2020

Coastal embayment rotation; morphological response to bi-directional wave climates and atmospheric forcing

Wiggins, Mark Andrew

UNIVERSITY OF
PLYMOUTH

COASTAL EMBAYMENT ROTATION; MORPHOLOGICAL RESPONSE TO BI-DIRECTIONAL WAVE CLIMATES AND ATMOSPHERIC FORCING

by

MARK ANDREW WIGGINS

A thesis submitted to University of Plymouth in partial fulfilment for the degree of

DOCTOR OF PHILOSOPHY

School of Biological and Marine Sciences

September 2020

Acknowledgements

First and foremost, I would like to thank my Director of Studies, Dr. Tim Scott for his guidance, support, and all-round motivation. Thank you for the opportunity and continued encouragement throughout this process, I look forward to working with you in the future.

I would also not be in this position without the assistance of my additional supervisors, Prof. Paul Russell and Prof. Gerd Masselink, both of whom have inspired and motivated me throughout. Additional thanks to Professor Masselink for facilitating the great opportunities I have experienced over the last few years.

Thanks to Jak “McCrack” McCarroll for all your tireless support with journal papers, as well as relentless energy levels at the beach. Extended thanks also go to everyone who has assisted in field work for this study, especially Peter Ganderton, Aaron Barrett, Rich Kenyon, Tim Poate and Kit Stokes.

I would also like to acknowledge and highlight the great work conducted by the entire Plymouth Coastal Observatory team, particularly Emerald and Josie for their support and provision of data throughout the last few years.

To the whole postgrad team, thank you for your support, assistance and most importantly friendship, especially Nieves (aka “Nievo”), Diego, Olivier, Oli, Marcus, Erin and Kris. It has always been great fun as a group, whether on the aeroplane to the USA, or in the van to Slapton Sands.

The greatest thanks of all go to my family. To my mother, father, and sister, you have always encouraged and supported me in everything I have done, and for that, I thank you. You can all now relax knowing I have almost finished university.

Finally, for your belief, support, and love, from beginning to end, you have earned this,

Mrs. Boss.

Author's declaration

At no time during the registration for the degree of Doctor of Philosophy has the author been registered for any other University award without prior agreement of the Doctoral College Quality Sub-Committee.

Work submitted for this research degree at the University of Plymouth has not formed part of any other degree either at the University of Plymouth or at another establishment.

The PhD supervisory team consisted of Dr Timothy Scott (Director of Studies), Prof. Gerd Masselink and Prof. Paul Russell from the School of Biological and Marine Sciences, University of Plymouth.

This research was in part funded by U.K. Natural Environment Research Council grant (NE/M004996/1; BLUE-coast project).

Relevant scientific seminars, project meetings and conferences were regularly attended throughout the duration of this thesis at which work was presented, and several papers were prepared for publication.

Word count of main body of thesis: 35,601

Signed...……

Date……07/09/2020……..…….……

Abstract

Name: Mark Andrew Wiggins

Title: Coastal embayment rotation; morphological response to bi-directional wave climates and atmospheric forcing

Beach rotation through longshore sediment transport can alter shoreline orientation, increasing erosional risks for coastal communities at short-term (storm events) and decadal to centurial time scales (long-term evolution). Identifying, predicting and planning for embayed beach rotation requires understanding of the morphological response to changes in directional wave climates driven by atmospheric forcing. Through assessment of annual to centurial datasets, this thesis aims to improve understanding of beach rotation at local (embayment) to regional (coastline) extents.

The multi-annual rotational response of a 12-km, longshore-dominated gravel embayment (Start Bay, Devon, UK) to a set of extreme and contrasting bi-directional winter wave conditions was assessed using multi-method topo-bathymetric surveys. Previously, the limited extent of intertidal measurements constrained insights into sediment pathways during rotational events; however, this study found that accounting for measurement uncertainty was critical in the calculation of robust total sediment budgets (sub-aerial to sub-tidal), allowing identification of full-embayment rotation.

Application of this new methodology revealed that under extreme directional wave energy (>1:50 year southerly winter season), full-embayment rotation (6.5×10^5 m^3 transport) is possible through headland bypassing (50% of total) and sub-tidal change (33% of total), providing new insights into sediment transport pathways for gravel beaches. Retrieval of beach volumes after rotational events requires sustained or equal extreme wave energy from opposing directions; however, only sub-embayment rotation was observed (under opposing easterly conditions), proposing that headland bypassing is asymmetrical, extending previously understood timescales of recovery.

Analysis of hindcast modelled wave data and a 10-year record of 36 intertidal beach profiles located across the full embayment of Start Bay, revealed that interannual to decadal scale beach rotation may be predicted by a new index of the normalized wave power directional balance (WDI), suggesting that subtle variations in bi-directional wave climate drive sustained changes in beach planform, increasing erosional risk at embayment extremities. Assessment of the modelled wave climate (1980 - 2018) highlighted that the two dominant wave directions (southerly and easterly) are correlated with winter averages of two key climate indices, the North Atlantic Oscillation (NAO) and West Europe Pressure Anomaly (WEPA). This is the first robust demonstration of the relationship between negative NAO and easterly wave power, indicating that atmospheric variability significantly explains the WDI and beach rotation at this location.

Spatial expansion of this analysis revealed that bi-directional wave climates are regionally comparable, extending throughout the length of the South coast of England. Similar correlations with both climate indices were exhibited, showing other rotational sites are controlled by the atmospheric influence of bi-directional wave climates. Examination of 10-15 years of intertidal beach profiles at 22 embayed South coast locations identified 11 sites exhibiting significant rotational responses, with regionally coherent common factors, including oblique shoreline orientation to bi-directional wave approach, steep slopes and coarser sediment. Beach rotation was shown to be correlated with the WDI for most sites, and significant direct correlations between beach rotation and WEPA at a number of locations, indicates the future potential skilful forecasts of atmospheric indices may have in predicting seasonal rotation at regional to basin-wide scales.

To explore the significance of recent (10-year) beach rotational behaviour in Start Bay within centurial timescales, a stepwise multi-linear regression model was developed to hindcast the WDI using long-term (1906-present) sea-level pressure records of the NAO and WEPA. It was found that combining the two indices vastly improved the predictive skill of the regression model when compared to using individual indices (R^2 of 0.66 between model data and index predicted values of the WDI).

Qualitative validation of beach rotation in response to the >100-yr hindcast WDI timeseries was achieved from proxy records of oblique photography and topographic maps, finding that low frequency (~60 years) phases of clockwise/anticlockwise beach rotation followed positive/negative phases of the detrended cumulative hindcast WDI record, over the period 1906 to 2018. This variability reflects observed multi-decadal fluctuations in phases of NAO (~60-80 year) and WEPA (~50-60 year), demonstrating atmospheric control of directional wave climate and beach rotation over centurial timescales, explaining historical accounts of coastal settlement relocation.

When examined in the context of millennial-scale proxy NAO reconstructions, the recent centurial-scale analysis does not capture the much greater magnitude and duration of past detrended cumulative variability observed over the last 3000 years, indicating that previously inferred phases of extreme coastal realignment may recur in the future, presenting a significant long-term issue for locations affected by beach rotation.

This work contributes new insights into embayment rotation at different spatial and temporal scales. Application of a new total sediment budget approach improves knowledge of full embayment rotation and recovery, whilst bi-directional waves are shown to predict beach rotation, driven by atmospheric forcing at medium to longer timescales. This thesis directly contributes towards new understanding of the past and future timescales of beach rotation, as well as proposing a mechanism for season ahead forecasting based on atmospheric variability.

PhD Outputs

Refereed Journal Publications

Wiggins, M.; Scott, T.; Masselink, G.; Russell, P.; McCarroll, R.J., 2019, Coastal embayment rotation: Response to extreme events and climate control, using full embayment surveys. Geomorphology, 327, 385–403. DOI: https://doi.org/10.1016/j.geomorph.2018.11.014

Wiggins, M.; Scott, T.; Masselink, G.; Russell, P., Valiente N. G., 2019, Regionally-Coherent Embayment Rotation: Behavioural Response to Bi-Directional Waves and Atmospheric Forcing. Journal of Marine Science and Engineering, 7(4), 116. DOI: https://doi.org/10.3390/jmse7040116

Wiggins, M., Scott, T., Masselink, G., McCarroll, R. J., Russell, P., 2020, Predicting beach rotation using multiple atmospheric indices, Marine Geology, 426, 106207. DOI: https://doi.org/10.1016/j.margeo.2020.106207

Valiente, N.G., McCarroll, R.J., Masselink, G., Scott, T., **Wiggins, M.**, 2019, Multi-annual embayment sediment dynamics involving headland bypassing and sediment exchange across the depth of closure. Geomorphology, 343, 48–64. DOI: https://doi.org/10.1016/j.geomorph.2019.06.020

McCarroll, R.J., Masselink, G., **Wiggins, M.**, Scott, T., Billson, O., Conley, D.C., Valiente, N.G., 2019, High-efficiency gravel longshore sediment transport and headland bypassing over an extreme wave event. Earth Surfaces Processes and Landforms. DOI: https://doi.org/10.1002/esp.4692

McCarroll, R.J., Masselink, G., Valiente, N.G., **Wiggins, M.**, 2020. The impact of a headland-associated offshore sandbank on shoreline dynamics. Geomorphology. 355, 107065. DOI: https://doi.org/10.1016/j.geomorph.2020.107065

Submitted Journal Publications

McCarroll, R. J., Masselink, G., Valiente, N. G., King, E., Scott, T., Stokes, C., **Wiggins, M.**, 2020, A general expression for wave-induced sediment bypassing of an isolated headland, EarthArXiv. DOI: https://doi.org/10.31223/osf.io/67rhx

Refereed Conference Proceedings

Wiggins, M., Scott, T., Masselink, G., Russell, P., Castelle, B., Dodet, G., 2017, The role of multi-decadal climate variability in controlling coastal dynamics: re-interpretation of the "Lost Village of Hallsands", In Proceedings of Coastal Dynamics, Helsingor, Denmark, 2017, pp. 96–107. Available at: http://coastaldynamics2017.dk/onewebmedia/195_wiggins.pdf

Wiggins, M., Scott, T., Masselink, G., Russell, P., 2019, Rotational beach response to directionally bi-modal wave climates, In Proceedings of Coastal Sediments, St Petersburg, Florida, 2019. DOI: https://doi.org/10.1142/9789811204487_0071

Scott, T., **Wiggins, M.**, Masselink, G., Castelle, B., Dodet, G., Saulter, A., 2019, Atmospheric climate control of directional waves in the United Kingdom and Ireland, In Proceedings of Coastal Sediments, St Petersburg, Florida, 2019. DOI: https://doi.org/10.1142/9789811204487_0063

McCarroll, R. J., Masselink, G., **Wiggins, M.**, Scott, T., Billson, O., Conley, D., 2019, Gravel beach cross- and alongshore response to an extreme event: beach length and headland proximity controls, In Proceedings of Coastal Sediments, St Petersburg, Florida, 2019. DOI: https://doi.org/10.1142/9789811204487_0234

Billson, O., Russell, P., Davidson, M. A., **Wiggins, M.**, McCarroll, R. J., Poate, T., Leonardi, N., 2019, observations of infragravity dominance in the swash zone of a steep gravel beach, In Proceedings of Coastal Sediments, St Petersburg, Florida, 2019. DOI: https://doi.org/10.1142/9789811204487_0161

Conference Presentations

Wiggins, M., Scott, T., Masselink, G., Russell, P., Castelle, B., Dodet, G., 2017, The role of multi-decadal climate variability in controlling coastal dynamics: re-interpretation of the "Lost Village of Hallsands.", Coastal Dynamics, Helsingor, Denmark, 2017.

Wiggins, M., Scott, T., Masselink, G., Russell, P., Stokes, C., Valiente N. G., 2018, Embayment Dynamics Using Multi-Method Surveys: An Assessment of Seasonal to Decadal Barrier Response to a Variable Bi-Modal Wave Climate, AGU Ocean Science, Portland OR, USA, 2018.

Wiggins, M., Scott, T., Masselink, G., Russell, P., 2019, Rotational beach response to directionally bi-modal wave climates In Proceedings of Coastal Sediments, St Petersburg, Florida, 2019.

Scott, T., **Wiggins, M.**, Masselink, G., Castelle, B., Dodet, G., Saulter, A., 2019, Atmospheric climate control of directional waves in the United Kingdom and Ireland, Coastal Sediments, St Petersburg, Florida, 2019.

McCarroll, R. J., Masselink, G., **Wiggins, M.**, Scott, T., Billson, O., Conley, D., 2019. Gravel beach cross- and alongshore response to an extreme event: beach length and headland proximity controls, Coastal Sediments, St Petersburg, Florida, 2019.

Published Datasets

McCarroll R. J., Masselink, G., **Wiggins, M.**, Scott, T., Billson, O., Conley, D., Valiente, N., Storm Emma, Start Bay, 2018 (BLUE-coast project). DOI: https://doi.org/10.24382/c3ee-6p96

Contents

List of figures and captions

List of tables and captions

Appendix A

List of key abbreviations

AMO – Atlantic Multidecadal Oscillation

AMOC – Atlantic Meridional Overturning Circulation

BMR – Beach Morphological Response

CCO – Channel Coastal Observatory

CUBE – Combined Uncertainty and Bathymetric Estimator

DEM – Digital Elevation Model

DJFM – December January February March

DJI – Da-Jiang Innovations

DoD – Digital elevation model of Difference

EACS – Environment Agency Control Stations

ENSO – El Nino Southern Oscillation

EOF – Empirical Orthogonal Function

GCP – Ground Control Point

GNSS – Global Navigation Satellite Systems

IPO – Inter-decadal Pacific Oscillation

LiDAR – Light Detection and Ranging

MBE – Multi-Beam Echosounder

LoD – Limit of Detection

MLWS – Mean Low Water Springs

NAO – North Atlantic Oscillation

ODN – Ordnance Datum Newlyn

PCO – Plymouth Coastal Observatory

PDO – Pacific Decadal Oscillation

PU – Plymouth University

RI – Rotation Index

RMSE – Root Mean Square Error

RTK-GPS – Real Time Kinematic Global Positioning System

RV – Research Vessel

SfM – Structure from Motion

SLP – Sea Level Pressure

SOI – Southern Oscillation Index

TLS – Terrestrial Laser Scan

TPU – Total Propagated Uncertainty

UAV – Unmanned Aerial Vehicle

UKHO – United Kingdom Hydrographic Office

WDI – Wave power Directionality Index

WEPA – West Europe Pressure Anomaly

WW3 /WWIII – Wave Watch 3 or Wave Watch III

1 Introduction

1.1 Context and motivation

Beaches often act as the first line of defence from elevated water levels and wave forcing, absorbing wave energy at the shoreline and providing protection from inundation for housing and infrastructure (Poate et al., 2016). Whilst there has been extensive research of beach morphological response to wave height (e.g. Davidson et al., 2013; López et al., 2018), and storm events (Karunarathna et al., 2014; Eichentopf et al., 2019) on exposed, cross-shore dominated locations, there is comparatively less insight into the response of alongshore dominated, semi-sheltered beaches, often experiencing incident waves from variable directions. In the United Kingdom (U.K.), such beaches make up a significant percentage of the coastline, and their response to wave forcing requires further attention.

Embayed and semi-sheltered coastlines can be highly dynamic and respond rapidly to changes in wave climate (Ruiz de Alegria-Arzaburu and Masselink, 2010; Bergillos et al., 2016b; Bergillos et al., 2017; Wiggins et al., 2019a). For embayed beaches with bi-directional wave climates, incident wave angles are often oblique to the shoreline, with morphological changes dominated by longshore processes, with sediment transported in the direction of wave approach (Short and Masselink, 1999). When wave directionality is sustained, embayed beaches erode and narrow at the up-drift extent and accrete and widen at the down-drift extent, with the subsequent change in planform orientation known as “rotation” (Klein et al., 2002). Changes in bi-directional wave forcing, and therefore beach rotational state can occur at short-term (e.g. Storm events, Ruiz de Alegria-Arzaburu and Masselink, 2010; Burvingt et al., 2016; McCarroll et al., 2019) and seasonal (Winter, Thomas et al., 2011a; Wiggins et al., 2019a, 2019b) timescales,

which present immediate challenges for coastal managers and communities (May and Hansom, 2003; Chadwick et al., 2005; Wiggins et al., 2017). The reduced beach volumes at one end of a rotated coastline may not offer the same level of protection from increasing coastal risk (e.g. wave overtopping, erosion, damage to infrastructure etc.). In the longer term, inter-annual variability in the winter-averaged wave climate is strongly affected by atmospheric changes over regional (Wiggins et al., 2019b) to basin-wide scales, (Bacon and Carter, 1993; Clarke and Rendell, 2009; Dodet et al., 2010; Castelle et al., 2017) with longer term trends in beach rotation being linked to multi-annual changes in atmospheric indices (Thomas et al., 2013; Plomaritis et al., 2015; Wiggins et al., 2017). This highlights the potential for climate indices to be effective predictors of bi-directional wave climates, and hence rotational coastline evolution over a range of timescales.

The work presented in this thesis is motivated by an increasing need to understand embayment scale rotation and its forcing mechanisms across a range of timescales (event scale to multi-decadal). The findings presented hope to contribute towards the improvement of effective planning and management of semi-sheltered coastlines, mitigating the risks posed by rapid or sustained rotational events, and allowing for proactive responses to variations in the incoming wave climate and atmospheric forcing. This requirement is increasingly pertinent, given the predictions of increased sea level rise over the next 100 years (Nicholls et al., 2011), in combination with longer term changes in coastal sea storminess (Feser et al., 2015), suggesting that the impact of coastal hazards is likely to increase significantly in the future.

1.2 Overview of thesis aims

The overall aim of this thesis is to advance our knowledge of coastal embayment rotation under bi-directional wave climates, understanding the driving mechanisms and

relationships with atmospheric climate variability. Further to this, embayment rotation over a range of temporal and spatial scales are investigated, including localised, event driven rotation, regionally coherent multi-annual response, and longer-term trends over multi-decadal to centurial timescales. Using Start Bay (South Devon, United Kingdom) as a natural field laboratory, and secondary data from the south coast of England, several methods are used to address these aims, including: (i) a robust multi-annual full embayment sediment budget analysis for Start Bay, using novel multi-method digital elevation models with associated uncertainty assessments, with data from a comprehensive field data collection campaign over three years (Chapter 2); (ii) an assessment of event and decadal scale rotational response, volumetric change and multi-annual recovery of a complete coastal sediment cell, including wave driven forcing and atmospheric controls (Chapter 2); (iii) decadal identification and quantification of regionally coherent embayment rotation using secondary topographic survey data and hindcast modelled wave data for many selected sites along the south coast of England, identifying regional characteristics of bi-directional wave climate, response to atmospheric forcing, and the factors controlling medium-term (decadal) beach rotation (Chapter 3); and (iv) development of a stepwise multi-linear regression model to hindcast wave climate and beach state in Start Bay, using long-term (centurial) records of atmospheric indices and historical proxy data to explore past beach volume variability (an hence beach rotation), placing the observed short to medium-term beach rotational response into a longer-term context.

1.3 Key concepts

Whilst each chapter introduces and discusses relevant processes and literature pertaining to its respective aims, methods and results, key concepts of this thesis are briefly introduced and explained in the following sections. This provides a clear overview of

the common themes, before briefly introducing the relevance of the main study site (Start Bay, U.K.), and describing specific research objectives and the thesis structure.

1.3.1 Beach rotation

Beach rotation has been studied worldwide, and is most prevalent at embayed beaches (Short and Masselink, 1999) where physical barriers (headlands or artificial structures) trap laterally moving sediment, driven by oblique incident wave angles, with an accretion at one end of the beach, and erosion at the other, resulting in shoreline advance or retreat, respectively (Figure 1.1). The resultant change in beach planform can leave certain stretches of coastline more vulnerable to wave attack, increasing risks of erosion, flooding and inundation. The driving mechanisms of beach rotation have classically been linked to changes in the incoming wave climate, in particular wave direction and period. These changes to oblique incident wave angles can occur over a range of timescales, leading to short-term event scale rotations (storm events), to seasonal, multi-annual and even multi-decadal phases of beach planform rotation.

In regions where wave climates are distinctly bi-directional (Klein et al., 2002, 2010; Wiggins et al., 2019b), rotation has been shown to be a common feature along headland embayed beaches (presented in Chapter 3). Storm events from different directions can drive rapid rotational responses, as shown by Ruiz de Alegria-Arzaburu and Masselink (2010), who identified that the relative balance of storm events from opposing directions controlled the planform shape of an embayed gravel barrier, driving considerable accretion and erosion at opposing ends of the beach. In such cases, annual variations in beach state under bi-directional waves may be a combined function of the relative energy, frequency and sequencing of wave events from opposing directions (Loureiro et al., 2012; Bergillos et al., 2016b; Grottoli et al., 2017; Pikelj et al., 2018). In cases like this, Klein et al. (2002) proposed that although rotational events may result

in a localised decrease or increase of beach volume alongshore, long-term sediment budgets within embayments remain balanced, with no net gains or losses to the embayment; however; several authors have shown that alongshore rotation under oblique waves, if sustained, can cause sediment losses through headland bypassing, either in the sub-tidal (Ojeda and Guillén, 2008; Goodwin et al., 2013; Thomas et al., 2013; McCarroll et al., 2019) or sub-aerial domain (Vieira da Silva et al., 2016). The rotational response of many beaches along the south coast of the U.K. was observed following a winter period (2013/14) dominated by Atlantic storms and found to be the most energetic winter wave season in Europe since at least 1948 (Masselink et al., 2015, 2016). Many south coast beaches rotated clockwise (west to east) in response to the sustained southerly wave climate (Burvingt et al., 2016, 2017; Scott et al., 2016); however, at some locations, net losses were observed within the intertidal zone, and sediment budgets were not balanced, suggesting cross-shore processes or headland bypassing were also accountable for some of the overall changes. Investigation into these observed losses (Wiggins et al., 2019a) is presented later in this thesis (Chapter 2).

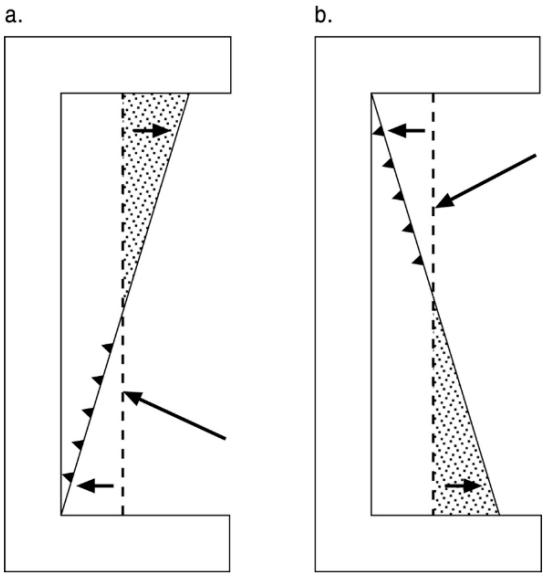

Figure 1.1. A simple conceptual model of longshore driven beach rotation in an embayed coastline, showing a) clockwise beach rotation under oblique southerly waves and b) anti-clockwise rotation under oblique northerly waves. Adapted from Short and Masselink (1999)

Whilst longshore transport driven rotation is well evidenced (Klein et al., 2002; Ruiz de Alegria-Arzaburu and Masselink, 2010; Wiggins et al., 2019a), further studies (Ranasinghe et al., 2004; Harley et al., 2011, 2015; Short et al., 2014), have suggested a cross-shore mechanism may also result in beach rotation. Harley et al. (2011) used Principal Component Analysis (PCA) on over 30 years of beach shoreline data surveyed at Collaroy-Narrabeen beach (south eastern Australia), concluding that the dominant mode of shoreline variability (60%) was controlled by variations in alongshore gradients in wave energy, resulting in increased or decreased cross-shore sediment exchange, known as beach oscillation. This lead to an out of phase erosion and accretion at embayment extremities, and when measured, this response manifests itself as a similar rotational observation (Figure 1.2), common along the beaches of south eastern Australia.

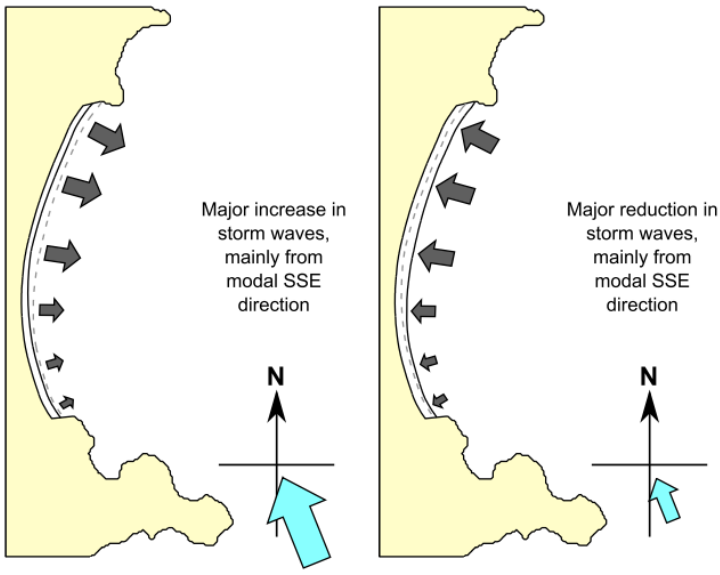

Figure 1.2. Conceptual model of cross-shore beach rotation observed on the south eastern Australian coastline. Dashed/solid shorelines represent the previous/current shoreline position. Black arrows indicate the direction of sediment transport processes and blue arrows the direction and relative magnitude of wave forcing. From Harley et al. (2011).

In addition, a follow up study by Harley et al. (2015) confirmed the cross-shore dominance on apparent beach rotation, and further identified a significant response in

beach berm slope, with opposing ends of the beach steepening or flattening in reaction to different cross-shore processes occurring in the surf zone, depending on the degree of shelter or exposure along the embayment.

Regardless of the dominant mechanism by which rotation is caused, wave height alongshore, and incident wave direction can both be altered by embayment alignment and curvature, refraction and shadowing from headlands and islands (Thomas et al., 2011b, 2011a) as well as the presence of offshore sand or mud banks (Anthony et al., 2010; Dolphin et al., 2011; Brunier et al., 2016).

1.3.2 Bi-directional waves

For beach rotation under longshore transport processes, wave bi-directionality can play a significant role in controlling the morphological response (Short et al., 2008; Ruiz de Alegria-Arzaburu and Masselink, 2010; Kelly et al., 2019; Wiggins et al., 2019b). The term “bi-directional” in this instance refers to a wave climate with two distinctly different dominant modal wave directions (Hemer et al., 2010; Romeu et al., 2013). The term “bi-modal” is sometimes used to describe such wave climates; however, this is incorrect in this context, and should strictly refer to a sea state in which both a swell and wind sea are present at the same time, regardless of direction (either the same or contrasting). Such bi-modal sea states have shown a limited annual occurrence around the coastlines of the U.K. (0-10% annual temporal average), but have been shown to cause complex morphological responses, such as increased berm crest erosion and breaching, due to the differing wave periods driving increased wave runup, overtopping and overwash (Mason et al., 2009; Bradbury et al., 2011; Thompson et al., 2018).

Bi-directional wave climates are driven by synoptic variations in weather patterns (Michelangeli et al., 1995; Sanchez-Gomez et al., 2009), driving winds from different directions, leading to distinct modes of directional wave generation (Mortlock and

Goodwin, 2015). At semi-sheltered coastlines, the geometry of the land mass can limit the directions in which waves can approach; however, swell wave propagation can allow waves generated far from the coast to arrive from several different directions (Mason et al., 2009; Malagon Santos et al., 2017). Additionally, shorter period, fetch limited wind waves may be present due to generation under different weather patterns. Around the coast of the U.K. and Ireland (UK&I), wave climates range from uni-directional to multi-directional, as highlighted in Figure 1.3 (Scott et al., submitted.).

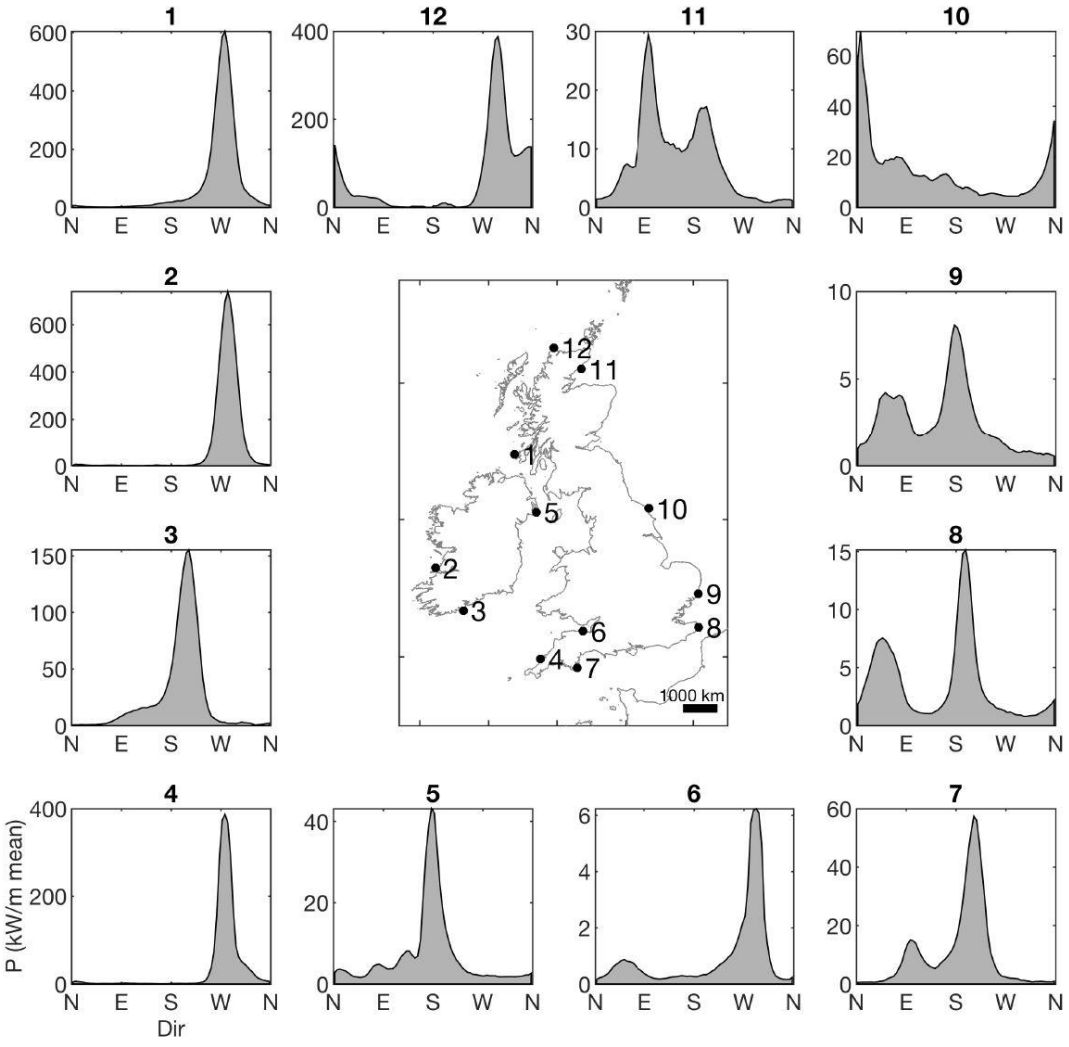

Figure 1.3. Example wave climate data from each region of UK&I demonstrating the variability in directional multi-modality. Insets show directional power distribution as 1980–2017 3-hourly average kW/m in 5˚ bins, adapted from Scott et al. (submitted).

Throughout many coastal environments, bi-directional wave climates can exhibit strong seasonal (Ruiz de Alegria-Arzaburu and Masselink, 2010; Mortlock and Goodwin, 2015; Bergillos et al., 2016a) to inter-annual (Wiggins et al., 2019a) variability, which can drive similar responses in beach rotation behaviour.

1.3.3 Atmospheric forcing

Atmospheric forcing has been linked to longer term variability in bi-directional wave climates throughout both the northern and southern hemisphere. This study focuses on the coasts of the U.K., and hence an overview of the two climatic indices used and discussed throughout this thesis are presented below.

1.3.3.1 North Atlantic Oscillation

Within the northern hemisphere, the North Atlantic Oscillation (NAO) is the primary mode of atmospheric variability (Hurrell, 1995), with significant implications for weather and climate, particularly in western Europe, and exerts a significant control during the colder period of the boreal winter.

Most commonly computed from sea level pressure (SLP) records of the sub-polar Icelandic Low and sub-tropical Azores High, the NAO index is a measure of the normalized SLP difference between the two (usually measured at Lisbon, Portugal and Stykkisholmur/Reykjavik, Iceland). Alternative calculations can be made from the principal empirical orthogonal function (EOF) of SLP hindcasts from numerical modelled weather data, which may provide more idealised depictions of the full spatial patterns of atmospheric variability, with reduced noise (Hurrell and Deser, 2009). Both the station-based SLP and EOF-derived NAO indices are closely matched, but physical measurements of SLP are often available further back in time, allowing for longer-term station-based records of the NAO to be computed.

Positive (negative) NAO phases occur (Figure 1.4) when the difference between the two centres is high (low). During positive phases, the strong low pressure and strong high pressure systems tend to result in a southward track of the jet stream, largely uninterrupted by Rossby waves, therefore driving increased westerly winds and storms over the North Atlantic, bringing milder, wetter weather to the north-west coasts of Europe, and an increase in westerly waves (Castelle et al., 2018). Conversely, negative phases of the NAO, characterized by a weakening in the pressure difference, allow for a "blocking" formation in the jet stream, resulting in a reduction in the number of westerly Atlantic storms, colder and drier conditions over northern Europe, with increased potential for the formation of easterly storms and wind conditions.

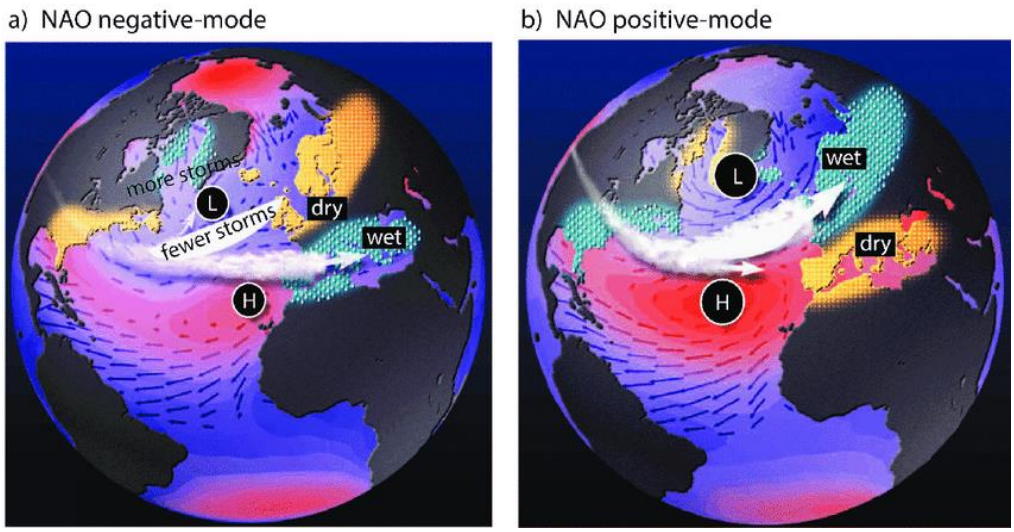

Figure 1.4. Model schematic of the North Atlantic Oscillation, showing a) negative NAO phase, decrease in associated storminess, reduced westerly winds and drier and colder temperatures in northern Europe, and b) positive NAO phase with more frequent storm activity, increased westerly winds, milder and wetter conditions in northern Europe (adapted from http://www.ldeo.columbia.edu/res/pi/NAO/).

The NAO has previously been linked to variations in wave climate throughout the North Atlantic (Bacon and Carter, 1993; Dodet et al., 2010; Castelle et al., 2018). Strong correlations between positive NAO and increased wave height anomalies (Figure 1.5) in the upper latitudes (>52° N) were presented by (Castelle et al., 2017). This correlation is

particularly strong during the winter months (Bromirski and Cayan, 2015; Burvingt et al., 2018; Wiggins et al., 2019a, 2019b), where storms play a critical role on wave heights and hence beach morphology.

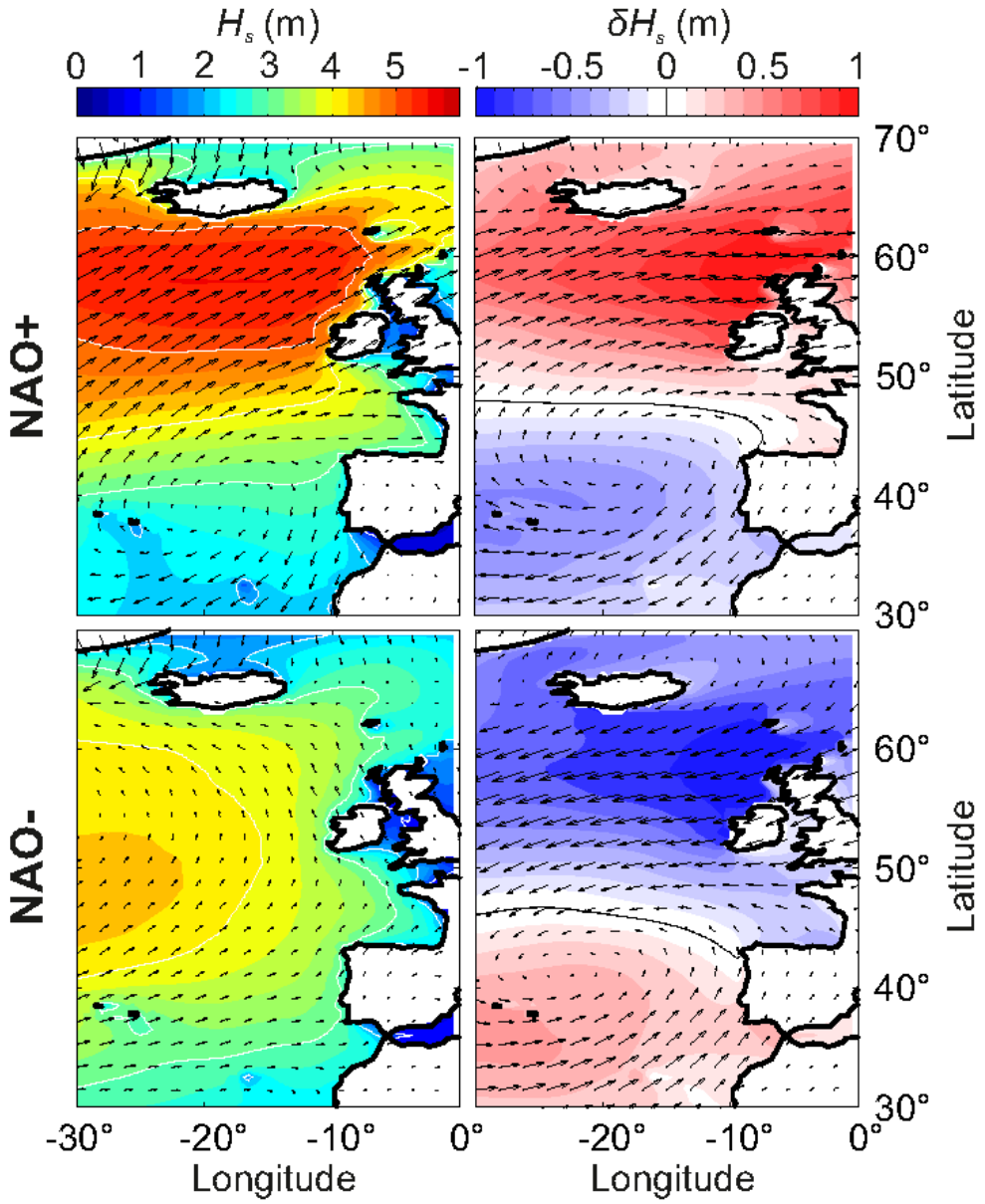

Figure 1.5. Influence of positive (top) and negative (bottom) NAO on winter averaged H_s (left panels) and corresponding anomaly (right), with 10m surface wind vectors overlaid. Positive and negative phases were addressed by averaging the five winters with the largest and smallest index values from 1950-2016. By order of decreasing importance, the five winter years considered for each index phase are NAO+ (2015, 1989, 1995, 2012, and 2000); NAO− (2010, 1964, 1969, 1963, and 1977), where, for instance, 1977 means the DJFM 1976/1977 winter. Published in Wiggins et al. (2017), adapted from Castelle et al. (2017)

1.3.3.2 West Europe Pressure Anomaly

Due to the lack of skill in the NAO capturing the unprecedented stormy winter of 2013/14, a new climate index was developed by Castelle et al. (2017), specifically created to capture the variability in wave height for the area of the North Atlantic southward of 52° N, affecting the western section of coastline between the U.K. and Portugal. Their study used reanalysis data (1948 to 2016) of SLP and 10 m wind fields at 2.5° x 2.5° grid points, to force a spectral Wave Watch III model at 0.5° grid resolution, covering the North Atlantic Ocean. Winter averages (DJFM) of significant wave height at six virtual wave buoys were correlated with all potential grid point pairs of normalised SLP difference, from anywhere in the domain. In this way, the pair of virtual SLP stations could be selected that best captures variability in wave height for western Europe. The optimal gradient capturing the greatest variability in wave height for the four southernmost virtual wave buoys, is both longitudinal and latitudinal, with the northern station located close to the island of Ireland; however, the southern virtual SLP station was located in the open ocean, restricting the use of land-based SLP station records. Given the need for a land-based station index, allowing for longer time series computations, the West Europe Pressure Anomaly (WEPA) uses the normalised SLP difference between Valentia in Ireland and Santa Cruz de Tenerife in the Canaries. These stations were selected as they were closest land-based SLP stations to the optimized virtual stations, and the resulting index accounted for 40-90% of wave height variability.

Positive phases of winter averaged WEPA are characterized by an intensified SLP gradient between the two stations, with an increase in wave heights (Figure 1.6) around 45°N, with southward tracking storms, passing over, and causing increased wave activity along the south coast of the U.K. (Malagon Santos et al., 2017; Burvingt et al., 2018; Castelle et al., 2018). Negative phases of WEPA result from a weakening of the

SLP gradient and are characterised by a reduction in wave height anomalies southward of the U.K. and Ireland (52°N), with northward tracking storm centres, passing over the top of the U.K. towards Scandinavia.

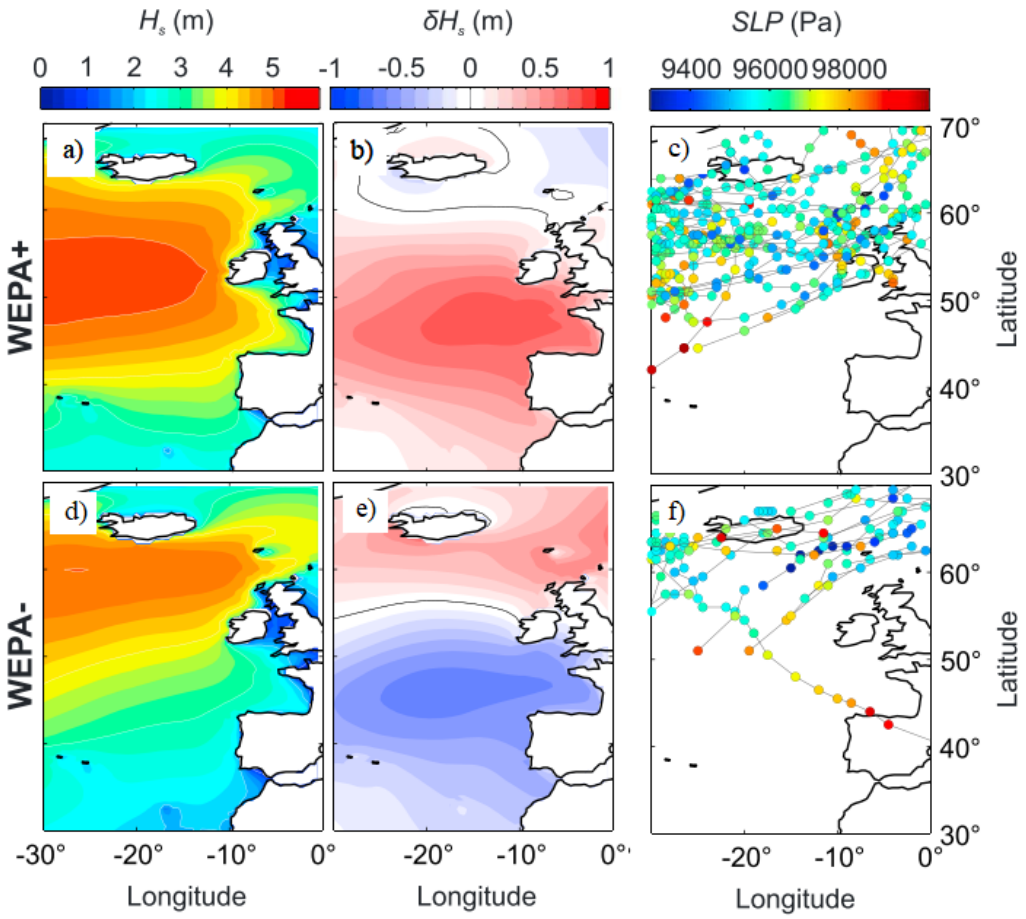

Figure 1.6. Influence of positive and negative WEPA indices on winter-averaged H_s (a, d), corresponding anomaly (δHs) (b, e) and storm tracks (c,f), with positive phase and negative phases of each index addressed by averaging the 5 years with the largest and smallest index values over 1950–2016. Superimposed storm tracks over the 5 years with the coloured circles indicating the sea level pressure at the center of the low-pressure system every 6 h. Note that for clarity and to focus on the more severe storms, only identified storms that have a low-pressure center deeper than 96,000 Pa are plotted. By order of decreasing importance, the five winter years considered for each index phase are WEPA+ (2014, 1994, 2001, 2016, and 1977); WEPA− (1992, 1953, 2005, 1976, and 1993), where, for instance, 1977 means the DJFM 1976/1977 winter. Adapted from Castelle et al. (2017).

This new index outscored all other North Atlantic climate indices in accounting for variability in both winter-averaged significant wave height, and winter-averaged extreme wave heights. Although the WEPA index appears to be simply a southward shifted version of the NAO, the two are not correlated, and WEPA is the climate index which best observed the unprecedented stormy winter of 2013/14 (Section 2.2.2).

1.3.4 Morphological response to climatic forcing

The link between atmospheric forcing and wave climate can further explain resultant variations in morphological beach response. Direct assessments of this idea have been explored by several authors worldwide. Within the North Atlantic, at seasonal to multi-annual scales, Masselink et al. (2014) showed that phases of the winter averaged NAO were able to explain variations in wave height and dimensionless fall velocity (Wright and Short, 1984) at an exposed sandy beach in south west England. They concluded that due to the strong correlation between wave height and beach state, that the NAO is therefore also correlated with multi-annual changes in nearshore bar morphology. Similar correlations have been discovered when addressing erosion and recovery rates of beaches in northern Brittany (Suanez et al., 2012), as well as the rotational state of an embayed sandy beach in west Wales, from annual to centurial timescales (Thomas et al., 2011a, 2011b, 2013).

Since it was devised by Castelle et al. (2017), WEPA has been used in the North Atlantic region to improve correlations between atmospheric forcing and beach state, especially in the region below 52°N. For the exposed western facing beaches of south west England, Burvingt et al. (2018) observed increased erosional cross-shore volume transport in line with positive phases of the WEPA index. Additionally, WEPA exhibited better correlations than NAO, with extreme supra-tidal boulder transport along the Brittany coastline (Autret et al., 2017).

In addition to the local and regional scale observations, basin-wide controls on beach morphological response have also been linked to climate indices, mainly the El Nino Southern Oscillation (ENSO) in the Pacific Ocean (Ranasinghe et al., 2004). For the eastern coast of Australia, Splinter et al. (2012) identified correlations between yearly modelled net longshore transport rates and positive phases of the Inter-decadal Pacific Oscillation (IPO) and the Southern Oscillation Index (SOI), highlighting that atmospheric indices may predict longer term beach response. In addition to the strong correlations between ENSO modes and directional wave climate (Mortlock and Goodwin, 2015), further work by Mortlock and Goodwin (2016) demonstrated that embayed beach planform is strongly controlled by different types of ENSO, controlling either a clockwise or anti-clockwise rotation. Phases of the ENSO were also found to control beach erosion at 48 different Pacific Ocean locations (Barnard et al., 2015), whilst an extremely strong El Nino event in 2015/16 was shown to cause widespread erosion along the American west coast of the North Pacific basin (Barnard et al., 2017). Beach rotation along the same stretch of coastline (Peterson et al., 1990; Anderson et al., 2018) has also been linked to phase differences in Pacific ENSO, highlighting the potential for such indices to control large scale beach morphological behavior.

Atmospheric forcing has shown significant controls on both wave climate variability and resultant beach morphological response, across a variety of spatial and temporal scales.

1.3.5 Start Bay: a site of scientific interest

This section introduces the main study site assessed throughout this thesis, Start Bay in South Devon. Further technical description is provided in relevant chapters, but an overview of the past and contemporary societal issues within Start Bay highlight its relevance to coastal geomorphological research.

Located on the south coast of Devon, U.K., Start Bay comprises four interconnected gravel sub-embayments, stretching over 15 km from Start Point in the south, to Blackpool Sands in the north (Figure 1.7). The main beaches are named from the south to north as; Hallsands, Beesands, Slapton Sands and Blackpool Sands, acting as barrier beaches, with freshwater lagoons behind. Between each sub-embayment lie rocky outcrops that separate each beach at high tide, trapping laterally moving sediment as it is transported alongshore. It receives a bi-directional wave climate (Figure 1.7) with diminished Atlantic swell waves arriving from the south-south-west and short fetch wind waves from the east. Due to the embayment alignment (SSW-NNE), geometry and local bathymetry, the angle of wave approach from the two dominant wave directions is oblique to the shoreline, driving northward (southward) sediment transport under southerly (easterly) waves, and southward. Although the barrier positions have remained relatively stable over the last 3000 years, allowing the sediment within the bay (mainly flint) to be reworked by the sea, the embayment continually realigns itself to the dominant wave approach, existing in a state of dynamic equilibrium.

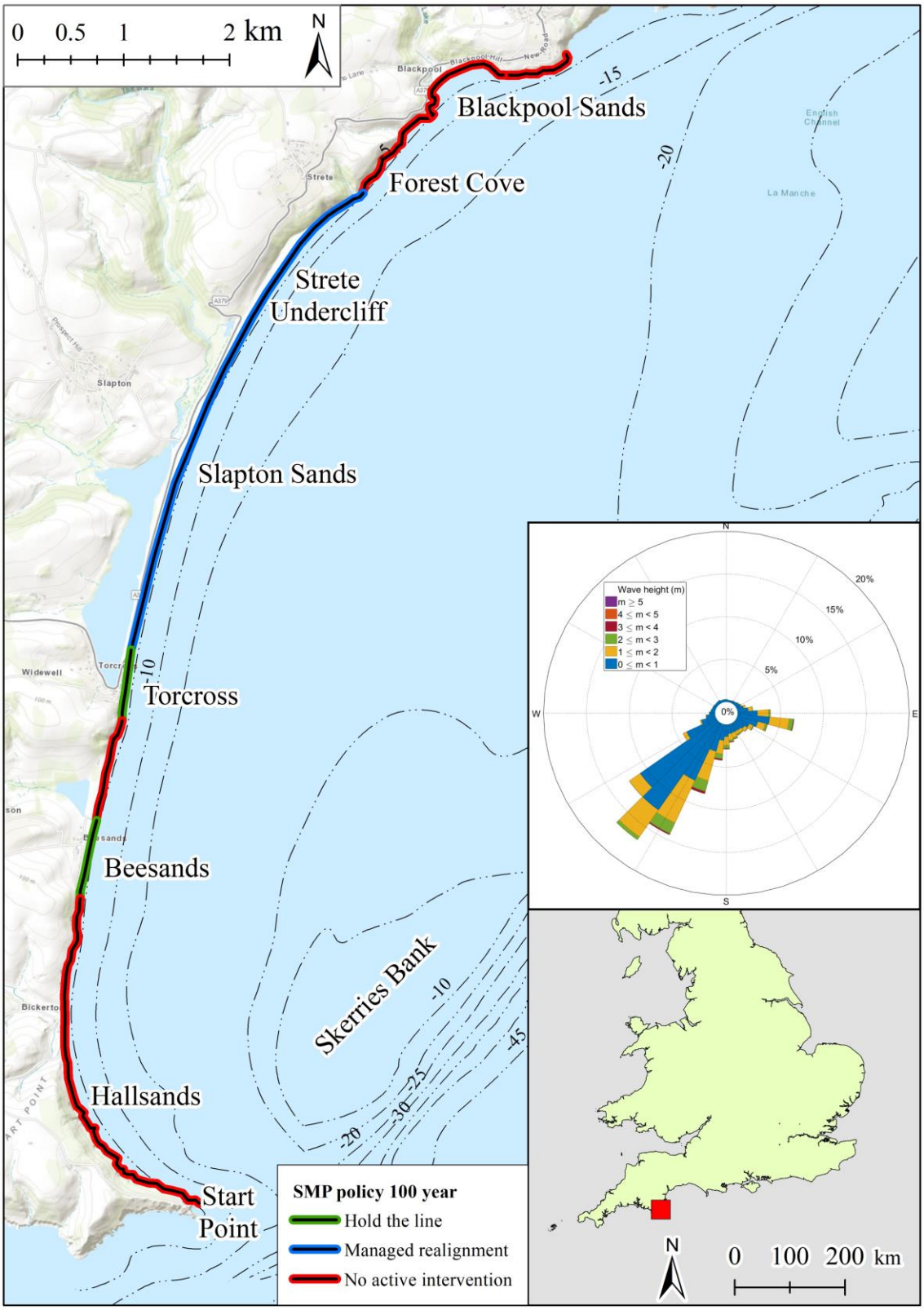

Figure 1.7. Location overview of Start Bay showing beach and settlement names and locations, as well as the A379 road over the Slapton Sands barrier. Shoreline Management Plan policy designations across the embayment are displayed by the coloured lines. The bi-directional nature of the wave climate for 1980 to 2017 is displayed in the inset wave rose.

Start Bay is a well-studied example of a closed sediment cell in which a bi-directional wave climate drives beach rotation under prevailing easterly and southerly wave conditions. Historically, the site has received significant attention in terms of coastal change and vulnerability, with numerous accounts of severe impacts to the communities and infrastructure. One of the most well-known coastal erosion case studies in the UK is the loss of Hallsands (Figure 1.7), which combines human intervention with complex coastal and atmospheric processes, which ultimately led to the demise of a small community.

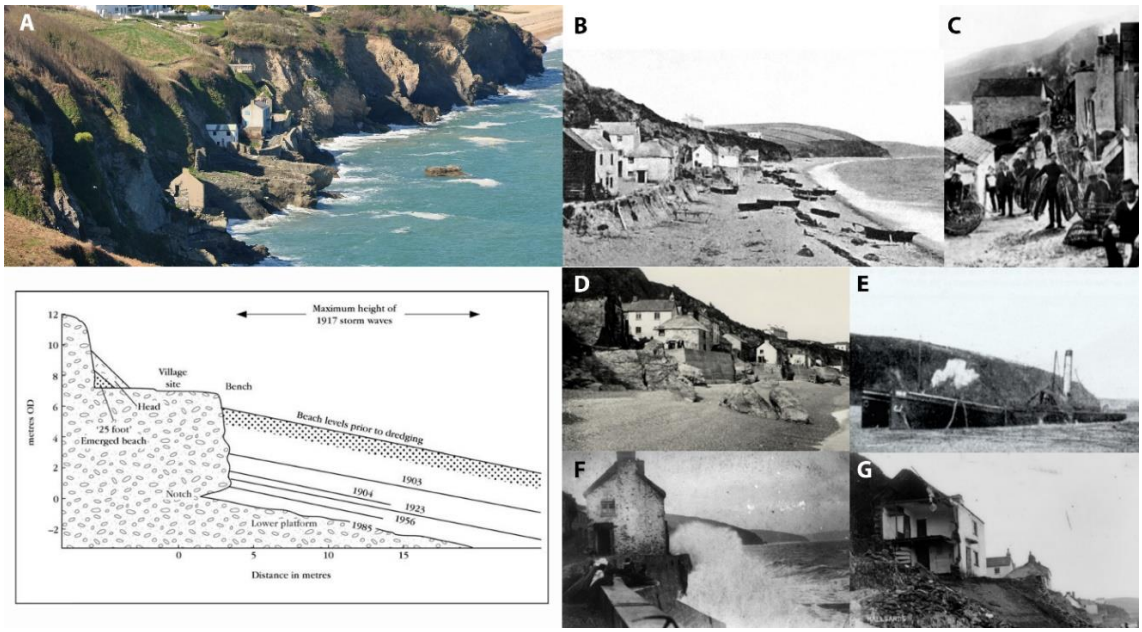

Figure 1.8. Photographic timeline before and after the loss of village (1894 – 2012). Photos courtesy of Cookworthy Museum, Kingsbridge, Devon. A) 2012, Hallsands, showing the rock platforms where the original houses stood; B) 1894, fishing boats on the beach; C) 1900, the road into the village; D) 1904, lowered beach levels following the commencement of dredging; E) 1898, dredging boats extracting shingle; F) 1901, storm waves reaching the village; G) 1917, and destruction of the village following easterly storms. Lower Left: Cross sectional surveys recorded through the 20th century showing the progressive lowering of the beach (Mottershead, 1986)

In 1897, an extension to the Devonport Dockyard in Plymouth (U.K.), required significant quantities of sand and other materials for its construction. The local contractor, Sir John Jackson began dredging from the beaches and nearshores of

Hallsands and Beesands (May and Hansom, 2003). Between 1897 and 1902 up to 1,600 tonnes was removed daily (Figure 1.8. d), and the beachface became progressively narrower (Figure 1.8. c). In November 1900, cracks began appearing in some of the houses and the sea wall foundations undermined. In the winter of 1900-1901, storms hit the village causing damage to sea walls (Figure 1.8. e), whilst removing shingle and gravel from gaps in the rock platform behind. The lack of foundations caused buildings to collapse at these points, and thus the dredging license was revoked in 1902 when the beach level had fallen by at least 3 m.

Civil Engineer, R. Hansford (Worth, 1904), refuted the claim that the beach would be resupplied with sediment from offshore, and conducted a set of beach level surveys in 1904, 1909 and 1923 (Figure 1.8. Lower Left). Using photographs from before and after the commencement of gravel removal, he estimated that approximately 400,000 m^3 of gravel was taken from Hallsands by the dredging operations (May and Hansom, 2003). Coastal defences were constructed behind the significantly narrower beach, and proved effective up until January 1917, when a north-easterly gale brought about a storm with reported waves allegedly over washing at heights greater than 12 m, crashing into the village during high spring tides. Most of the buildings were destroyed and the village was abandoned (Figure 1.8. f). At the time of the disaster, locals attributed the cause to the extraction of the gravel. Since then, work by Hails (1975a) has asked the question of whether this claim has ever been scientifically addressed. Further surveys were repeated by Robinson (1961), and concluded the beach had continued to erode to a level lower than ever previously recorded. To the south of the village there are no sediment sources to replenish the beach through longshore transport processes, and the beach at Hallsands has become progressively narrower over the last century (Figure 1.8. Lower left). At present, the site of the original village is devoid of almost any beach, and a rock

platform is exposed below the shelf on which the remnants of the original houses stand (Figure 1.8. g).

The story of Hallsands' lost village is often cited as an example of anthropogenic interference with a finely balanced system, and the catastrophic effects of exploiting natural resources, however; there is evidence to suggest that coincidental changes in wave climate occurring during the dredging and following years led to large scale rotations of the embayment, driven in part by multi-annual variations in atmospheric forcing (NAO), exacerbating or directly contributing to the eventual loss of Hallsands (Wiggins et al., 2017), explained further in Chapter 4. This explanation is supported by the abandonment of another village at the opposing northern end of the embayment, prior to the Hallsands disaster.

Strete Undercliff was a small fishing village (Figure 1.9) located at the northern end of Slapton Sands (Figure 1.7) and its earliest recording dates back to the early 17th century.

Figure 1.9. The lost village of Strete Undercliff, founded in the 17th century, and lost to the sea by 1780. Copyright © 2019 Stretewise, http://stretewise.co.uk/stretehistory.html

It was documented on early nautical maps, until its disappearance by 1780 (Stranack, 2017), at which point the earliest records of the village of Hallsands start to appear. Similar variations in wave climate, driven by multi-decadal phases of atmospheric forcing (Clarke and Rendell, 2006, 2009; Trouet et al., 2012) may have led to changes in beach planform, driving settlement locations of the past and present communities of Start Bay.

Within the last 20 years, Start Bay has experienced significant damage to infrastructure, under event scale and seasonal wave attack from both the southerly and easterly wave directions. In January 2001, an easterly storm with a duration of four days, combining a 1-in-1 year wave height (~3.5 m at break point) coinciding with a large spring tide, resulted in a 1:25 year combination event (Chadwick et al., 2005). Extensive erosion of the beach led to a section of the A379 road, which runs along the length of the Slapton Sands barrier crest (known as the Slapton Line), collapsing due to beach cutback, and the remaining road was moved back some 21 m in response.

In addition to the episodic easterly events, numerous southerly storms were experienced during the unprecedented energetic winter season of 2013/14 (Masselink et al., 2015, 2016; Burvingt et al., 2016; Scott et al., 2016; Wiggins et al., 2019a), described further in Section 2.2.2, with extensive damage recorded within Start Bay (Figure 1.10). At Beesands, a coastal road was completely eroded (Figure 1.10a), and the shoreline retreated well over 15 m in places (Siggery and Wiggins, 2014). In addition, overwash of beach gravel onto the A379 at Slapton Sands caused road closure, whilst overtopping of waves at the southern village of Torcross threw large volumes of gravel over a sea wall causing damage to numerous buildings. Beach levels in front of the sea wall continued to drop over the next two winters, with profile surveys showing the lowest levels ever recorded in February 2016. The foundations of an adjacent retaining wall were exposed, and it collapsed within a single tidal cycle, whilst the main sea wall's

foundations became exposed and had to be reinforced a year later. In 2018, an extreme easterly storm event (Storm Emma, March 2018) caused large scale erosion of the upper beach at Slapton Sands and Beesands, as well as large scale rotation of the embayments (McCarroll et al., 2019). Another section of the A379 road was lost to the sea as well as cut back of a coastal car park, and a full-scale midnight evacuation of Beesands at high tide due to coastal flooding. The road has again been moved back by 10 m but will not be replaced should it be breached again.

Figure 1.10. Contemporary storm damage issues in Start Bay a) Road destruction at Beesands following southerly waves brought in by Storm Petra, February 2014, b) undermining and collapse of sea wall at Torcross, Slapton Sands following sustained southerly incident waves and lowest recorded beach levels in February 2016, c) evacuation of residents following high tide impact of Storm Emma, March 2018, d) the second collapse of the A379 road atop the Slapton Sands barrier ridge following Storm Emma, March 2018.

The societal importance of the different storm impacts within Start Bay is further complicated by the variation in designation of the Shoreline Management Plan (SMP) for different sections of the embayment (Figure 1.7). The shoreline in front of the

villages of Beesands and Torcross is to Hold the Line, meaning government and Environment Agency (EA) funds are spent to preserve the current shoreline position, maintaining and improving the existing sea defences. Conversely, the beach and shoreline in front of the new village of Hallsands (just north of the original abandoned site) has a No Active Intervention designation, leaving only local self-funded defences to be maintained by residents as the only form of shoreline protection, causing controversy in the local communities (BBC, 2014). Elsewhere in the embayment, the main section of the road at Slapton Sands is designated as Managed Realignment (Wilson, 2006), meaning adaptation is required, in allowing the road to move back with barrier retreat, preserving the road for as long as possible.

Due to the rapid morphological response of Start Bay to variations in the wave climate, and its significant societal impacts on the local communities, regular coastal monitoring (including terrestrial and aerial topographic beach surveys, bathymetry and wave buoy data), has been undertaken since 2006, by both local government, through the South West Regional Coastal Monitoring Programme (SWRCMP), and academia, by Plymouth University (PU). This extensive dataset is used throughout this study.

The beaches of Start Bay, particularly Slapton Sands, are similar to many gravel barriers and beaches located along the south coast of England (Scott et al., 2011), and its morphological response is considered representative of other reflective gravel beaches in storm-affected, fetch-limited coastal environments.

1.4 Research objectives and thesis outline

The overarching aim of this thesis is to advance our knowledge of coastal embayment rotation under bi-directional wave climates, understanding its driving mechanisms and relationship with atmospheric climate variability. Several specific research objectives have been identified and are listed below in the context of the thesis outline.

Chapter 2 - Coastal embayment rotation: Response to extreme events and climate control, using full embayment surveys

Beach rotations at event to multi-annual scales are important morphological responses to storms and changes in bi-directional wave climates. These morphological responses pose immediate risk to coastal communities and infrastructure at timescales that may be critical to coastal management. In addition to providing a detailed introduction to the study site used throughout this thesis, and describing the unique set of wave conditions observed, the specific research objectives of chapter 2 are to:

i. **Quantify the short-term rotational response of an entire coastal embayment to bi-directional wave conditions.**

   The concept of longshore rotational response of embayed beaches to obliquely incident waves was introduced in section 1.3.1; however, to fully understand the sediment transport pathways and mechanisms driving embayment-scale rotation under an extreme set of bi-directional wave conditions it is important to capture all morphological changes within the full embayment, including all sub-embayments across both the sub-aerial and sub-tidal zones, extending to the depth of closure. In addition, to compute robust and meaningful inter-annual sediment budgets, a methodology must be developed which takes into account the uncertainties of the respective survey methods. In Chapter 2, a detailed description of a multi-method survey technique is introduced, along with the

calculation of essential uncertainty values for each method. At this point, a geomorphic change detection method, which has only previously been applied to fluvial settings, is used for the first time within a coastal environment, to evaluate morphological changes observed with Start Bay between 2013 and 2017. This period includes two distinctly different and unique sets of wave conditions, with both epochs showing significant, and contrasting deviations from the average, including a predominantly southerly set of winter waves (2013 to 2016) containing the unprecedented high energy winter of 2013/14, with the largest recorded 8-week average wave height in at least 60 years (Masselink et al., 2015, 2016), and a calmer winter with an increased proportion of easterly wave conditions (2016/17). Quantification of beach rotation at full and sub-embayment scale is made, and the volume of sediment transported between sub-embayments via headland bypassing is investigated. Finally, the morphological response is quantified in terms of sub-aerial and sub-tidal changes to beach volumes throughout the embayment.

ii. Assess the extent to which the bi-directional wave balance controls beach rotation over multi-annual timescales.

As suggested by previous authors (Ruiz de Alegria-Arzaburu and Masselink, 2010; Scott et al., 2016; Bergillos et al., 2017), wave power from opposing directions is a key driver of beach rotation. In Chapter 2, new insights into the control bi-directional wave climates impart on beach volume change are investigated. The creation of a new index which describes the winter integrated relative wave power directional balance (WDI) between the two dominant wave directions is assessed in relation to the spatial variations in beach volume over a 10-year topographic survey record.

iii. **Examine the relationship between climatic indices and bi-directional wave forcing.**

Once the rotational response of the embayment has been assessed and quantified in respect to the bi-directional wave climate, this third objective attempts to identify the forcing mechanisms controlling multi-annual variability. By exploring the potential relationship between atmospheric indices (NAO and WEPA) and the bi-directional wave climate, inferences can be drawn as to the potential longer term controls on beach rotation.

Chapter 3 - Regionally coherent, medium-term beach rotation and climate control

Whilst Chapter 2 examines beach rotation within a single coastal embayment, for a unique set of wave conditions, Chapter 3 looks to identify the relevance of the findings on a broader scale. The relationships and responses identified in Chapter 2 may be applicable to similar environments. Expansion of the analysis across a larger spatial domain requires the assimilation of vast third-party data sets (beach topography and modelled wave data). This chapter presents the results of applying the multi-annual methodology used in Chapter 2 (Objectives ii-iii), to the full extent of the south coast of England, assessing wave climate, morphological response and climatic forcing throughout. The specific research objectives of Chapter 3 are to:

i. **Investigate the regional coherence of bi-directional wave climates and relationships with atmospheric indices.**

Using a 36-year hindcast wave record, an assessment of wave climate bi-directionality is made along the entire south coast of England to establish regions where beach rotational response would be expected. The relationships between atmospheric indices and wave climate directionality are made and compared to the Start Bay site-specific analysis as discussed in Chapter 2.

ii. **Identify and quantify regional beach response, in order to examine the extent to which wave bi-directionality controls beach rotation.**

In order to quantify regional beach response, a 10-year coastal monitoring dataset (cross-shore beach profiles) was exploited to develop new parameterisations of beach morphology and relative extents of rotational behaviour. Physical environmental controls of the quantified morphological response were then examined leading to an assessment of the extent to which associated 10-year hindcast wave climate records, and hence wave bi-directionality, explain observed rotational behaviour at relevant sites.

Chapter 4 - Predicting beach rotation using multiple atmospheric indices

Based on the findings of Chapter 3, which investigates the regional value in using bi-directional wave climates to predict beach rotation, Chapter 4 examines the possibility of using climate indices to directly predict bi-directional wave climates and beach rotation, providing a valuable tool to coastal managers.

The research objectives of Chapter 4 are to:

i. **Evaluate the skill of atmospheric indices for predicting beach rotation through multivariate modelling.**

Chapter 3 identifies some localised value in this concept, by correlating beach rotation with winter values of NAO and WEPA at two locations; however, skill was limited due to a short, 10-year data set. Chapter 4 explores this further, returning to Start Bay, as a case study, but expanding the analysis temporally as far back as records allow. Using 38 years of winter station-based SLP derived NAO and WEPA, in addition to contemporary modelled wave data, a stepwise multi-linear regression (SMLR) model wis developed to maximise the predictive capability of climate indices.

The SMLR then hindcasts the novel wave directionality index (WDI) as described in Chapters 2 and 3, with the predicted WDI values compared with modelled wave data derived WDI values. Further validation is conducted against a contemporary rotation index computed from the winter averaged volume change of cross-shore profile surveys (2007 to 2018).

ii. **Validate long-term hindcasts of wave directionality index (WDI) against proxy records of beach rotation.**

To assess whether the SMLR predicted WDI record held any applicable value to real world beach rotation, long-term (centurial) records of winter NAO and WEPA are used to hindcast the WDI back to 1906. Hindcast values are then validated against a qualitative record of beach width (used as a proxy for beach rotation) devised from historical photographs and topographic maps.

iii. **Place the contemporary beach rotational behaviour into a longer-term context of climatic variability.**

Long-term (centurial to millennial) records and proxy reconstructions of the NAO are compared with the predicted WDI and contemporary NAO variability. Contemporary event to centurial scale variability in beach rotation and associated proxies, are put into historical context, providing a unique perspective of the representativeness of observed variability and understanding of the parameter space.

Chapter 5 – Synthesis and conclusions

This section brings together the main findings of Chapters 2, 3 and 4. Some of the key findings are visually summarised, highlighting the mechanisms of beach response and rotation identified throughout the research, in addition to a summary of the final thesis conclusions at the end.

2 Coastal embayment rotation: Response to extreme events and climate control, using full embayment surveys

This chapter contains work published in the following papers:

Wiggins, M., Scott, T., Masselink, G., Russell, P., Castelle, B., Dodet, G., 2017, The role of multi-decadal climate variability in controlling coastal dynamics: re-interpretation of the “Lost Village of Hallsands.”, In Proceedings of Coastal Dynamics, Helsingor, Denmark, 2017, pp. 96–107.

Wiggins, M.; Scott, T.; Masselink, G.; Russell, P.; McCarroll, R.J., 2019, Coastal embayment rotation: Response to extreme events and climate control, using full embayment surveys. Geomorphology, 327, 385–403.

2.1 Introduction

Rotation-dominated embayments in bi-directional wave climates are sensitive to extreme storm events from particular directions. Masselink et al. (2015) and Scott et al. (2016) observed significant south coast rotation following a series of southerly storms (see Section 2.2.2), where wave approach was oblique to the shoreline. The volumetric response was observed in detail at Slapton Sands (Start Bay, South Devon, U.K.), a semi-sheltered, embayed gravel barrier. Critically, Scott et al. (2016) identified that net intertidal volume change was negative between pre and post winter surveys, indicating sediment loss through either cross-shore processes (offshore transport and/or barrier over wash), or between sub-embayments via subaqueous headland bypassing (Ojeda and Guillén, 2008).

The lack of understanding of the fate of observed intertidal sediment losses in the alongshore (Harley et al., 2015; Burvingt et al., 2017), between sub-embayments (Thomas et al., 2010; Goodwin et al., 2013), and on/offshore (Davidson et al., 2013; Poate et al., 2015), limits the understanding of the mechanisms driving spatial and temporal morphological change, specifically beach recovery from extreme wave events (Corbella and Stretch, 2012; Scott et al., 2016; Burvingt et al., 2018). Robust calculations of total sediment budgets are difficult within the coastal zone and often only sub-aerial (e.g. Burvingt et al., 2016), or sub-tidal (e.g. Shaw et al., 2008) beach changes are assessed. The resultant temporal comparisons may lack consideration of uncertainty induced by the survey technique, sampling and interpolation, producing estimates of geomorphic volume change with limited confidence (Williams, 2012). Recent advances in fluvial geomorphology (Wheaton et al., 2010; Milan et al., 2011) have developed approaches to account for uncertainties when estimating volume change with combined survey techniques. In riverine environments, where significant elevation change is of the same order of magnitude as measurement uncertainty, these advances have allowed robust calculations of complete geomorphic volume change with associated uncertainty and significance testing. In the coastal environment, where study sites may be large (on the order of kilometers), with significant regions of limited change (e.g. near the depth of closure), it is important to robustly deal with uncertainty as errors can rapidly propagate to misrepresent large proportions of the observed change. Until now, there has been a distinct lack of full embayment supra- to sub-tidal sediment budget assessments within the coastal environment, due to the lack of coexisting spatial and temporal data sets, and the difficulty/lack of accounting for uncertainty in survey methods (Schimel et al., 2015).

In the longer term, inter-annual variability in the winter-averaged wave climate is strongly affected by atmospheric changes (Bacon and Carter, 1993; Clarke and Rendell,

2009; Dodet et al., 2010; Castelle et al., 2017). Strong relationships exist between phases of climatic indices and variations in wave height and storm characteristics. On a basin-wide scale, Barnard et al. (2015) found that coastal erosion across 48 different Pacific Ocean beaches, was significantly linked with variations in the El Nino Southern Oscillation (ENSO), whilst Mortlock and Goodwin (2016) showed on a regional scale, that different modes of ENSO produced variations in wave power from subtly different directions, causing a discrepancy between erosion and recovery rates within an embayed headland beach in south east Australia.

In the Northern Hemisphere, the North Atlantic Oscillation (NAO), is known to affect the incoming wave climate in the northern latitudes of the Atlantic Ocean (e.g., Dodet et al., 2010), with particularly strong influence during winter months (e.g., Bromirski and Cayan, 2015), explaining multi-annual cross-shore change in exposed sandy beach morphology (nearshore bar configuration) in South West England (Masselink et al., 2014). Longshore rotation of macrotidal, headland embayed sandy beaches has been well correlated to phase changes in the NAO over multiple timescales (Thomas et al., 2010, 2012, 2013), highlighting the possibility of the NAO's use as a predictor of coastline evolution. Castelle et al. (2017) presented a new climate index, the West Europe Pressure Anomaly (WEPA), based on the normalized sea level pressure difference between Ireland and the Canary Islands. Positive WEPA winters better describe increasing winter wave heights and increased southerly storm tracks, whilst exhibiting no significant correlation with NAO itself. Recent improvements in both the forecast skill of winter-averaged NAO (Dunstone et al., 2016), and understanding of its relationship with bi-directional wave climates (and hence beach rotational response), could provide significant advances in coastal management.

The overarching aim of this chapter is to assess and quantify the morphological response of an entire gravel barrier embayment, to episodic and decadal bi-directional

wave forcing. A unique series of directionally contrasting wave conditions in south west England are assessed to investigate the controls on rotational response mechanisms, from the sub embayment to full embayment extent. This chapter exploits a comprehensive morphological dataset collected within Start Bay (South Devon, U.K.), including multi-method full embayment sediment budgets, decadal records of intertidal beach profiles and new interpretations of connections between longer term wave climate and atmospheric variability, to further our understanding of response and recovery mechanisms within these timescales. A future goal is to improve coastal vulnerability assessment and management for coastal embayments that are sensitive to directional wave climates.

2.2 Regional setting study site

2.2.1 Embayment alignment and beach composition

Start Bay is a 12-km long embayment located on the south coast of Devon, U.K. (Figure 2.1). Meso- to macrotidal with neap and spring tidal ranges of 1.8 m and 4.3 m, respectively, the embayment comprises four sub-embayment gravel barrier beaches, named from the south to north as; Hallsands, Beesands, Slapton Sands and Blackpool Sands. Between each sub-embayment lie short headlands/rocky outcrops, extending to approximately 1-4 m below mean low water springs (MLWS), that separate each beach at high tide, trapping laterally moving sediment as it is transported alongshore. Behind the barrier at both Slapton Sands and Beesands, freshwater is held above mean sea level in two lagoons known as Slapton Ley and Widdecombe Ley (Austin et al., 2013). The gravel barrier at Slapton Sands rises to 5–6 m above mean sea level with a steep reflective beachface ($\tan\beta = 0.1$) composed of fine gravel (D_{50} = 2–10 mm), with the toe of the barrier extending to an average depth of -7.5 m Ordnance Datum Newlyn (ODN) (Kelland, 1975). The barrier position has remained relatively stable over the last 3000

years, allowing the sediment (mainly flint) to be reworked by the sea (Hails, 1975b). Within Start Bay, gravel is finer to the east due to the lateral grading of material (Chadwick et al., 2005), with coarser grains transported south west with larger, steeper easterly waves, and finer grains being well sorted and transported north east with smaller but more frequent southerly swells (Morey, 1976).

South of the bay lies Start Point, a rocky headland offering shelter from longer period southerly waves. Skerries Bank, an offshore banner bank, sits east of the main beaches in the southern half of the embayment and is -5 m (ODN) at its shoalest (Hails, 1975a). These two features modulate the wave climate in Start Bay. Refraction and dissipation of large southerly waves around Start Point allows waves to reach the southern sub-embayments of Hallsands and Beesands, however wave energy is reduced, resulting in an alongshore gradient in inshore wave conditions, with significant wave heights (H_s) increasing from the south to north along the embayment (Ruiz de Alegria-Arzaburu and Masselink, 2010).

Maximum water depth between the gravel barrier and the shallowest part of the Skerries Bank is -15 m ODN, deeper than the estimated depth of closure (-10m ODN). This fact, combined with the distinct difference in sediment type between the four gravel barriers and the finer shelly sands of Skerries Bank, suggests there is no movement of sediment between the two (Hails, 1975a). Furthermore, the entirety of Start Bay is bound by large headlands, and the system is considered a closed sediment cell, with no sediment sources except for some confined areas of cliff erosion (Ruiz de Alegria-Arzaburu and Masselink, 2010).

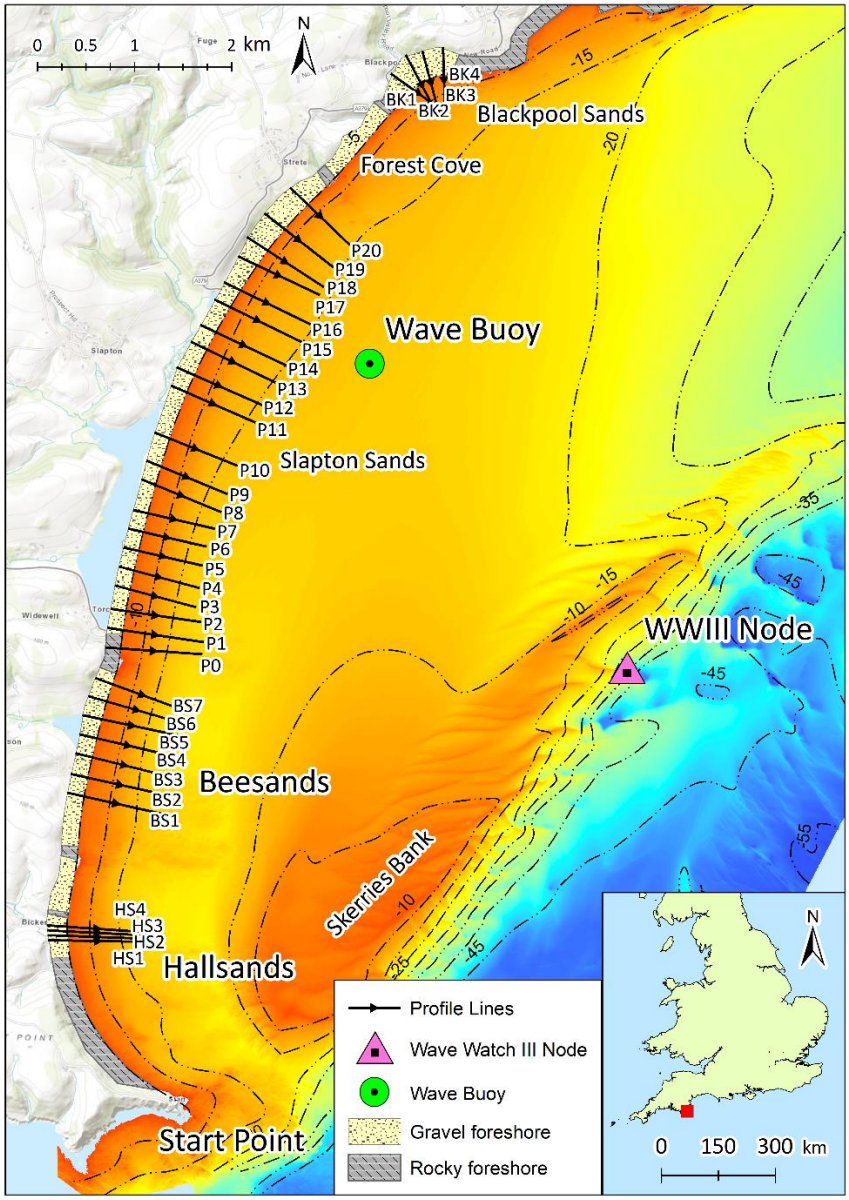

Figure 2.1. Location map showing Start Bay, South Devon, U.K. Nearshore bathymetry from 2013 (UKHO, http://aws2.caris.com/ukho/) and associated contours (m, ODN), highlight the location of Skerries Bank. Survey profile locations for each beach are shown as arrows pointing offshore and are labelled accordingly. The foreshore is identified as either gravel or rock, and the location of the Directional Wave Rider Buoy (http://southwest.coastalmonitoring.org/), and the WaveWatchIII Model Node is shown to the east of Slapton Sands.

2.2.2 Wave climate

The local inshore wave climate has been measured since April 2007 by a Wave Rider Directional Wave buoy, located in the centre of the embayment (Figure 2.1) at approximately 12 m ODN water depth sampling at 30-min intervals (Plymouth Coastal

Observatory, 2017). In addition to the measured data, the U.K. Met Office have provided long-term 3-hourly hindcast wave data from their 8-km WaveWatchIII (WW3) model, between 1980 and 2017 for a node location offshore of Start Bay, in approximately 20 m water depth (Figure 2.1).

The bay is aligned SSW-NNE and receives predominantly short period (mean annual Te ~5-6 s) wind driven waves from both the south and east (Ruiz de Alegria-Arzaburu and Masselink, 2010). The long-term wave rose (U.K. Met Office hindcast) clearly shows the bi-directionality of the waves within the embayment, with a dominance of south-westerly over easterly waves (Figure 2.2, bottom panel). At the model node location, south-westerly waves are propagating in the offshore direction (from the south west); however, they are refracted and attenuated towards the shoreline by interaction with Skerries Bank (Figure 2.1). Previous studies (Ruiz de Alegria-Arzaburu and Masselink, 2010; Wiggins et al., 2017) have shown, through comparison with directional wave buoy records, that the dominant south-westerly waves rotate to a southerly direction at the nearshore (-12 m ODN) and easterly waves maintain their original angle. Despite nearshore transformation, the long-term offshore model hindcast record is used here for further analysis as the wave buoy data represented a relatively short time series and contained storm dropouts. Later analysis highlights the value of the longer-term offshore wave data.

The time-series of hindcast H_s (Figure 2.2, top panel) shows a seasonal trend with wave heights increasing in winter (H_s = 1 – 1.3 m) and decreasing in summer (H_s = 0.5 – 0.6 m). Storm events are classified as having peak H_s exceeding 2.17 m ($H_{s5\%}$ calculated over the entire modelled wave record), with a duration of at least 6 hours and separated by at least 24 hours (Harley, 2017).

Since 1980, southerly waves (> 110° and < 240°) make up 69% of wintertime (December, January, February and March, DJFM) wave directions (Figure 2.2, second panel), with a mean H_s of 1.23 m. Easterly waves (angles >60° and <110°) make up 23% of the wave directions for winter months, with average H_s of 1.15 m across the model record. High-energy southerly winter storm events are more frequent than those from the east from year to year, with a 5:1 ratio per winter; however, each year is highly variable and there are periods of dominance of storms from one direction or another.

During the winter of 2013/14, the south west of England experienced numerous, exceptionally high-energy Atlantic storms, producing the largest recorded 8-week average wave height in at least 60 years, considered the most energetic since at least 1948 (Masselink et al., 2016) with 22 storms (H_s > 5.9 m) between October 2013 and April 2014 recorded at the Seven Stones Light Vessel (50.102˚ N 6.100˚ W) (Masselink et al., 2015). The modelled wave data shows 15 winter storm events at the Start Bay node, characterized by a series of southerly storms with minimal input from easterlies (Figure 2.2, third panel). 84% of winter waves were southerly for this period, with average winter H_s of 1.65 m, with only 10 % from the east with mean wave heights of 0.70 m (Figure 2.2, Second Panel). Locally, the most destructive storms within Start Bay occurred on the 04/02/2014 and the 14/02/2014 with H_s recorded at the inshore wave buoy reaching 4.69 m and 5.25 m, respectively. Compared to similar magnitude storms in this period, both incoming storms tracks from the Atlantic were south of 50° latitude and resulted in larger waves reaching the south coast of the U.K. As a result, these two storms were calculated as having wave height return periods greater than 50 years (Siggery and Wiggins, 2014) and caused the most extensive impacts on the beaches of Start Bay (Burvingt et al., 2016; Scott et al., 2016).

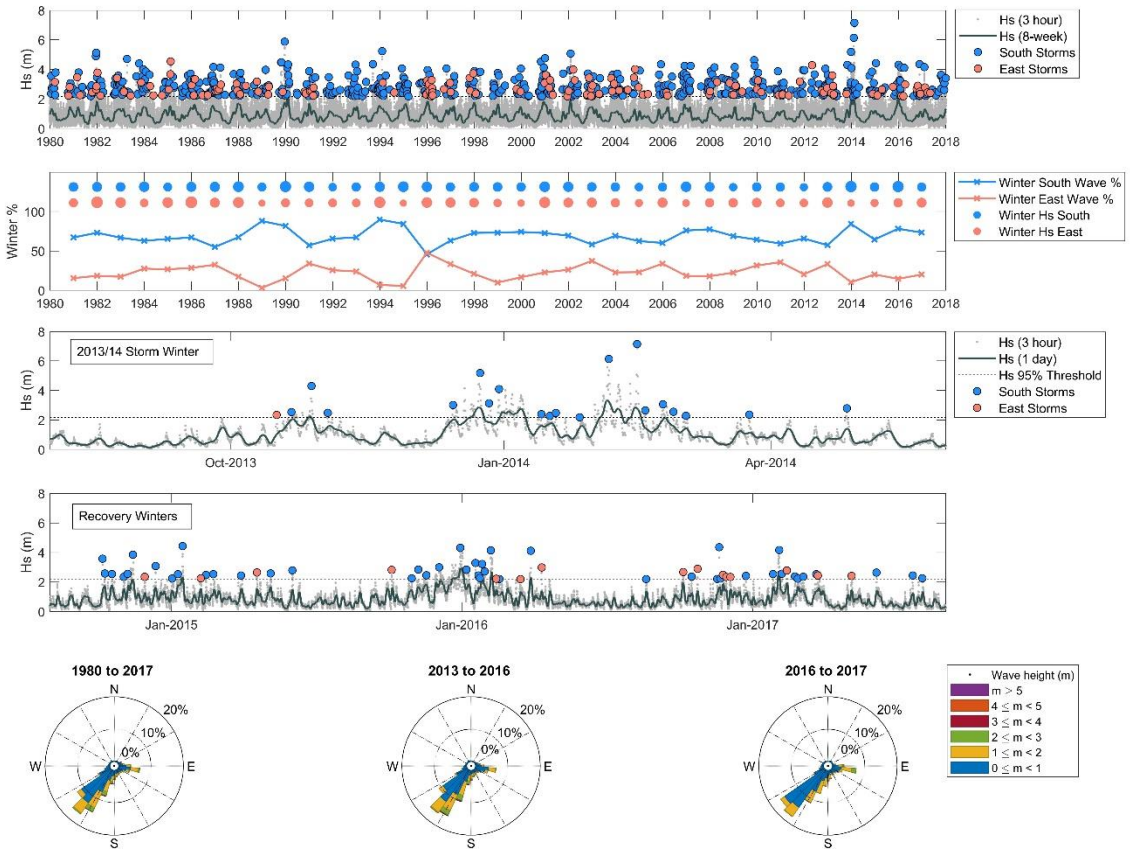

Figure 2.2. Top Panel; Met Office WaveWatchIII modeled hindcast data showing significant wave heights every 3 hours (grey dots) and 8-week moving average (grey line) from 1980 to 2017. Associated storm events (Waves greater than $H_{s5\%}$ = 2.17 m) from both the south and east are shown by the blue and red circles respectively. Second Panel; Total winter percentages of southerly (blue) and easterly (red) wave contributions, with average wave heights for each shown by the circle size in the upper section of the panel. Third Panel; Significant wave heights of the exceptionally stormy winter of 2013/14 with a one day moving average (grey line), showing the lack of easterly storm events. Fourth Panel; Significant wave heights of the three most recent winters, with associated storm peaks highlighting the increased easterly storms of the winter of 2016/17. Bottom Panel; Wave roses from the full time series (left), 2013 to 2016 (middle) and 2016 to 2017 (right).

In the 3-year period following the winter of 2013/14, the first two winters maintained a dominance of southerly over easterly waves with the winter of 2014/15, being 65% southerly and 20% easterly in direction with average H_s of 1.14 m and 0.84 m, respectively. Further southerly waves were experienced in the winter of 2015/16, with 78% southerly waves (average H_s of 1.62 m) and only 15% easterly (average H_s of 1.12

m). A reversal in the trend occurred between 2016 to 2017, with 11 easterly storms observed between October 2016 and May 2017. Average winter values for that season show southerly waves make up 73% of wave contributions, with 20% coming from the east. Mean southerly wave heights drop to 1.06 m for that year (the lowest value for 5 years), and easterly winter waves increase to an average 1.24 m (the highest value since 2012/13).

For the purpose of the following morphological response analysis, the southerly-dominated period between 2013 and 2016, which includes the unprecedented storms of 2013/14 is considered a 'southerly' period. The significant change to easterly wave conditions from 2016-2017 can be considered an associated 'easterly' period, and as such, both 'southerly' and 'easterly' periods, and their effects on embayment morphology are assessed further in this chapter.

2.3 Data and methods

2.3.1 Full embayment sediment budgets

In order to calculate total sediment budgets and morphological change in a coastal embayment, it is essential to combine topographic and bathymetric survey data from different time periods. Consideration must be given to the survey instrumentation and data collection techniques, as well as the inherent uncertainty in both point cloud and gridded position and elevation (Wheaton et al., 2010). Described below are the morphological data sets used for the full embayment response analysis, as well as the approaches to gridding and addressing uncertainty.

2.3.2 Unmanned aerial vehicle (UAV) intertidal surveys

A quadcopter UAV (DJI Phantom), as seen in Figure 2.3, facilitated a full inter/supra-tidal survey of Start Bay in both 2016 and 2017. Implementing a structure-from-motion

(SfM) approach (Westoby et al., 2012), overlapping aerial photographs were aligned and georeferenced using Real Time Kinematic (RTK) Global Positioning System (GPS) measured ground control points (GCP), deriving a high-resolution (> 50 pts/m^2), three-dimensional point cloud, which was then interpolated to a 1 m grid digital elevation model (DEM) of inter/supra-tidal beach topography. This methodology allowed full coverage of the beaches and interconnecting bays around a single set of spring tides, without significant event driven changes occurring during the data collection.

Figure 2.3. DJI Phantom Quad Copter, used throughout the study for sub-aerial surveys of Start Bay.

2.3.3 Multibeam bathymetry

Extending the spatial coverage of the embayment surveys into the sub-tidal domain, multibeam bathymetry was used from a range of sources. United Kingdom Hydrographic Office (UKHO) supplied multibeam data collected during January 2013 (UKHO, 2013), whilst Plymouth University (PU) conducted two separate surveys in June 2016 and June 2017 using the universities research vessel, RV Falcon Spirit (Figure 2.4). These data sets were surveyed at high resolutions (typically, 25 pts/m^2

point density) and exported at 1 m, providing comparable DEM's from approximately Chart Datum to below the depth of closure (< -10 m ODN).

Figure 2.4. The university of Plymouth research vessel, RV Falcon Spirit, conducting a multi-beam bathymetric survey of Start Bay in June 2016, capturing data as close as possible to the intertidal shore face. Copyright Mark Wiggins (2016).

2.3.4 Light Detection and Ranging (LiDAR)

Environment Agency U.K. LiDAR data is captured as part of the ongoing south west regional coastal monitoring programme (http://southwest.coastalmonitoring.org/). Datasets over Start Bay were collected during March 2012, March 2016 and April 2017, using the Environment Agency ALTM ORION SN14SEN342 LiDAR instruments, mounted on aerial survey platforms. Swath width for surveys are quoted at 850 m, with beam divergence of 0.25 mrad and a laser footprint of 0.22 m. Data is supplied in a 1 m raster grid format, and an assessment of the measurement uncertainty has been conducted by the contractor and a reported value is supplied as part of the deliverables.

2.3.5 Real Time Kinematic (RTK) Global Positioning System (GPS) surveys

RTK-GPS continuous data was surveyed on foot at 1 Hz and covers the intertidal extent of Start Bay in areas where the UAV was unable to be utilized (due to permissions). Individual surveyors (Figure 2.5) walked at 5 m spaced alongshore lines, with attention paid to capturing changes in topography and breaks in slopes (berms, crests etc.). This method was utilized for the 2013 epoch, and in some instances 2016 and 2017 to provide complete coverage of the embayment in areas where UAV surveying was not possible due to permissions or safe flying protocol.

Figure 2.5. Surveyor with RTK-GPS survey pole conducting a 3D walking survey in Start Bay.

2.3.6 Full embayment Digital Elevation Models (DEM's)

The full supra/intertidal and sub-tidal extents of Start Bay were surveyed using the above multiple methods over three epochs, providing 'pre-southerly' (2013), 'post-southerly' (2016) and 'easterly' (2017) morphological datasets. The spatio-temporal coverage of data sets meant that multiple surveys could be combined (Figure 2.6)

producing DEMs spanning supra, inter and sub-tidal extents of the entire embayment to an average depth of < -10 m ODN (Figure 2.7).

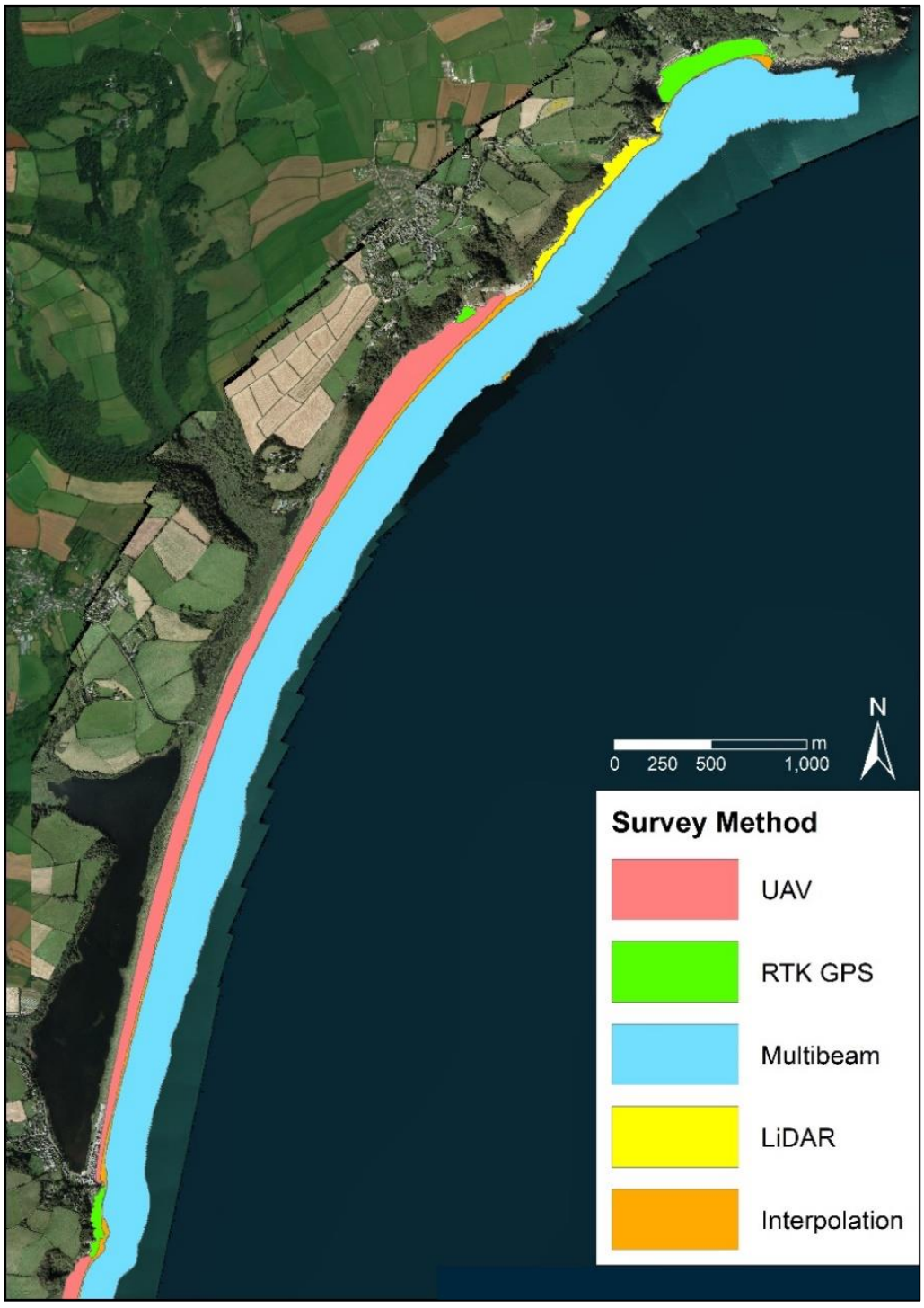

Figure 2.6. Example of multimethod survey masks for the northern section of the combined morphological surveys from 2016. Each colour represents the respective spatial extent covered by the individual survey techniques.

The datasets used in this analysis and their temporal structure are summarized in Table 1. In all cases data were interpolated to a 1 m raster DEM using a natural neighbour interpolation (Sibson, 1981), which utilizes a weighted average of neighbouring points based on their respective areal contribution. It is effective in processing a high number of irregularly spaced input points and has been shown to well represent surfaces interpolated from LiDAR point data (Bater and Coops, 2009).

Table 2.1. Temporal survey method chart highlighting the morphological survey methods used within each epoch of DEM analysis.

	Year					
Morphological Survey	**2012**	**2013**	**2014**	**2015**	**2016**	**2017**
UAV Intertidal (DEM 1 m)					**Jun**	**Apr**
Multibeam Bathymetry (DEM 1 m)		**Jan**			**Jul**	**Jun**
LiDAR (DEM 1 m)	**Mar**				**Mar**	**Apr**
RTK GPS Continuous (DEM 1 m)	**Jul**	**Aug**			**Jun**	**Apr**

Partial coverage

Full coverage

2013 Epoch

2016 Epoch

2017 Epoch

While the ‘pre-southerly’ DEM comprised datasets that spanned 10 months, it was deemed appropriate in capturing the changes caused by the 2013/14 winter after assessment of a decadal, intertidal 2D morphological dataset from Start Bay, showing the significance of the event (see Section 4.3).

2.3.7 Quantifying full embayment geomorphic change

The basic principle of measuring geomorphic change involves the subtraction of two independent DEM surfaces to produce a DEM of Difference (DoD, Wheaton et al.,

2010), with each grid cell value representing a measure of the vertical elevation difference. Individual cells can then be integrated to estimate total volume changes within the spatial extent of the DoD. A key principle when utilizing DoD's for the purpose of geomorphic change detection, is accounting for the vertical uncertainty across each DEM, and therefore an ability to discern the probability that the observed change is real (and not due to measurement or sampling error). This is particular important when attempting to detect small vertical changes (with respect to uncertainty) over broad spatial extents (Wheaton et al., 2010).

Each individual dataset has its own inherent uncertainty, based on a combination of instrument, measurement (sampling), systematic and interpolation errors. In the case of morphological surveys, variables such as the underlying surface roughness, dynamic gradients of slope, and variability in environmental conditions all contribute to the potential uncertainty of any given surface (Wheaton, 2008). Within this study, estimates of uncertainty (δz_{DEM}) for each survey technique were obtained (through the use of a reference survey experiment (Section 2.3.8), and applied to respective regions of the DEM (Figure 2.6).

Table 2.2. Summary of survey method, uncertainty type, calculated value and the source of analysis.

Survey Type	**Uniform or Variable**	**Calculated Uncertainty (σ)**	**Source of analysis**
RTK – GPS Topographic continuous	Uniform	0.054 m	Reference surface comparison
UAV structure from motion	Uniform	0.038 m	Reference surface comparison
Airborne LiDAR (2012/2017)	Uniform	0.150 m	GPS ground truth
Multibeam Bathymetry 2013	Fixed	0.270 m	IHO Order 1a specification
Multibeam Bathymetry 2016	Variable	0.08 - 1.830 m	Spatially variable CUBE surface
Multibeam Bathymetry 2017	Variable	0.03 - 0.158 m	Spatially variable CUBE surface

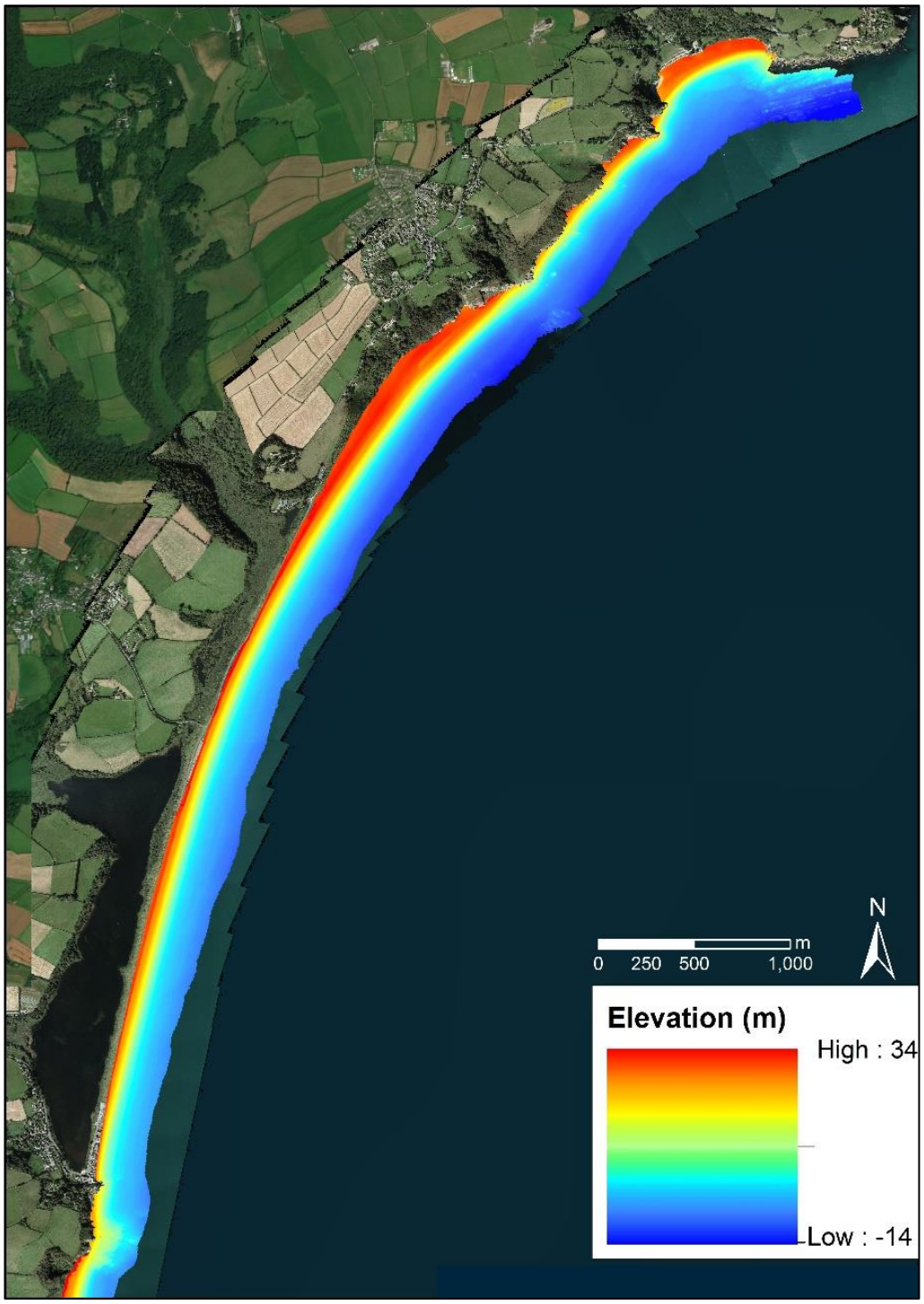

Figure 2.7. Example sub-section of the resultant DEM produced from a combination of survey methods.

These uncertainty estimates can then be propagated into the DoD using standard independent error propagation (Brasington et al., 2000) with the resultant propagated uncertainty (δU_{DoD}) defined as a minimum level of detection (minLoD);

$$minLoD = \delta U_{DoD} = \sqrt{(\delta z_{DEM1})^2 + (\delta z_{DEM2}{}^2)} \quad \text{Eq. (1)}$$

where δz_{DEM1} and δz_{DEM2} are some metric of uncertainty from the first and second DEM respectively (Taylor, 1997). Changes measured below this minLoD are thresholded from the DoD and excluded from the total calculated change. This can be done on a cell-by-cell basis if DEM uncertainties are spatially variable.

A further conservative step can be taken when thresholding the DoD's, incorporating a probabilistic approach to assess whether the observed change is real, as set out by Lane et al. (2003). If the estimates of DEM uncertainty (δz_{DEM}) are approximated as their standard deviation of error (σ_{DEM}), and are represented by a normal distribution, a critical threshold error (U_{crit}) can be obtained using;

$$U_{crit} = t\sqrt{(\sigma_{DEM1})^2 + (\sigma_{DEM2}{}^2)} \quad \text{Eq. (2)}$$

where σ_{DEM1} and σ_{DEM2} are the standard deviations of error for the first and second DEM respectively, and t is the critical t-value for a two tailed students t-test at a chosen confidence interval (Williams, 2012). By utilizing the propagated error of the DoD on a cell by cell basis, a t score can be derived from the actual change observed such that;

$$t = \frac{|Z_{DEM_2} - Z_{DEM_1}|}{\sigma_{DoD}} \quad \text{Eq. (3)}$$

where σ_{DoD} is equal to δU_{DoD} evaluated at each cell of the DoD grid, and Z_{DEM_1} and Z_{DEM_2} are elevations from two different DEMs. The resultant t value can be related to the probability of the elevation difference occurring due to measurement error alone by utilizing the cumulative distribution function for the two tailed t test. Assuming a large number of samples is used to estimate σ_{DoD}, the t distribution is nearly identical to the normal distribution (Wheaton, 2008), such that if $t \geq 1$, the change is significant at the 68% confidence interval (1 σ).

2.3.8 Reference survey assessments

To apply a spatially variable limits of detection thresholding technique to the geomorphic change detection, an estimate of the uncertainty (δz_{DEM}) is required for each survey method and subsequent DEM. Various approaches can be taken, ranging from simple instrument accuracy values quoted by manufacturers, to full investigations into the error budget of a single survey (Lichti and Gordon, 2004). In this study, independent analysis was conducted to obtain reasonable uncertainty values that can be applied to the various survey methods used for each DEM. In each case, the uncertainty estimate represents the total combined integration of all individual sources of error including instrument, measurement, systematic and interpolation, and is therefore site-specific.

2.3.8.1 Sub-aerial uncertainty

To quantify uncertainty estimates for both the UAV and RTK-GPS continuous data, a reference surface was produced for comparison with each survey method. A typical stretch of the embayment was surveyed using a Leica terrestrial laser scanner (TLS), with reference targets measured with a total station, tied into a local network of high-quality Environment Agency Control Stations (EACS), surveyed in to E1 grade (> 8 hours). This allows the total combination of all sources of uncertainty to be incorporated, using the same sampling methods employed during data collection. The resultant laser scan (Figure 2.8) was used as a reference point cloud (>100 pts/m^2), with vertical errors relative to the control network, below one centimetre (RMSE = 0.005 m).

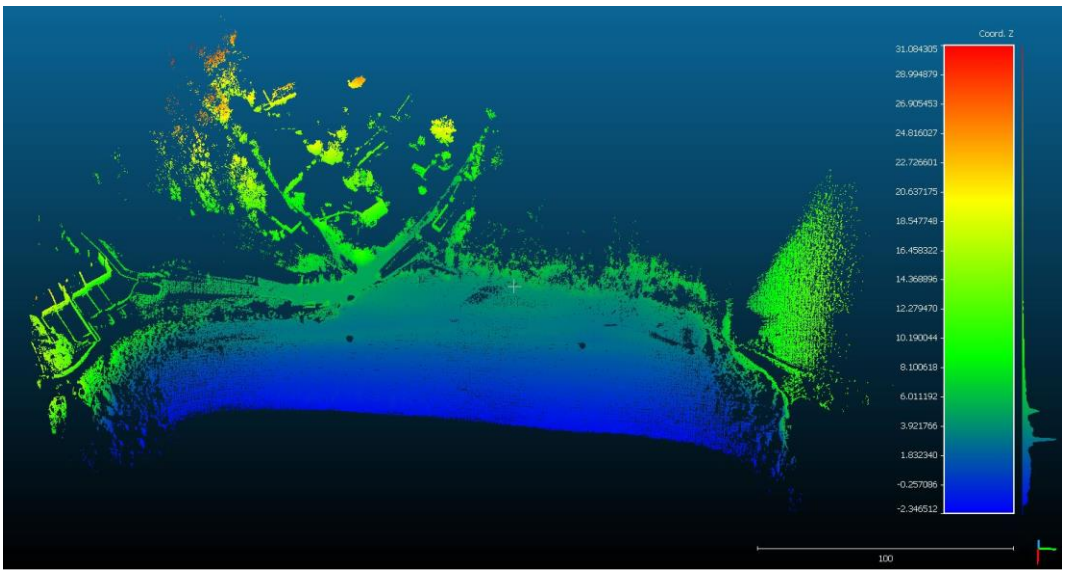

Figure 2.8. Reference survey point cloud created from a terrestrial laser scan, referenced to total station control points.

A UAV survey was conducted simultaneously, using ground control points surveyed using RTK GPS (RMSE < 0.030 m). In addition, a surveyor conducted a continuous topographic survey (Figure 2.9) on the same stretch of beach, walking with an RTK-GPS rover measuring position and elevation data at 1 Hz.

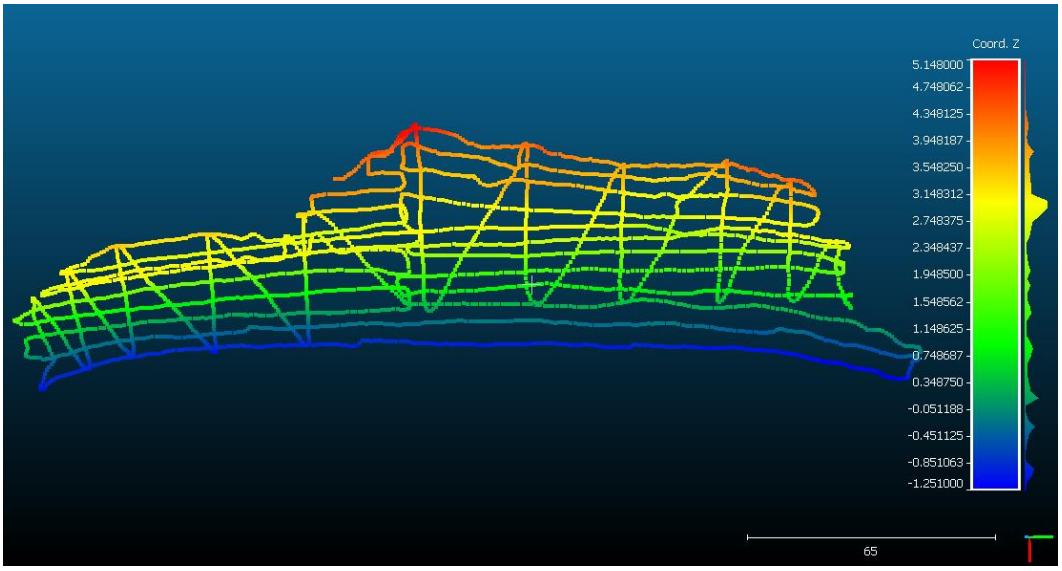

Figure 2.9. Point cloud derived from an RTK-GPS walking survey over the same reference surface as the terrestrial laser scan survey.

The reference survey surfaces were interpolated to a 1 m grid, using the same technique as applied to the final multimethod DEM's. Each respective raster was subtracted from

the laser scan surface providing a direct measure of uncertainty and results are summarized and presented in Figure 2.10 and Table 2.3.

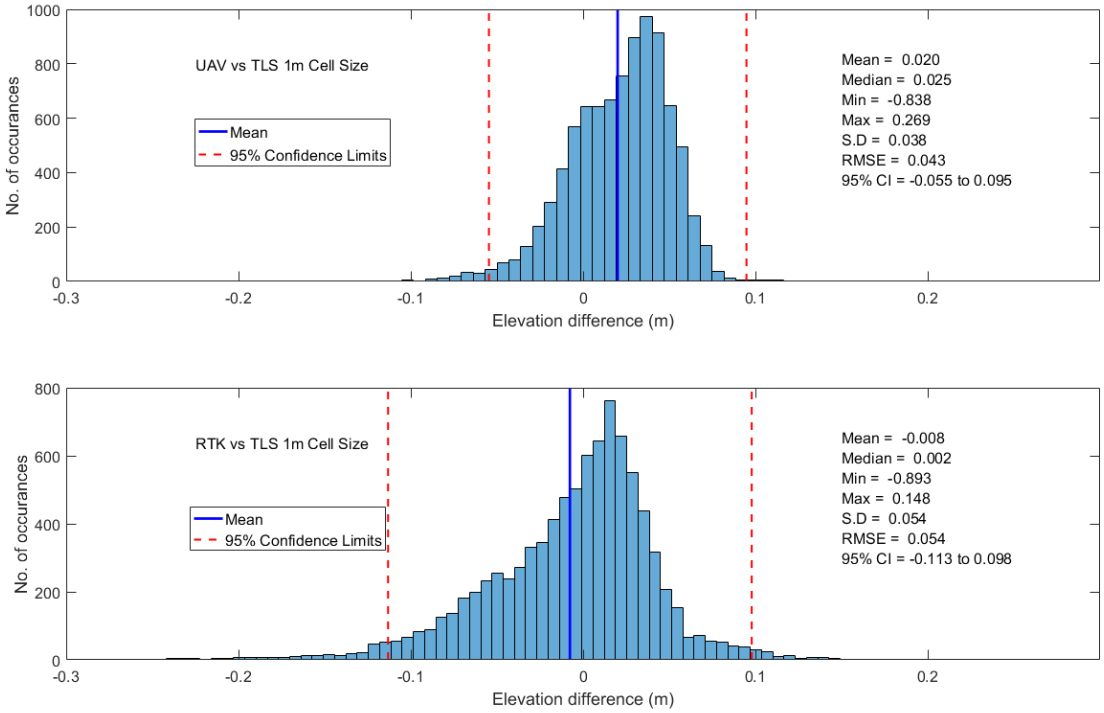

Figure 2.10. Upper; histogram of elevation differences between 1m DEM created from TLS reference survey, and DEM from UAV survey. Lower; Histogram of elevation differences between 1m DEM created from TLS reference survey, and 1m DEM from RTK GPS walking survey.

In all cases, third-party processed LiDAR point data passed ground truth comparisons with RTK-GPS data points on immovable objects, and results quote a vertical accuracy within 1σ of 0.150 m. LiDAR data has been used from 2012 and 2016 where there are no other sources of topographic data. In other instances, where notable change has occurred, for example at the back of the active beach, LiDAR has been used in combination with other data sources to extend the spatial extent of individual DEMs.

Table 2.3. Comparison of UAV and RTK GPS surveys against a laser scan reference survey. Statistics are presented for the raster to raster comparison.

Comparison with laser scan reference	**Raster to Raster 1m cell Z differences (m)**							
	Mean		**Median**		**S.D**		**RMSE**	
	Vector	Absolute	Vector	Absolute	Vector	Absolute	Vector	Absolute
UAV	0.020	0.031	0.025	0.029	0.038	0.030	0.043	0.043
RTK GPS	-0.008	0.037	-0.002	0.027	0.054	0.040	0.054	0.054

2.3.8.2 Sub-tidal uncertainty

An alternate methodology was needed to address the uncertainty within the multibeam surveys, as it was not possible to obtain an absolute sub-tidal reference control surface. A combined statistical and error budget modelling approach was taken based on *a priori* estimates of uncertainty of system components, computed in QPS QIMSy/Qimera survey acquisition software, to generate total propagated uncertainty (TPU) values for each individual sounding. These were then gridded across the multibeam survey region using the Combined Uncertainty and Bathymetric Estimator (CUBE) algorithm, which provides a statistically robust method for generating spatially variable residual uncertainty surfaces (Calder and Mayer, 2003; Calder and Wells, 2007; Schimel et al., 2015). The range of uncertainty values for the 2016 and 2017 data are given in

Table 2.4, with the highest values occurring over high roughness regions (rock reefs) and at swathe edges, and lowest values over flatter sandy regions directly beneath the sonar. As no TPU values were available for the 2013 survey (secondary dataset) a conservative estimate based on the known survey specification (International Hydrographic Organization Order 1a; IHO, 2008) was used, providing a spatially

uniform uncertainty value (1 standard deviation from the mean (σ) quoted as ± 0.270 m).

To address the lack of an absolute control surface to assess influence of systematic error between the surveys, a reference surface analysis was conducted across a flat immobile rocky seabed region 50 m x 50 m and at -14 m ODN depth. The roughness length scale of the selected region was an order of magnitude less than the width of the control region to minimize incorporation of significant vertical errors due to any horizontal misalignment. To minimize random error orthogonal lines were run and only data from beam angles between ±45 degrees were used to compute the mean elevation differences from 0.5 m gridded surfaces for each survey. Due to the lack of immobile reference region options, no other areas could be compared so it is unknown if these error values are variable across the domain. Therefore, based on this analysis and using 2017 survey as a reference (utilized GNSS Post Processed Kinematic heighting), appropriate fixed vertical offsets (representing systematic errors) were applied during volume change calculations.

Table 2.4. Elevation difference statistic for reference region (0.5-m gridded).

Survey	Start Bay 2017 - 2016	Start Bay 2017 - 2013
Area	50m x 50m (-14 m ODN)	50m x 50m (-14 m ODN)
S.D	0.07 m	0.08 m
Mean	-0.05 m	-0.20 m
Median	-0.06 m	-0.19 m
RMSE	0.07 m	0.22

2.3.9 Decadal morphology and wave climate assessment

A decadal record of quasi-quarterly RTK-GPS topographic cross-shore profiles have been collected regularly throughout Start Bay since 2007, as part of an ongoing coastal monitoring program (http://southwest.coastalmonitoring.org/). Hallsands, Beesands and Slapton Sands are surveyed three times per year on average (Spring, Summer and Autumn), whilst Blackpool Sands is surveyed twice a year (Spring and Autumn). Profile locations are shown on the map in Figure 2.1, with an average line spacing of 50 m at Hallsands and 200 m at Beesands, Slapton Sands and Blackpool Sands. Measurements are made from the back beach to mean low water springs (-2 m ODN), with a maximum distance of 5 m between successive points, and additional points are taken to capture all breaks in slope to accurately represent the beach morphology. Unit volume differences relative to the first survey were then calculated for each profile.

To explore direct relationships between bi-directionally wave forcing and morphological change, the wave energy flux equations were used to compute the total wave power, P for the WaveWatchIII modelled time series for the location of the model node (Figure 2.1), using;

$$P = \frac{1}{16}\rho g H_s^2 C_g \qquad \text{Eq. (4)}$$

where ρ = water density, g = gravity, H_s = the significant wave height and C_g = the wave celerity based on the wave energy period T_e and local water depth h, using linear wave theory for intermediate depths.

Wave power was then split into components of southerly (240°> and >115°), and easterly (<60° and <115°) directions, and the total of each directional bin was time integrated over the winter period of December to March for each year. An index of the normalized balance of the two contributions was obtained by equation 5;

$$\mathrm{WDI} = \frac{(P_{south} - P_{east}) - \overline{(P_{south} - P_{east})}}{\sigma(P_{south} - P_{east})} \quad \text{Eq. (5)}$$

where $(P_{south} - P_{east})$ is the difference between the southerly and easterly wave power, $\overline{(P_{south} - P_{east})}$ is the long-term average of those winter differences, and $\sigma(P_{south} - P_{east})$ is the long-term standard deviation of winter differences, calculated over the entire model record from 1980 to 2017.

This index, hereinafter referred to as the wave power directionality index (WDI), was calculated for each time interval between successive morphological surveys at each profile. The WDI index can be described as a normalised disequilibrium parameter, describing the deviation in wave power directional balance in relation to the mean conditions. Positive and negative values of the WDI represent the dominance of southerly and easterly waves respectively, in comparison to the long-term mean. The index was then plotted against the measured volume changes between morphological surveys, and linear correlation coefficients were obtained for the relationship between the two. This correlation was further split from total correlations (using the entire record), into winter correlations (using only volume changes and wave power indexes observed during winter months (December to March).

2.3.10 Climatic indices and wave variability

The influence of climate indices on waves in the North Atlantic is stronger in the winter months due to the increased occurrence of storm events; hence, in this chapter, and throughout the thesis, a normalized winter-averaged (DJFM) value of the station-based NAO index is utilized (Hurrell, 2018). Further to the NAO, winter-averaged values of WEPA (Castelle et al., 2017) are presented as an additional climate index, and both are assessed against with the long-term winter modelled wave record.

2.4 Results

2.4.1 Multi-annual southerly and easterly full embayment response

Computed significant morphological change across the southerly period (2013-2016) indicated strong northward transport of sediment within the embayment as a whole, and within individual sub-embayments, manifesting in a pronounced clockwise rotational response (Figure 2.11, left). Significant sub-aerial erosion was recorded at the southern end of sub-embayment beaches, whilst accretion was observed at the northern ends with material collecting at rocky headlands.

The net change across the whole embayment is highlighted in Figure 2.12 (top) and shows the balance of erosion and accretion. Overall, a total thresholded volume of 641,900 m^3 of erosion was observed, with a thresholded deposition of 593,300 m^3. A net volume thresholded change of -48,600 m^3 was observed, which falls within the propagated uncertainty of the analysis (+- 91,300m^3) and is therefore not significant at the 95% confidence limit. As a result, the system has to be observed as closed, with no significant detectable net loss or gain of sediment through either barrier over wash, offshore transport or longshore flux beyond the extreme southern or northern extents of the embayment.

During the easterly phase (2016-2017) the geomorphic change analysis highlights a reversal in the rotational response of Start Bay (Figure 2.11, right). Erosion is observed at the northern ends of all sub-embayments, with an associated accretion observed at the southern ends. The strongest areas of erosion occurred at the northern end of Slapton Sands and Forest Cove. The thresholded DoD analysis (Figure 2.12, bottom) shows the full embayment experienced a total erosion of 289,700 m^3 whilst gaining 241,500 m^3. The net change equates to -48,200 m^3, which, like the 2013 to 2016 analysis, is within the associated uncertainty of the analysis (+-61,900 m^3), suggesting that there has again

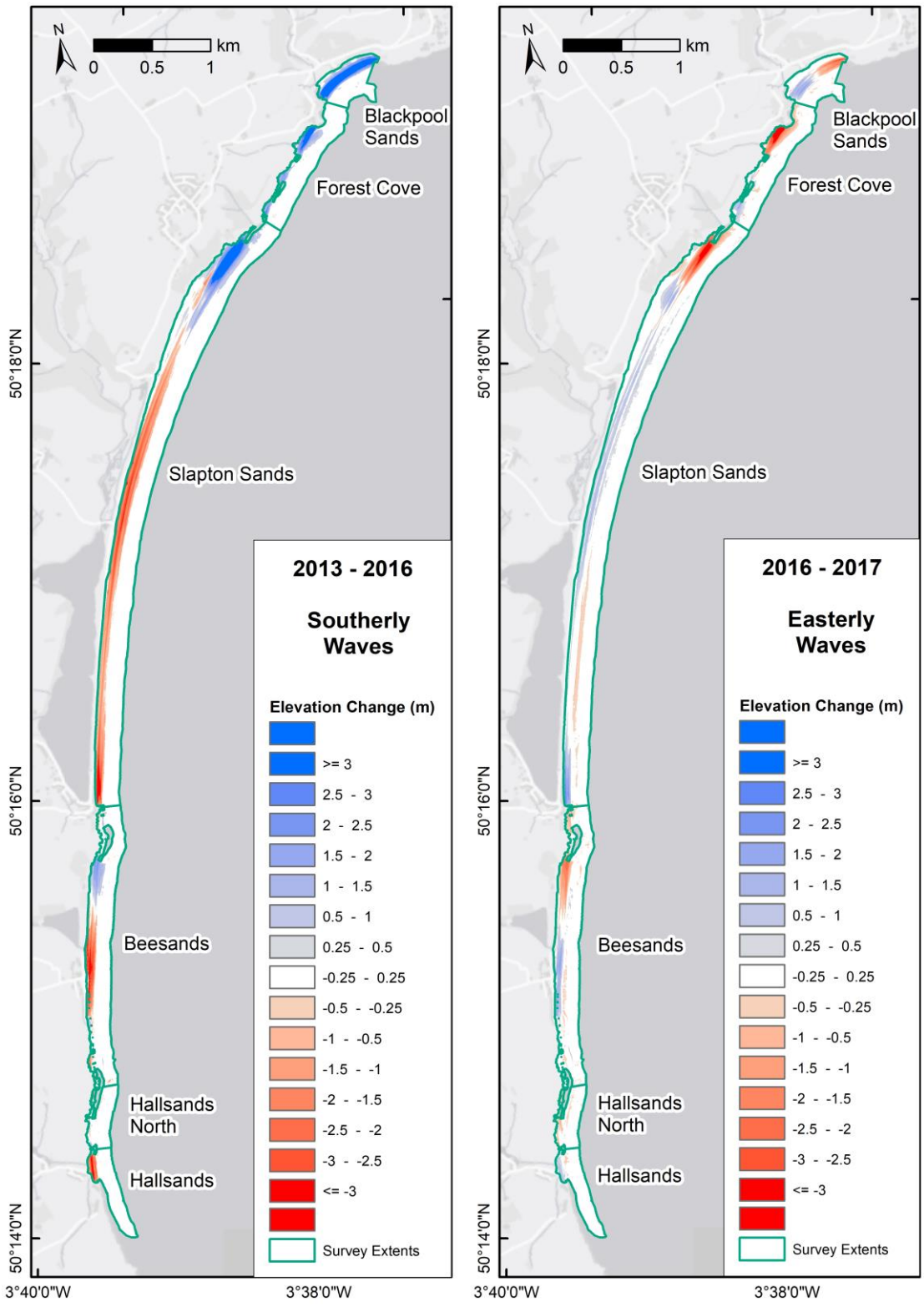

Figure 2.11. Thresholded DoD's for the southerly period between 2013 to 2016 (Left) and easterly period between 2016 to 2017 (Right). Elevation changes between epochs are represented as colour intensity from red (erosion) to blue (accretion), with no detectable change represented as a lack of colour.

been no detectable net loss or gain of material within the embayment. A distinct pivot point for the full embayment is observed across both epochs at the northern end of Slapton Sands, around the location of P18 (Figure 2.1), where erosion and accretion are clearly delineated. The total volume changes past this point were calculated for both epochs, with 529,500 m^3 (± 54,500 m^3) transported north of this point between 2013 and 2016, and only 139,218 m^3 (± 24,630 m^3) passing southward of this point between 2016 and 2017.

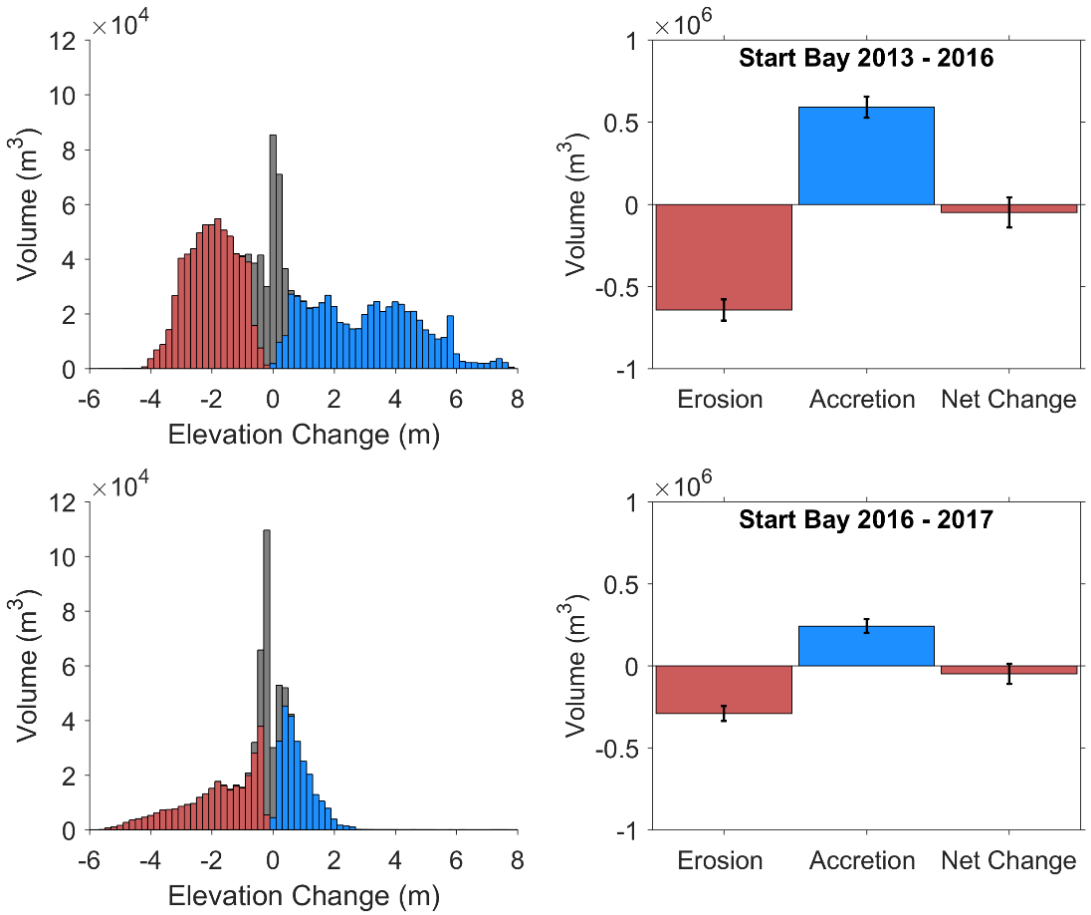

Figure 2.12. Thresholded volume change within Start Bay between during the southerly period of 2013 and 2016 (top panel), and easterly period between 2016 to 2017 (bottom panel). Volume elevation changes are expressed in terms of erosion (red) and accretion (blue) (Left Panels). Grey bars represent volume change in which elevation differences were below the LoD , and hence were thresholded from the total volume calculation. Total and net volume changes within the embayment (Right Panels), expressed in terms of erosion (red) and accretion (blue). The black error bars represent the propagated volume uncertainty at the 95% confidence interval associated with the result.

Comparisons of the two epochs show that total detectable volume change measured from 2016 to 2017 is 45% of 2013 to 2016, however; this anti-clockwise rotation occurred within a single annual cycle, spanning a winter period containing a higher percentage of easterly waves than the previous two (Figure 2.2, Bottom Right), highlighting the importance of wave direction in controlling beach morphology.

2.4.2 Sub-embayment morphological response

Dividing the full embayment into individual sub-embayments (Figure 2.11, green boundaries), definitive erosional and accretional responses are observed across the measured time periods. Sub-embayments were defined as beach sections between clear protrusions of rock headlands, or where clear interfaces were observed in the rotational response. The spatial redistribution of sediment is shown though volume change histograms for each sub-embayment (Figure 2.13), including the associated uncertainty from the DoD calculations.

Large volumes of sediment were lost and gained during the southerly dominated 2013-2016 epoch (Figure 2.13, Left column), with significant and detectable net losses in all four southern sub-embayments (Hallsands, Hallsands South, Beesands and Slapton Sands). Net volume gains were observed at the northern sub-embayments of Forest Cove and Blackpool Sands. The resultant imbalance of erosion and accretion within individual sub-embayments, but insignificant net full embayment change, suggests there is either cross-shore exchange of sediment, or an alongshore flux of material bypassing headlands and transitioning between sub-cells.

To assess the cross-shore element of sediment transport within sub-embayments, profiles were extracted across the full-embayment surveys at 50 m intervals, and the relative contributions of sub-aerial (> -2 m ODN) and sub-tidal (< -2 m ODN) volume change was calculated (Figure 2.14).

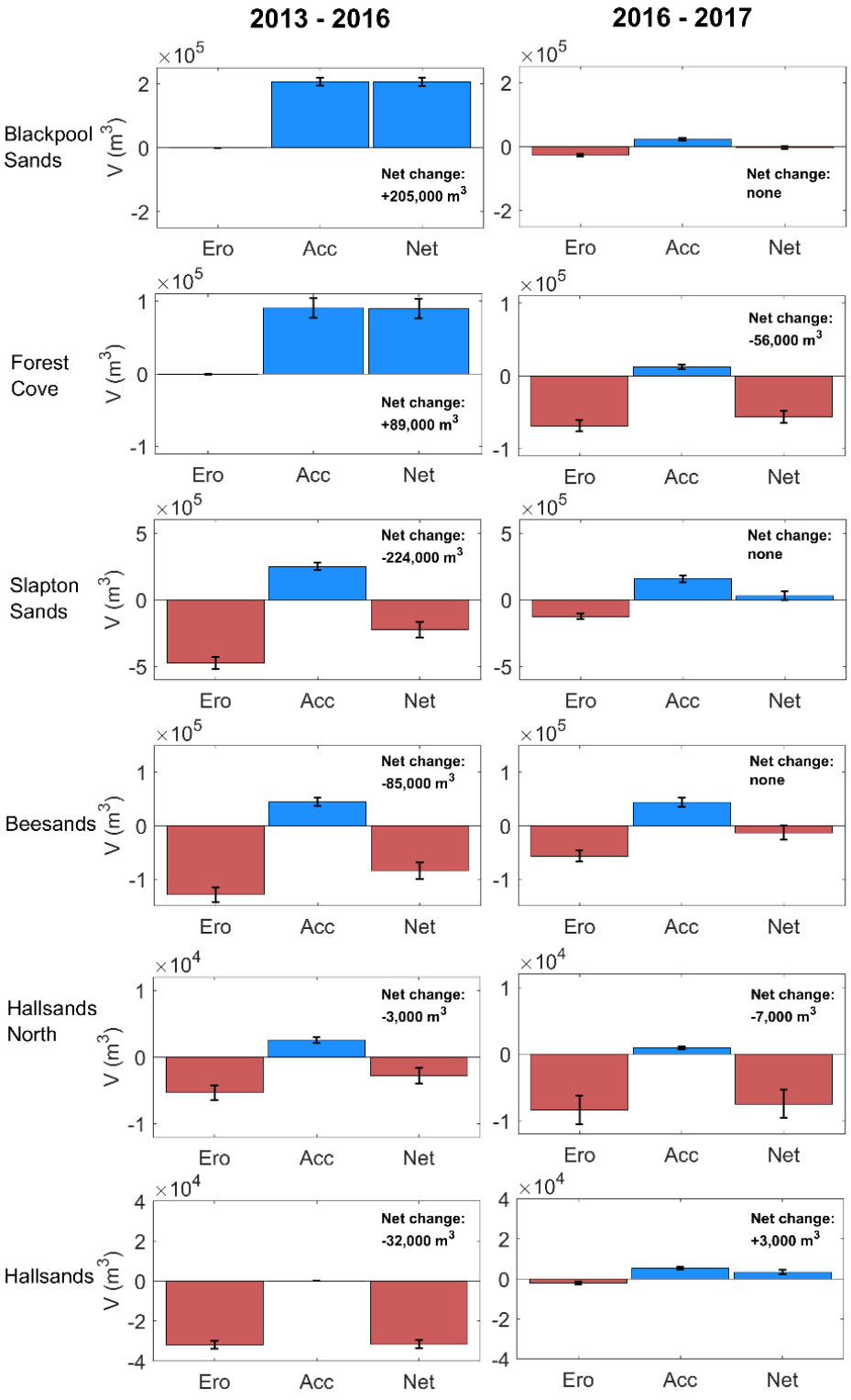

Figure 2.13. Total volumetric change within sub-embayments from 2013 to 2016 (Left) and 2016 to 2017 (Right) – note the differing Y axis limits between sub-embayments. Black bars represent the uncertainty estimates for the total combined erosion, accretion and net change. Net detectable change is displayed on each plot. Where change was less than the total propagated uncertainty, no net change is quoted.

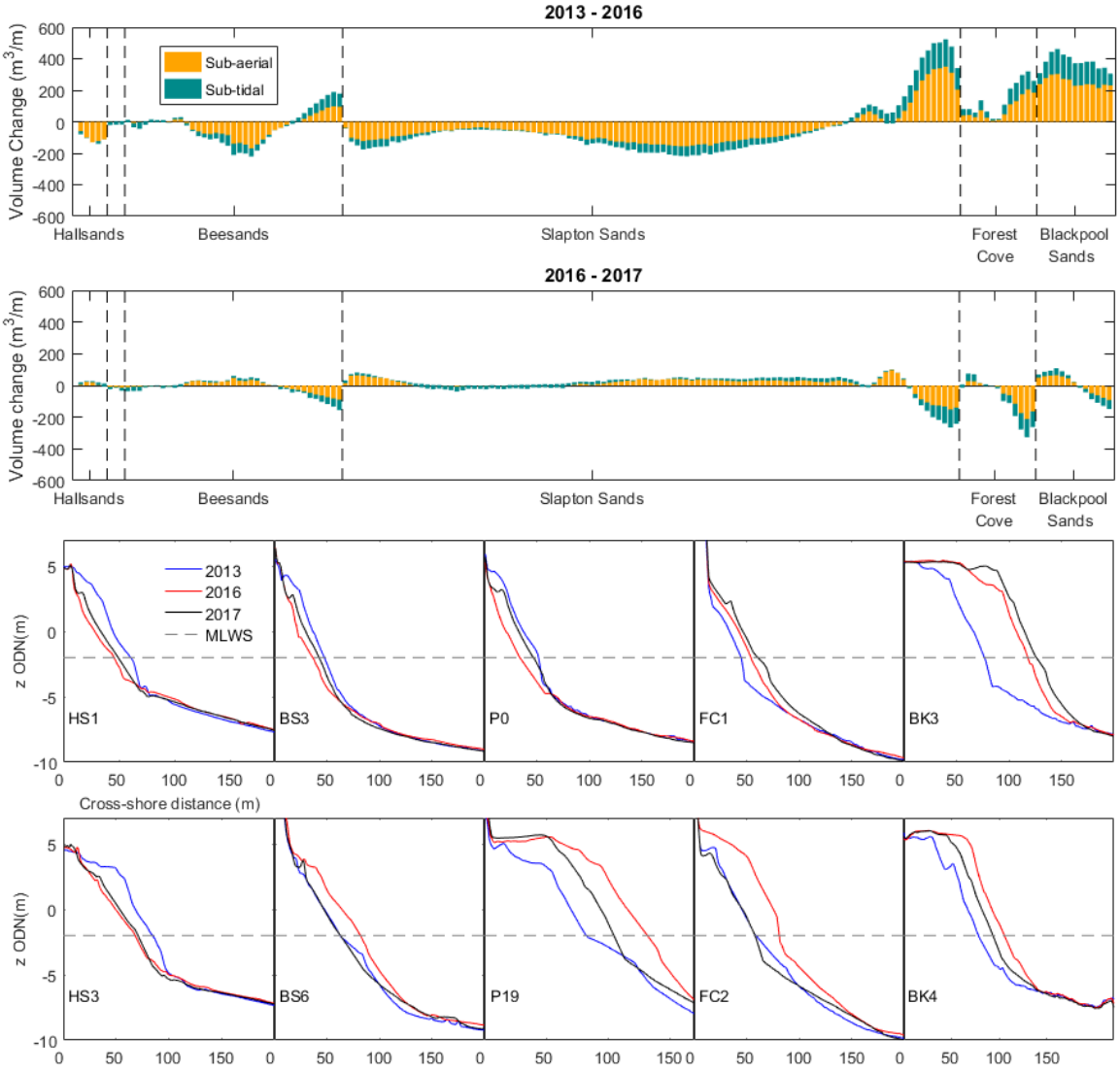

Figure 2.14. First and second panel. Extracted profile volume change from 2013 to 2016, and 2016 to 2017, showing intertidal and sub-tidal (< -2 m ODN) contributions from south to north of the embayment . Vertical dashed lines represent the relative location of headlands between sub-embayments. Profile elevations are presented in the lower panels and are cropped to display upper elevation changes. All profiles close at the sub-tidal extent.

During the 2013 – 2016 epoch (Figure 2.14, upper), substantial in-phase change occurred in both the sub-aerial and sub-tidal elevations, particularly at the northern extents of Beesands, Slapton Sands and Blackpool Sands. Within Beesands, profile BS1 at the southern extent lost 91 m^3/m, with 32% occurring in the sub-tidal extent. The northernmost profile, BS7, gained 178 m^3/m with sub-tidal changes making up 47% of the total volume accreted. Similar results are observed at Slapton Sands, with P1 losing

126 m^3/m in the south (20% sub-tidal losses) and P20 gaining 524 m^3/m (33% sub-tidal accretion) in the north. Throughout the embayment, the sub-tidal sediment volume changes are in phase with sub-aerial changes and the detectable depth of closure has been reached (Figure 2.14). These results, in combination with the balanced total sediment budget for both epochs suggest that there is no significant cross-shore exchange causing the net volume disparity within sub-embayments, and that the only mechanism for the large-scale changes is bypassing of material around headlands from one embayment to the next. The integrated volume change in the sub-tidal extent is approximately 33% of the total volume changes observed across all profiles within the full embayment, illustrating the significant contribution sub-tidal change makes to the total sediment budget.

During the 2016-2017 easterly epoch, sub-embayment anti-clockwise beach rotation was observed at Beesands, Slapton Sands and Blackpool Sands (Figure 2.14, Right), although no significant net gains or losses were detected (Figure 2.13, Right). This suggests that there has been no detectable flux of sediment into or out of the three major sub-embayments. The only significant sub-embayment net volume change (in comparison with that lost during the southerly epoch) was within the north of the embayment. Forest Cove experienced a net loss of -56,000 m^3, compared to a gain of +89,000 m^3 between 2013 and 2016. As Forest Cove represent a transition cell between Blackpool Sands and Slapton, this loss is explained as a detectable southward flux of sediment out of the sub-embayment into Slapton Sands.

The measured geomorphic changes during the southerly and easterly epochs show that the entire embayment rotated in a clockwise direction under the extreme southerly-dominated conditions of 2013 to 2016, with headland bypassing evidenced as large-scale redistribution of material between sub-embayments. Under the easterly conditions of 2016 to 2017, anti-clockwise rotation was observed within sub-embayments, with

absolute change approximately 40% of the southerly epoch; however, minimal net changes occurred through headland bypassing, indicating volume changes induced across the entire embayment in 2013-2016 have not returned.

2.4.3 Decadal morphological change and forcing mechanisms

Whilst spatially integrated total embayment response provides invaluable understanding of response and recovery mechanisms to extreme variability in the wave climate, an extended temporal record is required to quantify the relationship between wave forcing and morphology.

The changes to the intertidal (> -2m ODN) beach profile volumes across the embayment over the last ten years (Figure 2.15) show there is an underlying trend of accretion at profiles in the northern embayment of Blackpool Sands (BK1 and BK2 gaining 31 and 38 m^3/m per year respectively), and the northern end of Slapton Sands, with P19 accreting at 23 m^3/m per year. The central and southern section of Slapton Sands has shown a negative trend in volume difference since 2007, with P9 and P2 losing at respective rates of -8 and -12 m^3/m per year. The trend is similar at Beesands, with volume losses in the south (BS2 eroding at -10 m^3/m per year) matched by gains in the north (BS7 accreting at 3 m^3/m per year). Profile volumes at Hallsands have shown a semi-stable response, with positive and negative changes occurring from 2007 until the stormy winter of 2013/14, after which the beach volume has significantly decreased, remaining depleted in the years since.

The significance of the 2013/14 southerly storm response is clear from the volume change plots, as the largest profile volume changes occurred over this period. The effect of this winter on the long-term profile volume trends is significant, in many cases doubling the rates of erosion or accretion calculated between 2007 and summer 2013.

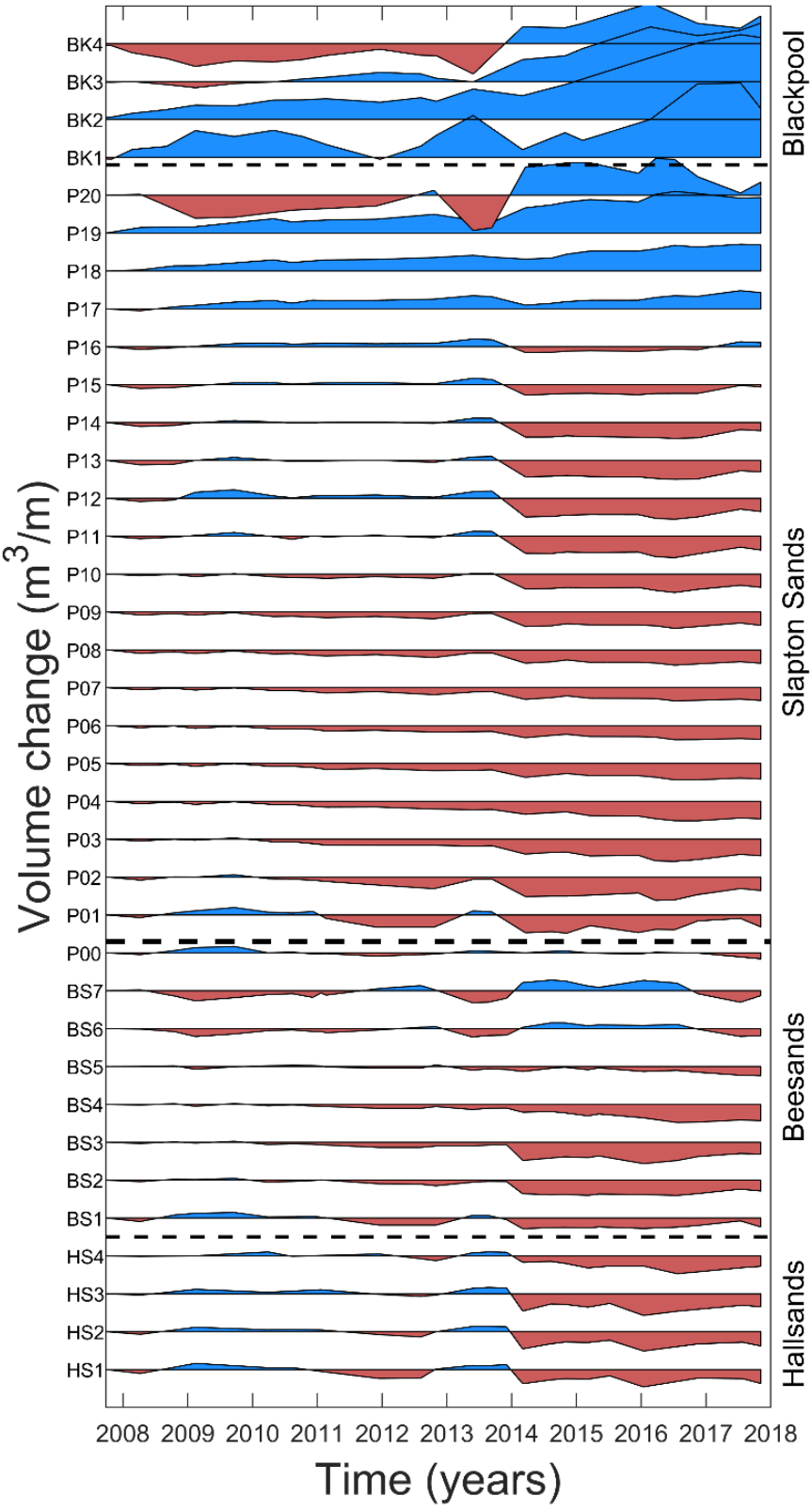

Figure 2.15. Intertidal volume change time series for intra annual profiles in Start Bay, collected between 2007 and late 2017 by PCO. Profiles are displayed from north to south (top to bottom), with Blackpool Sands at the top of the figure, and Hallsands at the bottom. The red dashed line indicates the separation of sub-embayments by headlands. Volume change at each profile is shown relative to the first survey in 2007 and represents volume change as a unit of beach width (m^3/m).

Profiles in the northern sections of sub-embayments, which accreted during the storms, have generally remained stable, and in some cases, continued to increase in volume since 2014. Conversely, southerly profiles have continued to erode and only shown signs of accretion in the last year from 2016 to 2017. The 2013/14 winter is the only event in the time series that experienced significant full embayment rotation with headland bypassing.

Correlations between the WDI and short-term (~3-monthly) morphological change over a decade of observations show that the balance of southerly to easterly wave power directly controls the spatial variation of beach volumes, with correlations stronger in the winter when absolute wave energy is greater (Figure 2.16).

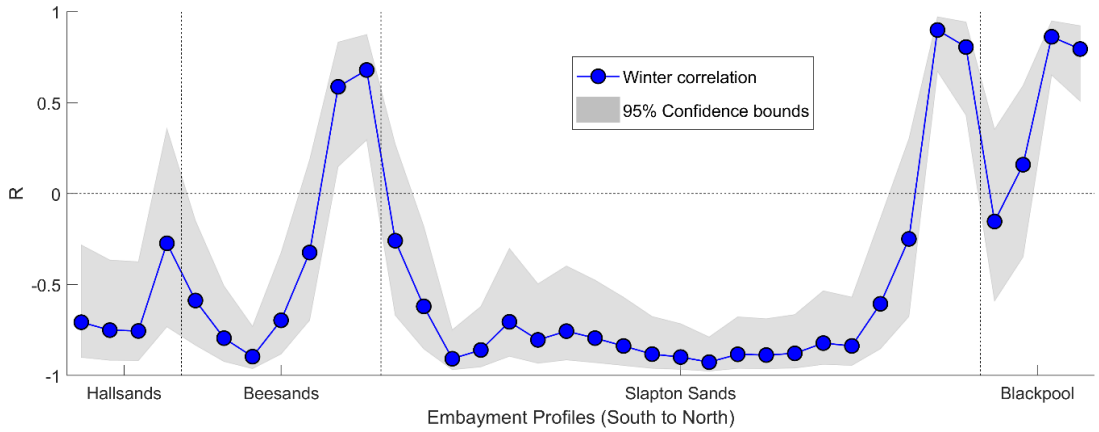

Figure 2.16. Winter correlation coefficients (with associated 95% confidence intervals) between observed intertidal volume change and the WDI for the decadal time series of intertidal beach profiles within Start Bay.

Profiles at the southern (northern) extents of sub-embayments show the strongest negative (positive) correlations. Where the correlation is strongly positive (> 0.7), such as at the northern extents of Beesands, Slapton and Blackpool Sands, profiles gain volume under southerly dominated wave conditions, and lose volume under predominantly easterly wave conditions. The converse is true, for example at Hallsands and the southern extents of Beesands and Slapton Sands, where negative correlations (< -0.7) indicate a loss of sediment under southerly waves, and a gain of material under

easterly dominated conditions. Two distinct rotational pivot points are evidenced by the alongshore correlations at both Beesands and Slapton Sands (Figure 2.16). Between profile BS5 and BS6, correlations switch from negative to positive, meaning under southerly dominated wave conditions, the Beesands sub-embayment erodes to the south of this point and accretes to the north. A similar pivot point is observed at the northern end of Slapton Sands, with correlations again switching from negative to positive around profile P18. The full embayment difference models (Figure 2.11) also evidence these two pivot points, with clear transitions from erosion and accretion found in similar locations under both southerly and easterly wave conditions.

Strong correlations (both positive and negative) between the WDI and beach volume change at sub-embayment extremities, shows that the offshore modelled waves are well correlated to measured beach morphology, despite not being transformed inshore, suggesting that directionality of incoming wave power is a key component in predicting beach change.

2.4.4 Role of atmospheric variability

The wave climate presented in Figure 2.2 shows that the winter-averaged contribution from each directional mode varies dramatically on a multi-annual to decadal timescale. From the morphological response in the short-term, it is clear that this has a significant impact of the direction and magnitude of embayment rotation. The next intuitive step is to examine the link between climate indices and dominant wind and wave directions to investigate their explanatory power for multi-annual winter-average bi-directional balance and hence long-term morphological response.

The long-term winter modelled wave data since 1980 shows the dominance of southerly over easterly wave power (Figure 2.17, Upper); however, the offshore waves cannot be compared in absolute terms, due to the lack of inshore transformation.

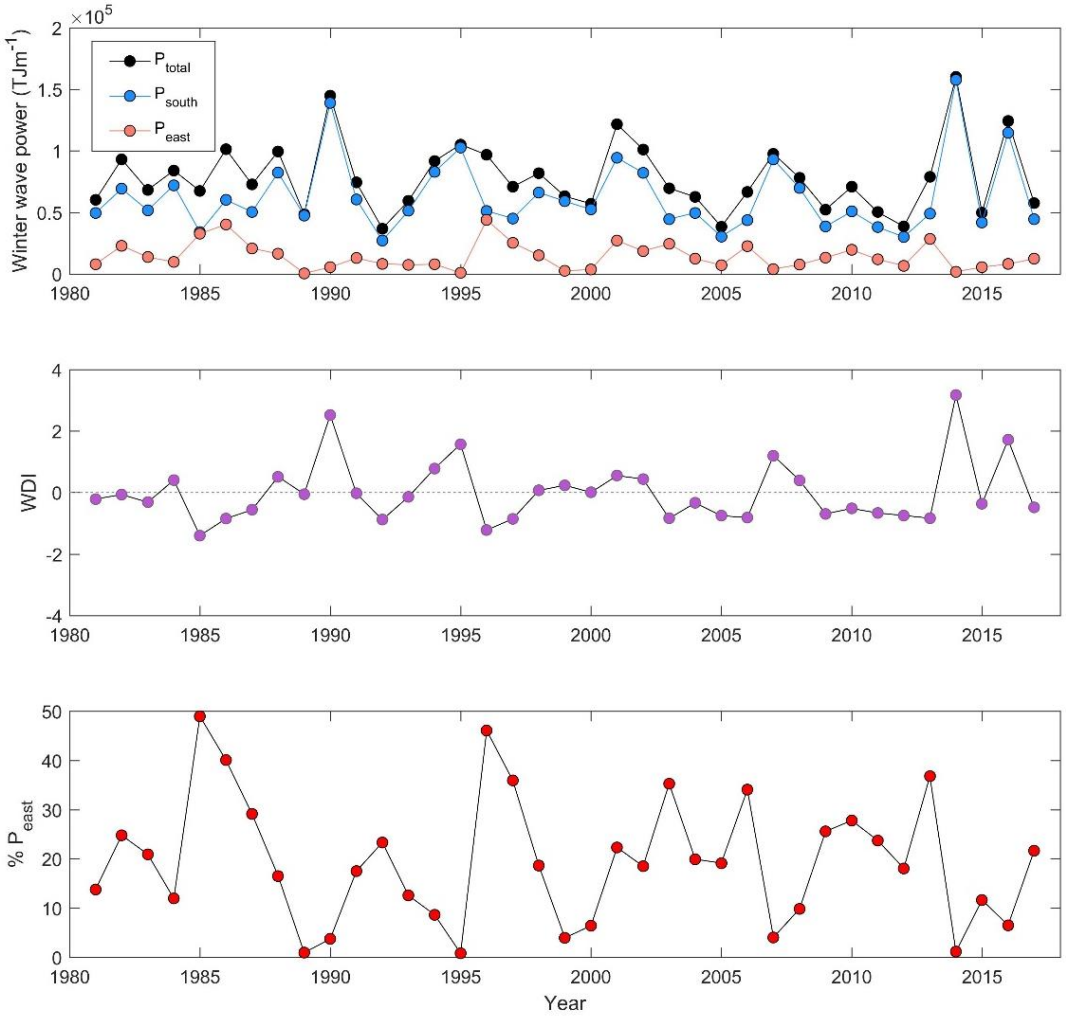

Figure 2.17. Upper; winter (DJFM) wave power total (black), westerly (blue) and easterly (red). Middle; Southerly to Easterly wave power index (WDI) computed for the winters of the modelled wave record. Lower; easterly wave power as a percentage of the total wave power for each winter.

The most energetic winters within the model record were 1990 and 2014 and are attributable almost exclusively to southerly wave events. Easterly wave power contributes less than 40% of the total winter wave power with the exceptions of 1986 and 1995 (Figure 2.17, Lower). The WDI for the entire modelled record is shown in Figure 2.17 (Middle), and highlights where the balance of winter wave power is either more southerly dominated than average (positive) or more easterly dominated than average (negative). Multi-annual periodicity linked to variations in incident wave direction are evidenced by sustained periods of positive or negative winter WDI values, for example the five-year positive period between 1998 and 2002 and the following

four-year negative phase between 2003 to 2006 (Figure 2.17, Middle). This leads to an assessment of whether fluctuations in atmospheric climate indices can account for or predict changes in the direction of the incoming wave climate and therefore the rotational beach morphology observed at this location.

Winter-averaged values of the NAO and WEPA index from 1980 to 2017 are plotted against the winter-averaged wave parameters and presented in Figure 2.18.

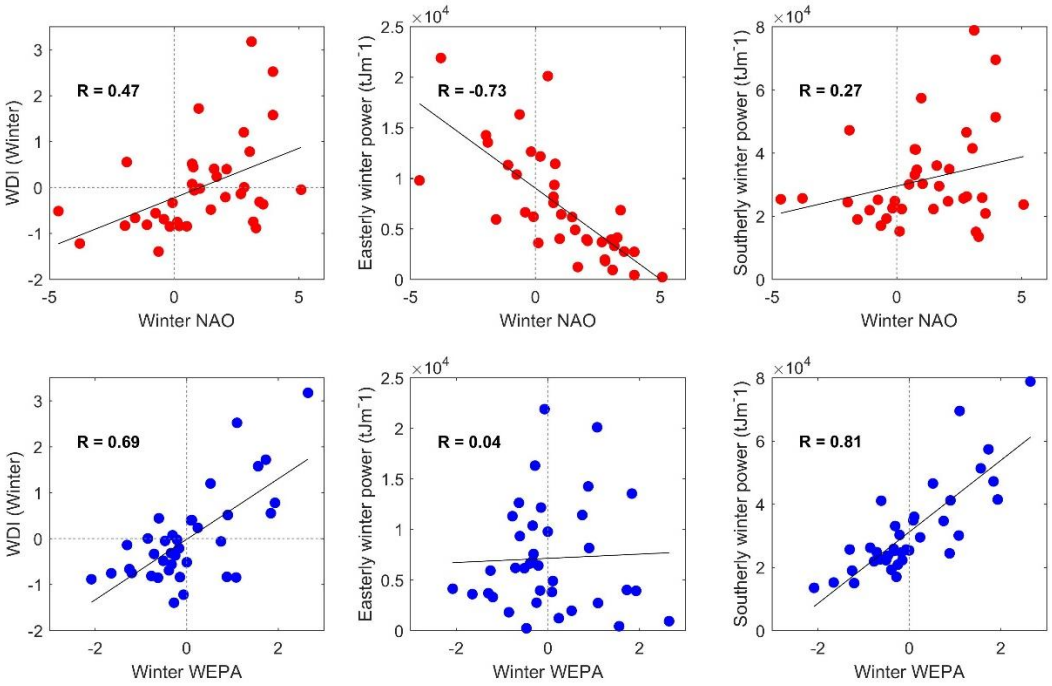

Figure 2.18. Upper; Winter NAO versus winter wave parameters: WDI (upper-left panel), easterly wave power (upper-middle panel), southerly wave power (upper-right panel). Lower; Winter WEPA versus wave parameters: WDI (lower-left panel), easterly wave power (lower-middle panel), southerly wave power (lower-right panel).

The WDI exhibits only a moderate positive correlation with winter NAO values (R = 0.48; p = 0.0043), however; there is a significant negative correlation between winter NAO and easterly deep-water wave power (R = -0.73; p = 0.0000). Further examination shows southerly winter wave power is weakly correlated with winter NAO (R = 0.27; p = 0.1116). Therefore, it can be assumed the low correlation with southerly waves is reducing the relationship with the WDI. This could be explained by the southerly wave

power dependence on storm track latitude which is ill-defined by the NAO as elaborated by (Castelle et al., 2017), therefore the NAO may provide skill in describing the balance of easterly and southwesterly wave events through the presence or lack of easterly wave events at this location.

The WEPA index, developed by Castelle et al. (2017) for explaining lower latitude wave climate (western Europe), provides an improved relationship with bi-directional waves, especially those from the southwest (Figure 2.18, bottom panels). A significant positive correlation between winter WEPA and both the WDI ($R = 0.69$; $p = 0.0000$) and southerly winter wave power ($R = 0.81$; $p = 0.0000$) is observed. There is no significant correlation between winter WEPA and easterly winter wave power (Figure 2.18, Lower-middle).

2.5 Discussion

2.5.1 Full embayment extreme winter response

Beaches dominated by a rotational response to wave forcing occur worldwide, particularly semi-exposed coastlines with bi-directional wave climates, where headlands or structural constraints trap sediment transported alongshore at embayment extremities. This chapter has quantified and examined the full morphological response of a semi-sheltered gravel embayment to a multi-annual bi-directional wave climate, including a >1:50 year winter storm season. Similar to previous studies of rotational beaches, the findings here highlight that beach rotation is a function of wave direction over a variety of timescales. At event and winter-averaged seasonal scale (e.g. Ruiz de Alegria-Arzaburu and Masselink, 2010; Thomas et al., 2011a), energetic storms prevailing from one direction have the ability to cause significant and rapid changes to the planform shape and sediment distribution within rotational embayments. Klein et al. (2002) suggested that seasonal rotation often results in erosion and accretion at opposite ends

of an embayment, but does not lead to net sediment losses; however, under the exceptionally southerly-dominated storm conditions during the winter of 2013/14, initial assessments of a single sub-embayment (Slapton Sands, Scott et al., (2016) highlighted the net loss of sediment from the intertidal extent. These losses were accounted for in this study, by the calculation of total sediment budgets including all sub-embayment beaches within the full embayment, at both sub-aerial and sub-tidal extents. Through well-defined and thoroughly assessed uncertainty bounds, following Wheaton et al. (2010), significant changes were identified to have occurred between sub-embayments with a new level of confidence, accounting for more of the total sediment budget, across all sediment pathways (e.g. Goodwin et al., 2013), improving the understanding of spatial patterns of embayment response to storms. The occurrence of full embayment rotation between 2013-2016, with 33% of significant geomorphic changes occurring in the sub-tidal extent (up to 47% in some locations); represents a considerable proportion of the sediment budget that would have been unaccounted for using conventional intertidal or sub-aerial measurements alone. Furthermore, net sediment losses and gains from individual sub-embayments highlight sediment bypassing headlands, being transported from one sub-embayment to the next, as suggested by Burvingt et al. (2018). The robust methodology for capturing geomorphic changes, as applied within this chapter, have allowed significant insights into the mechanisms and pathways for embayment scale changes to be presented with a confidence level not seen in many similar studies (Burvingt et al., 2016; Scott et al., 2016). The findings here suggest future sediment budgets calculated in coastal locations should follow the same approach, accounting for spatial variability in uncertainty between different survey techniques, propagating through to the DoD analysis and incorporating probabilistic thresholding, allowing reliable volume change calculations and some level of confidence in inferences to observed morphological processes.

Application of this method would be valuable at other locations worldwide, including cross-shore dominated sites; however, the expected vertical changes would need to be greater than the uncertainties in employed survey techniques. Additionally, for larger, intermediate to dissipative beach locations, with finer sediment and macrotidal ranges, total sediment budgets may be difficult to obtain, due to the expansive areas of small scale vertical changes (offshore), and greater depth of closure (Valiente et al., 2018), increasing the difficulty and cost in obtaining sufficient data. Nevertheless, recent application of the total sediment budget approach, using combined multi-method surveys of the supra- to sub-tidal shoreface at an exposed, macrotidal, beach-dune system (Perranporth, U.K) by Valiente et al. (2019), highlighted the longshore uniform cross-shore response of the intertidal extent, whilst also identifying a partial decoupling from the sub-tidal zone. Unlike the results presented here, additional volume calculations at Perranporth over multi-annual time frames highlighted the inner embayment was not closed or balanced, particularly in the sub-tidal extent; however, similar mechanisms were proposed for the loss of volume, suggesting sediment fluxes into and out the embayment through headland bypassing within the sub-tidal zone.

Further application of the total sediment budget approach would be valuable at locations experiencing a cross-shore rotational response (Harley et al., 2015), as insights into beach rotation mechanisms have highlighted complex feedback loops with offshore sediment transport and sand bar coupling (Van de Lageweg et al., 2013; Harley et al., 2015).

2.5.2 Sub-embayment counter rotation to easterly waves

The anti-clockwise (southward) sub-embayment rotation observed between 2016 and 2017 following the increased but moderate easterly wave conditions (20% contribution of winter easterly waves compared to the long-term mean of 23%) of that winter

resulted in volume changes that were ~50% less than those observed between 2013 and 2016. As a consequence, sub-embayments counter-rotated but sediment exchange between headlands was minimal. Scott et al. (2016) hypothesized that a rebalance of an embayment towards its pre-storm state would require aggregated equal and opposite wave events from the east. The changes observed in this study suggest that for sub-embayments to restore pre-storm sediment volumes, specific wave conditions must prevail that drive not only reversals in sediment transport direction but occur at absolute magnitudes and timescales that allow sediment to traverse back around headlands already bypassed, resulting in full embayment rotation. These conditions were not met during the 2016-2017 epoch of this study, and headlands acted to constrain sediment changes to sub-embayment rotation only.

Many geological, geometrical and hydrodynamic factors affect the facilitation of transport around headlands, including the bathymetric slope angle, headland apex ratio, protrusion length or size, as well as the occurrence of a shore platform (George, 2016). The headlands within Start Bay are complex and varied and hydrodynamics and geological orientation will play equally important roles. Headland bypassing within embayed coastlines may be asymmetrical, with some headlands “open” to transport under one set of wave conditions, but “closed” under another. This has significant implications for the understanding of recovery of sediment losses, suggesting full embayment rotation is dependent on the occurrence of headland bypassing, requiring a specific cumulative threshold of absolute wave power from one direction, rather than simply a reversal of wave angle. If such conditions are not met, recovery of sediment may be impossible without human intervention, and coastal vulnerability at up-drift locations may be permanently increased. Future work underway will look to improve our understanding of the mechanisms governing gravel (bedload transport) bypassing of

headlands and conditions required to allow sediments to transition from one sub-embayment to the next.

2.5.3 Decadal embayment response to wave climate variability

Over longer timescales, this study developed and utilized the WDI, a new equilibrium parameter, used here to describe the imbalance of opposing southerly and easterly wave power relative to the long-term mean. For the interim period between morphological profile surveys over a decadal scale, strong correlations (both positive and negative) were observed between the WDI and beach volume change at sub-embayment extremities. These results suggest that the direction of longshore transport and its control on beach morphology is linked with not just the occurrence of high-energy episodic wave events, but also the dynamic balance of incident wave power from southerly and easterly directions. Observed correlations with beach morphology are strongest for changes measured during the winter months (Figure 2.16), due to high energy wave events in the North Atlantic occurring most frequently between December to March (van Nieuwkoop et al., 2013; Woolf and Wolf, 2013), where the seasonal clustering of storm events is greatly affected by atmospheric oscillations (Castelle et al., 2017). Peak period (spectral energy) from the WW3 hindcast data was used for wave power calculations. This approach does not resolve the spectral contributions of wind and swell (bi-directional or otherwise). This is deemed acceptable as the focus is on alongshore transport (rotation) rather than cross shore profile shape. Previous studies have shown that gravel barrier shape responds differently to spectral contributions of swell and wind waves (e.g. Bradbury et al., 2011; Mason et al., 2009).

Whilst morphological response here is well correlated with incident wave direction, the long-term winter wave climate shows significant multi-annual variability for both the total wave power, and the southerly and easterly contributions to the bi-directional wave

balance (Figure 2.17). Previous studies have identified links between atmospheric climate variability and incident wave heights, with particular focus on the North Atlantic Oscillation (Bacon and Carter, 1993; Masselink et al., 2014) and the El Nino Southern Oscillation (Barnard et al., 2015, 2017; Mortlock and Goodwin, 2016) for the Atlantic and Pacific Oceans, respectively. Castelle et al. (2017) identified that the NAO index did not capture the unprecedented stormy winter of 2013/14, characterized by increased southerly storm tracks (Masselink et al., 2015) and full embayment rotation at Start Bay, and devised the WEPA index to better characterize increased wave heights in more southern latitudes of the European North Atlantic coast. Malagon Santos et al. (2017) explored the link between the magnitude and frequency of extreme wave heights around the U.K. and concluded that WEPA is better suited to predicting wave action in the south west than the NAO; however, their dataset was temporally limited to 10 years of wave buoy data per site, and direction of wave events was not considered. In this chapter, it is shown for the first time, that the two dominant winter wave directions, easterly and southerly, are significantly correlated with winter-averaged NAO ($R = -0.73$) and WEPA ($R = 0.81$), respectively.

Long-term wave climate controls over the 37-year record are summarised in Figure 2.19, with the four winter variables (NAO, WEPA, WDI and relative wave power) showing two distinct modes, representing northward (clockwise) and southward (anti-clockwise) rotation. The top-right quadrant (Figure 2.19) indicates winters with positive NAO (suppressing easterlies), and positive WEPA (increased southerly storm tracks). These winters are typically dominated by large southerly storms (large red circles, Figure 2.19, left) and are associated with the strongest northward transport. The bottom-left quadrant represents periods of negative NAO (allowing easterly wave conditions to develop), and negative WEPA (fewer southerly storm tracks), associated with a relative dominance of easterly conditions (WDI is uniformly negative), and dominant southward

transport within Start Bay. The top-left and bottom-right quadrants of Figure 2.19 indicate periods where the relevant climate indices are in opposition, and net rotation direction is uncertain.

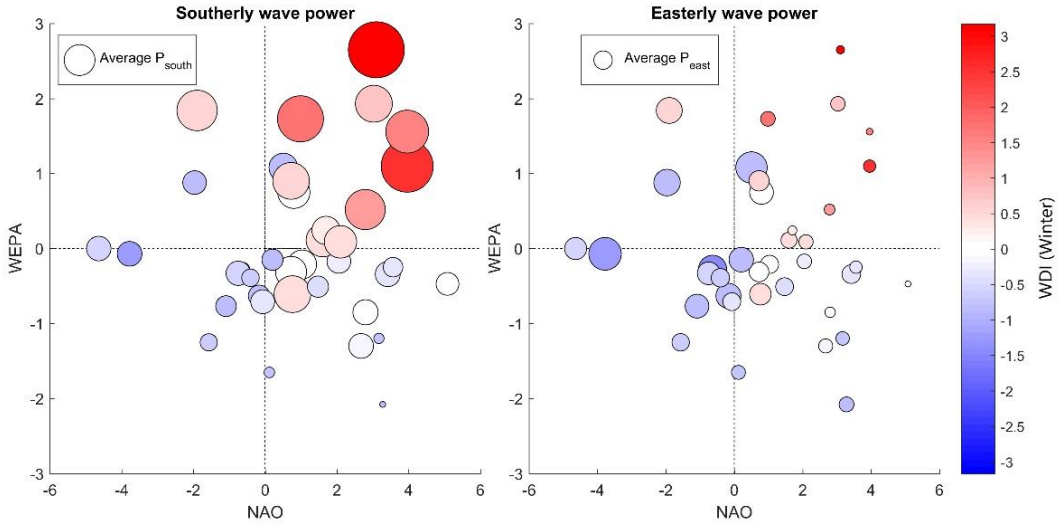

Figure 2.19. Summary plot of winter values for NAO vs WEPA, with WDI values represented by circle colour, and winter contributions of relative wave power from southerly (Left) and easterly (Right) waves represented by circle size.

These findings are consistent with the correlation found between cross-shore volume transport and the WEPA index, on the northern exposed coastline of the south west U.K. (Burvingt et al., 2018). This suggests that climate indices are useful predictors of morphologic change on a wide range of exposed, to semi-exposed coastlines.

These findings indicate that, respectively, winter-averaged NAO and WEPA are effective in explaining the easterly and southerly wave components driving morphological change in Start Bay. Therefore pressure-driven climate scale indices can account for the observed bi-directional periodicity in wave climate in this study. It is therefore expected that atmospheric indices like the NAO, may skillfully explain long-term wave climate variability in other (semi) sheltered environments significantly influenced by bi-directional waves. Further work in this thesis will explore the use of WEPA and NAO to hindcast seasonal changes to wave climate and beach morphology.

Recent modeling breakthroughs in seasonal forecasting of the winter NAO (Dunstone et al., 2016) suggest there may be an applicable level of skill in 3-month forecasting of winter NAO (Stockdale et al., 2015). The recent growth in ensemble size is increasing the skill of such models, allowing predictions of winter NAO to take place up to one year in advance (Scaife et al., 2015; Dunstone et al., 2016; Wang et al., 2017). If these models can be validated and improved, allowing the combined prediction of NAO and WEPA (Castelle et al., 2018), governments and coastal engineers may be able to plan using event and seasonal scale forecast wave conditions, acting before potential changes in beach morphology result in increased coastal vulnerability.

2.6 Conclusions

This chapter examines extreme event and decadal sub- and full-embayment rotation within a headland embayed gravel coastline with a bi-directional wave climate. It highlights the importance of antecedent morphology and storm sequencing in transitioning from sub-embayment to full embayment rotation. Over multi-annual timescales, morphological change is correlated with the wave power balance from the two dominant directions, which in turn are correlated with atmospheric indices.

1. Under the dominance of a particular wave direction, individual sub-embayments may rotate; however, if persistent seasonal or extreme energy levels exceed a given threshold, significant headland bypassing can occur, leading to full-embayment rotation.

2. During a >1:50 year energetic southerly winter (2013/14), extreme wave events from one direction resulted in full embayment rotation; whereas, persistent moderate energy from the alternate easterly wave direction (2016-2017) resulted in sub-embayment rotation, failing to reach the threshold required for headland bypassing and full embayment rotation.

3. The application of a novel total sediment budget approach, including all sub-embayments and sub-tidal extents (with robust spatial uncertainty assessments), is essential to fully understand the geomorphic response mechanisms in rotational embayments, and should be applied to all future sediment budget analyses.

4. Beach rotation can be parameterized by a new index that quantifies the deviation in the directional wave balance between the two dominant directions from the long-term average.

5. Winter wave direction is correlated with two distinct climate indices, suggesting that atmospheric oscillations may explain periodicity and multiannual morphological changes at embayed rotational sites with bi-directional wave climates.

Findings presented here help advance our understanding of event-scale, annual, and decadal embayment morphological response mechanisms. This new knowledge should help improve coastal vulnerability assessment and management in embayments sensitive to directional wave climates.

3 Regionally coherent, medium-term beach rotation and climate control

The previous chapter has identified beach rotation over a full embayment to sub-embayment scale, under distinctly different winter wave conditions. The WDI has been developed and identified as the key mechanism for controlling beach rotation within the site-specific example of Start Bay, and this next chapter aims to expand the analysis spatially into the region of the south coast of England, U.K.

This chapter contains work published in the following paper: Wiggins, M.; Scott, T.; Masselink, G.; Russell, P.; Valiente, N.G. Regionally-Coherent Embayment Rotation: Behavioural Response to Bi-Directional Waves and Atmospheric Forcing. Journal of Marine Science and Engineering, 2019, 7 (4), 116.

3.1 Introduction

Coastal rotation is observed worldwide at many semi-sheltered, often embayed locations, particularly where wave climates are bi-directional (Klein et al., 2002). Alongshore transport of sediment as a result of opposing wave directions, especially following storm events, can lead to an imbalance of erosion and accretion at embayment extremities. This can leave coastal communities and infrastructure vulnerable to damage from future storm events (Bergillos et al., 2017; Burvingt et al., 2017), seasonal changes in wave climate (Wiggins et al., 2019a) and atmospheric changes over decadal timescales (Thomas et al., 2013). To mitigate these impacts, identification of rotational beach behaviour, its drivers and controls is required for planning and management of the coastal zone, given future predictions of sea level rise (Nicholls et al., 2011), increased storminess (Suursaar et al., 2015) and coastal squeeze (Pontee, 2013).

Many site-specific studies of beach rotation (Ruiz de Alegria-Arzaburu and Masselink, 2010; Dolphin et al., 2011; Thomas et al., 2011b; Bergillos et al., 2017; Wiggins et al., 2017) have identified variability in the local bi-directional wave climate as a key control of the beach morphological state. Chapter 2 identified that winter changes in beach profile volume change, at opposing ends of a single semi-sheltered gravel embayment (Slapton Sands, U.K.; facing south-east up the English Channel), are well correlated to the relative balance of the normalized contributions of winter wave power from opposing directions. This power balance, and the individual contributions of directional wave power, were also shown to be significantly correlated with both the North Atlantic Oscillation (NAO) and the newly-devised West Europe Pressure Anomaly (WEPA) (Castelle et al., 2017). The work presented in Chapter 2 did not directly compare beach rotation with atmospheric indices; however, several authors have identified direct links between changes in beach morphology and different phases of climatic oscillations, including the El Niño/La Niña Southern Oscillation (ENSO) (Ranasinghe et al., 2004; Barnard et al., 2015; Harley et al., 2015), NAO (Thomas et al., 2011b; Masselink et al., 2014), and WEPA (Autret et al., 2017; Burvingt et al., 2018).

This chapter firstly assesses whether, across a regional domain, wave climates exhibit bi-directional characteristics and whether similar correlations with atmospheric indices (NAO and WEPA) are observed for the whole south coast of England, U.K. Secondly, this chapter assesses whether beach rotational behaviour can be identified at a multitude of different sites, by evaluating the decadal morphological response of 22 different coastal locations. Where rotation can be identified, this chapter assesses to what extent the wave climate balance and shoreline orientation are controlling factors. Lastly, it is investigated whether climate indices can be directly correlated to beach rotation. If wave climate and beach rotation are regionally coherent beyond a few single case studies and well correlated to climate indices, then improved “season ahead” forecasts

of NAO (Scaife et al., 2015; Dunstone et al., 2016) and WEPA (Castelle et al., 2018) may lead to direct predictions of beach rotation and subsequent coastal vulnerability at regional scales.

3.2 Data and methods

3.2.1 Wave data

For the length of the south coast of England, wave data were obtained for 14 offshore node locations (Figure 3.1), comprised of 3-hourly hindcast Wave Watch III model data (obtained from the U.K. Meteorological Office), spanning the years from 1980–2016.

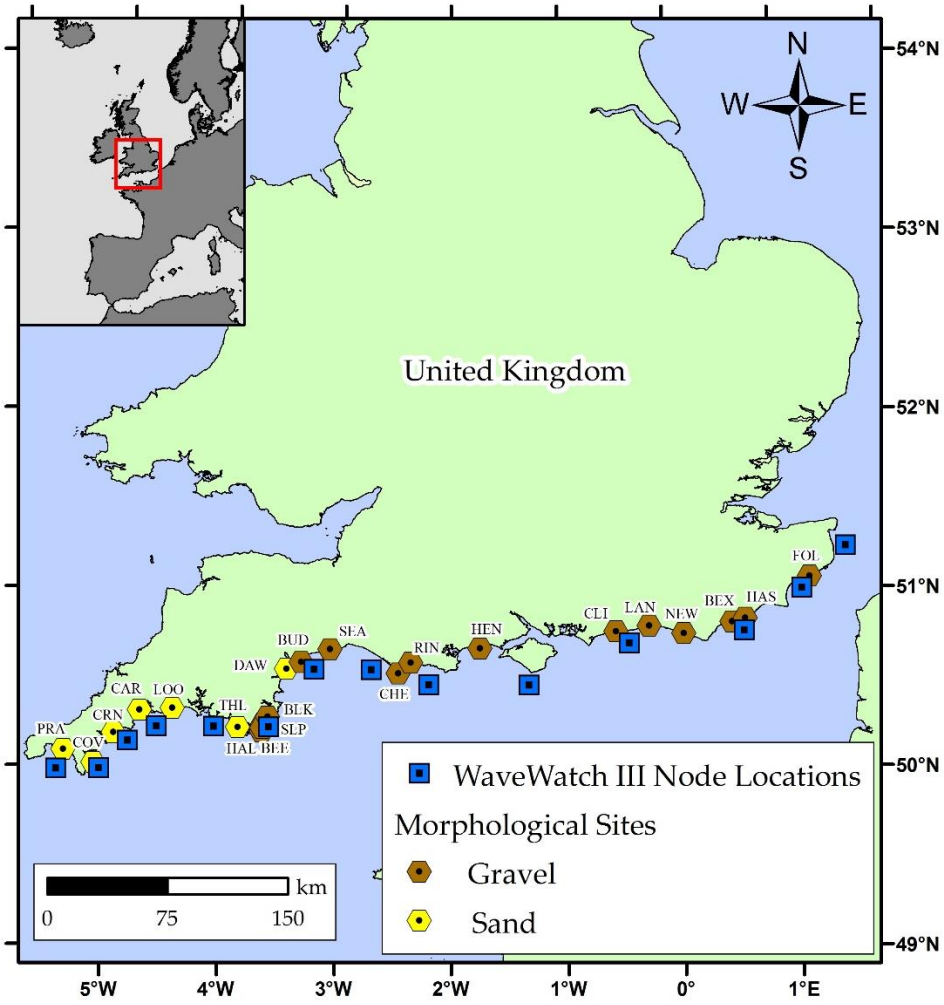

Figure 3.1. Wave Watch III model wave nodes (squares) and morphological study site locations (hexagons) along the south coast of England, U.K. Site location names are abbreviated here and used

when presenting further results. An index of site locations, morphological parameters and survey schedules is located in Appendix A, Tables A1 and A2.

Offshore, significant wave height, mean wave energy period and peak direction were utilized in assessing directional wave power variability in wave climate across all node locations. The same method as Chapter 2 was applied, with wave power (P) calculated at each model node using the same equation (Section 0):

$$P = \frac{1}{16}\rho g H_s^2 C_g \qquad \text{Eq. (6)}$$

where ρ is water density, g is acceleration due to gravity, H_s is significant wave height and C_g is wave celerity calculated with linear wave theory using wave energy period (T_e) and local water depth (h).

Additional short-term records (up to 13 years, 2003–2016) of inshore measured wave conditions were obtained from a wave buoy network (obtained from the Channel Coastal Observatory), for a limited number of locations along the length of the coastline. These were used to compare the inshore wave climate to the modelled conditions offshore.

3.2.2 Wave power directionality index

At all locations, an assessment of the primary (P_{Dir1}) and secondary (P_{Dir2}) wave directional modes was made. Wave power was then subdivided into contributions coming from these two directions, and the index of the relative balance of the two was computed, as per Section 2.3.9 in Chapter 2, again named the Wave power Directionality Index (WDI), using the equation:

$$\text{WDI} = \frac{(P_{Dir1} - P_{Dir2}) - \overline{(P_{Dir1} - P_{Dir2})}}{\sigma(P_{Dir1} - P_{Dir2})} \qquad \text{Eq. (7)}$$

where $(P_{Dir1} - P_{Dir2})$ is the residual wave power between the first and second directional modes, $\overline{(P_{Dir1} - P_{Dir2})}$ is the long-term mean and $\sigma(P_{Dir1} - P_{Dir2})$ is the long-term standard deviation of that difference. High positive values of WDI indicate that the primary directional mode is more prevalent than the long-term average, whereas high negative values indicate that the wave climate has a higher proportion of the secondary directional mode than average.

The wave power for each directional mode, as well as the WDI was calculated for the period spanning December, January, February and March (DJFM), to give a winter average of each variable over the 36-year period at each node location. These wave characteristics were later correlated with atmospheric controls and morphological change, described next.

3.2.3 Morphological data

Extensive morphological datasets of intertidal, cross-shore beach profiles were collated from a multitude of coastal sites, along the length of the south coast of England (Figure 3.1; further site information and survey schedules are provided in Appendix A, Tables A1 and A2). Unfortunately, quantitative records of beach grain sizes were not available across the full extent of the surveyed beaches; however, a qualitative distinction between gravel ($\varphi < -1$ or $D_{50} > 2$ mm) or sand ($\varphi > -1$ or $D_{50} < 2$ mm) was made for each site. Beach surveys were conducted during Mean Low Water Spring (MLWS) tides, using Real-Time Kinematic Global Positioning Systems (RTK-GPS), providing vertical accuracy of <30 mm. The frequency of surveys varied within and between site records, ranging from 4-monthly to yearly, with records spanning from 10–15 years. For each survey date, cross-shore beach volumes were calculated at equally-spaced profiles (between 150 and 250 m depending on location). Individual cross-shore profile volumes at adjacent locations were averaged over representative alongshore beach lengths for

opposing ends of beach extents (Figure 3.2), to produce a representative mean volume for the eastern (northern) and western (southern) sections. These beach sections, and profile locations were chosen based on their proximity to embayment headlands/structures, and further informed by observed historical trends of beach rotation, obtained from annual reports written by Plymouth Coastal Observatory.

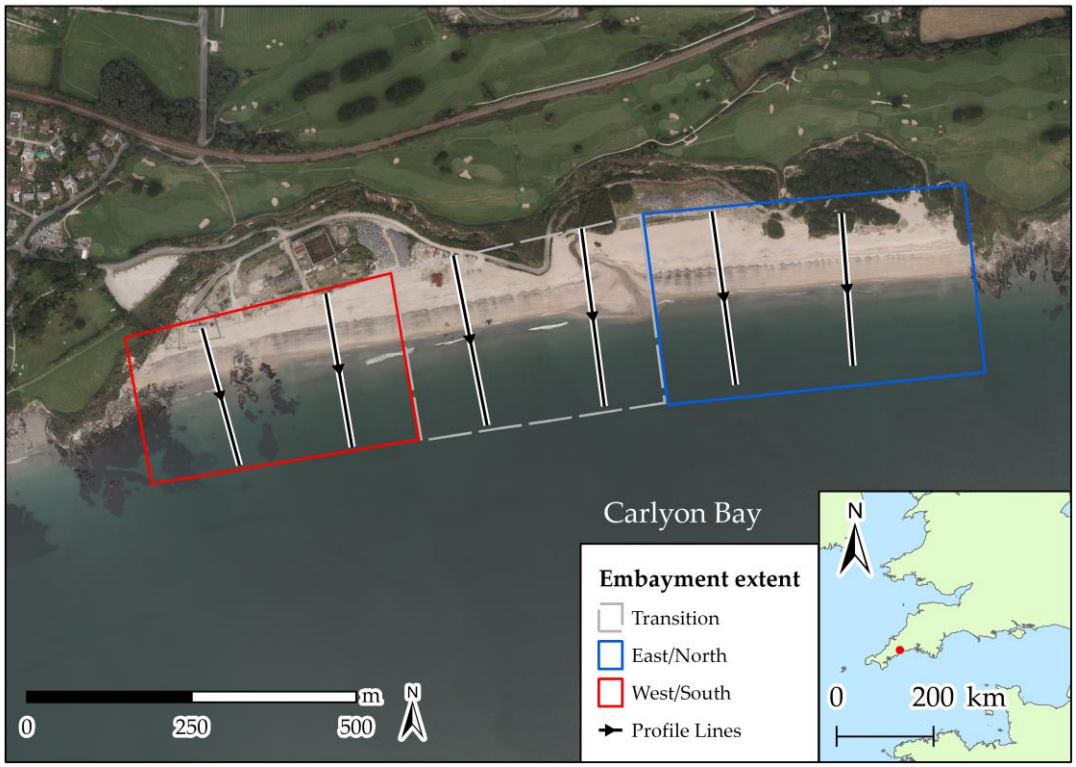

Figure 3.2. Example of beach morphology extents for Carlyon Bay (CAR). The black arrowed lines represent measured profile locations. Beach volumes for the east (west) or north (south) extents are averaged along the length of the blue (red) box. The grey dashed box represents the central nodal point of the embayment, and as such, the beach volume for this region is omitted.

Feature scaling (normalization) of the timeseries of resultant average volumes (for each beach section) by their mean and range produced a normalized time series of volume values (V_i) ranging between 0 (lowest volume, most eroded) and 1 (highest volume, most accreted).

Volume change ($\mathrm{d}V_i$) at opposing ends of the embayment was then calculated for each time-step (V_i) by subtracting the previous normalized volume (V_{i-1}) such that:

$$\mathrm{d}V_i = V_i - V_{i-1} \quad \text{Eq. (8)}$$

3.2.4 Beach morphological response

Assessment of the behaviour for each coastal location was then conducted by calculating a Beach Morphological Response (BMR), defined as the correlation coefficient of the linear regression of western (southern) volume change $\mathrm{d}V_i$ $(west)$, against the eastern (southern) volume change $\mathrm{d}V_i$ $(east)$. Where the correlation and hence BMR values were positive, both ends of the beach were responding together, suggesting that the behavioural response was cross-shore dominated. Conversely, at locations where values were negative, the two ends of the beach were responding out of phase, with one end gaining volume, whilst the other losing, suggesting a longshore transport of beach material, and hence rotational response. An example of this regression is shown for Carlyon Bay (CAR) in Figure 3.3a and Figure 3.3b, showing the two beach ends responding out of phase.

3.2.5 Rotation Index

To quantify the strength and direction of the beach rotational response for each site, at each time step, a Rotation Index (RI) was calculated by subtracting the western (southern) volume change from the eastern (northern) volume change such that:

$$RI = \mathrm{d}V_i\ (east) - \mathrm{d}V_i\ (west) \quad \text{Eq. (9)}$$

When RI was highly positive, the beach response exhibited a strong clockwise rotation, whereas high negative values indicated an anti-clockwise rotation. Where values of RI

tended towards zero, both ends were responding in phase, and beach rotation was minimal. The time series of the RI for Carlyon Bay is shown in Figure 3.3c, highlighting the phases of clockwise and anti-clockwise rotation. The WDI and RI for each site were also correlated against each other, as seen in Figure 3.3d, with results for the remaining sites presented later in Section 3.3.2.

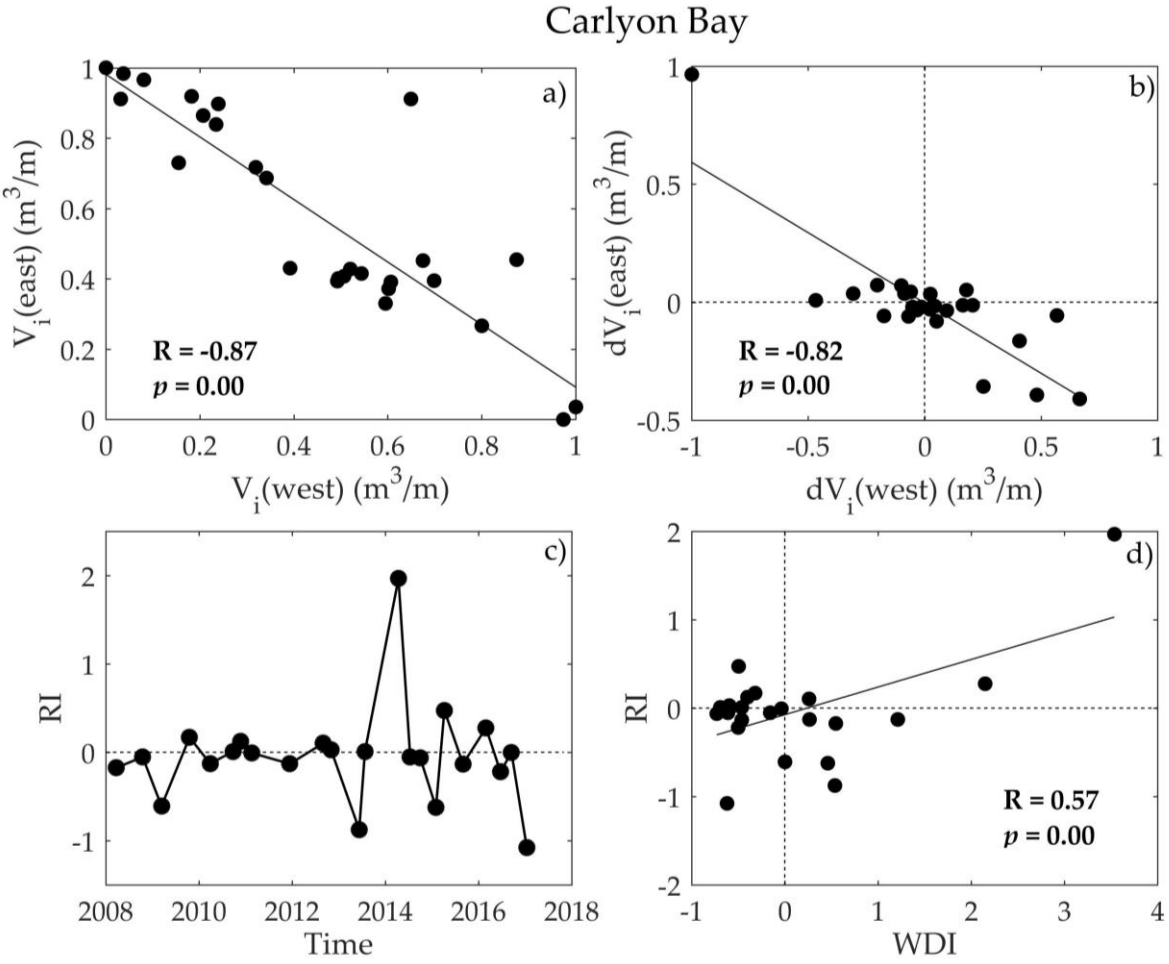

Figure 3.3. Example of the morphological workflow and parameters for the embayed sandy beach of Carlyon Bay, Cornwall, U.K.: (a) Linear regression of the normalized beach volumes at the western and eastern ends of the beach. (b) Linear regression of the normalized volume change of the same western and eastern beach ends, with the correlation coefficient giving the BMR value, in this case -0.82, indicating a rotation beach response. (c) Time series of the Rotation Index (RI) for the duration of the survey record. (d) Linear regression of the Wave power Directionality Index (WDI) against the RI, highlighting the beach rotational response to increased dominance of one wave direction over another.

3.2.6 Atmospheric indices and climate control

In addition to the wave climate and morphological datasets identified above, winter averages of both NAO and WEPA were obtained for the time period of the modelled wave data. Winter averages (DJFM) of NAO (Hurrell, 2018) and WEPA (Castelle et al., 2017) were derived from station-based differences of sea level pressure.

3.3 Results

3.3.1 Wave climate spatial variability

The offshore modelled wave climate was predominantly bi-directional along the length of the south coast (Figure 3.4). In all locations, the primary wave direction was from the south west (greater than 180° and less than 270°). Secondary modes, where apparent, were from easterly directions (less than 180°).

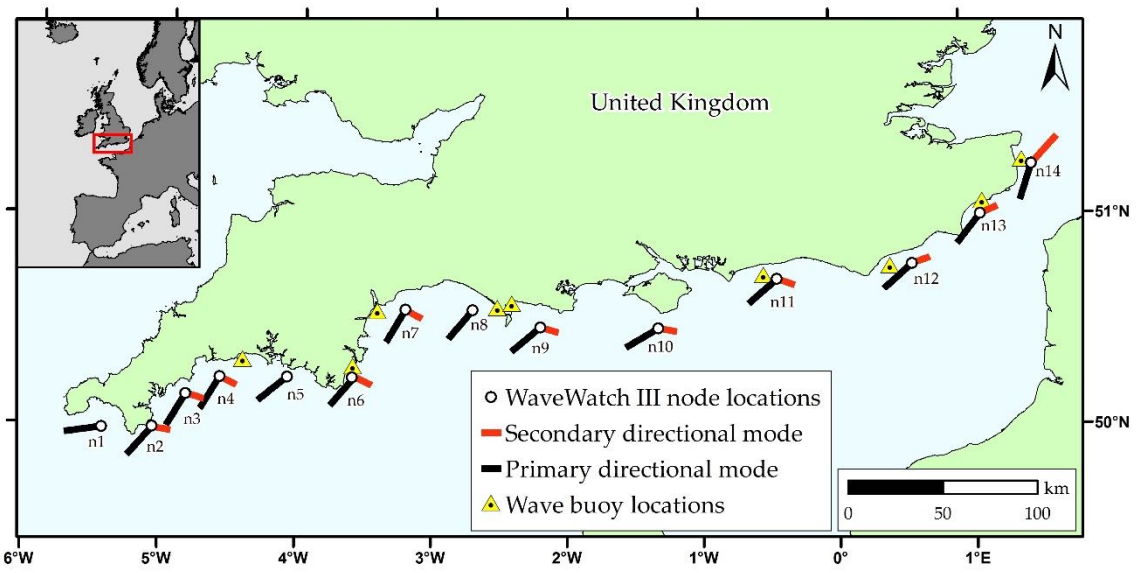

Figure 3.4. Bi-directional wave climate along the south coast of the English Channel, showing the primary directional mode in black and the second directional mode in red, averaged from a 36-year Wave Watch III modelled record. Inshore wave buoy locations are indicated by yellow triangles.

Despite the bi-directional nature of the wave climate, winter averages (DJFM) of directional wave power across all node locations for the 36-year period showed that south-westerly wave power was greater than easterly wave power (Figure 3.5a). The imbalance of directional wave power was less pronounced at inshore locations, as the wave characteristics were often modified by coastline orientation, potential shelter, refraction and shoaling due to inshore bathymetry and headlands. In addition to the modelled wave data, measured data from inshore wave buoy locations (Figure 3.4) were used to calculate the balance of southerly to easterly waves, with results displayed in Figure 3.5.

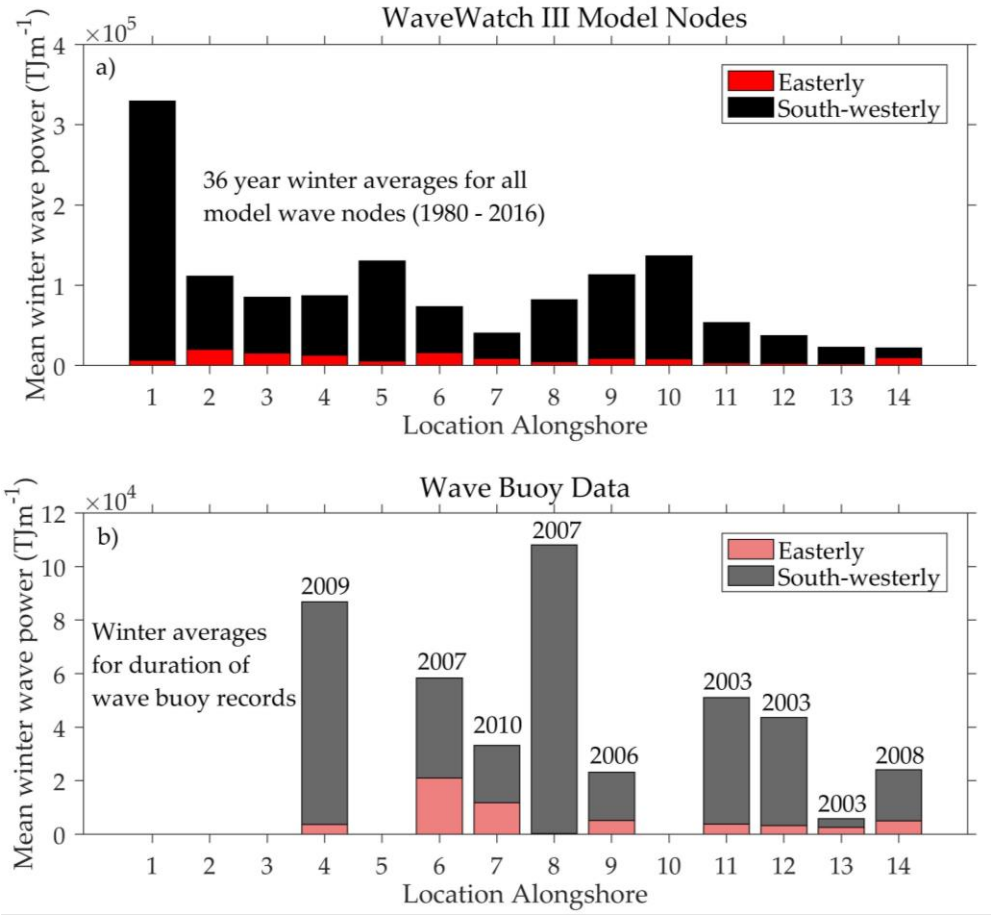

Figure 3.5. (a) Thirty-six-year long-term averages of winter (DJFM) wave power from both easterly (red) and southerly (black) directions for each offshore Wave Watch III model node, numbered from west to east (for locations, see Figure 3.4). (b) Average winter (DJFM) wave power from both easterly (red) and southerly (black) directions for inshore wave buoys closest to the respective node location. The year of wave buoy installation is labelled above each bar, and the record period runs from that year until 2016.

At locations where there was a degree of shelter from south-westerly waves (e.g., buoy locations closest to Nodes 6, 7 and 9), measured inshore total wave power averages were lower than those modelled offshore, and easterly waves contributed a larger percentage to the winter average balance of the two wave directions. For example, over the same time period (2007–2016), the winter averaged contribution of easterly wave power increased from 16% offshore at Node 6 to 39% of the total wave power measured at the closest inshore wave buoy (Start Bay, Devon). Similar increases in easterly wave contributions were seen at Node 7 (15% offshore to 45% inshore) and Node 9 (5% offshore to 28% inshore).

Despite the average dominance of south-westerly to easterly waves, at all bi-directional node locations, there was significant inter-annual variability between directional dominance. As a result, calculated values of WDI indicated years where south-westerly or easterly waves were higher than average. An example time series is shown in Figure 3.6 and highlights the inter-annual variability for Node n6.

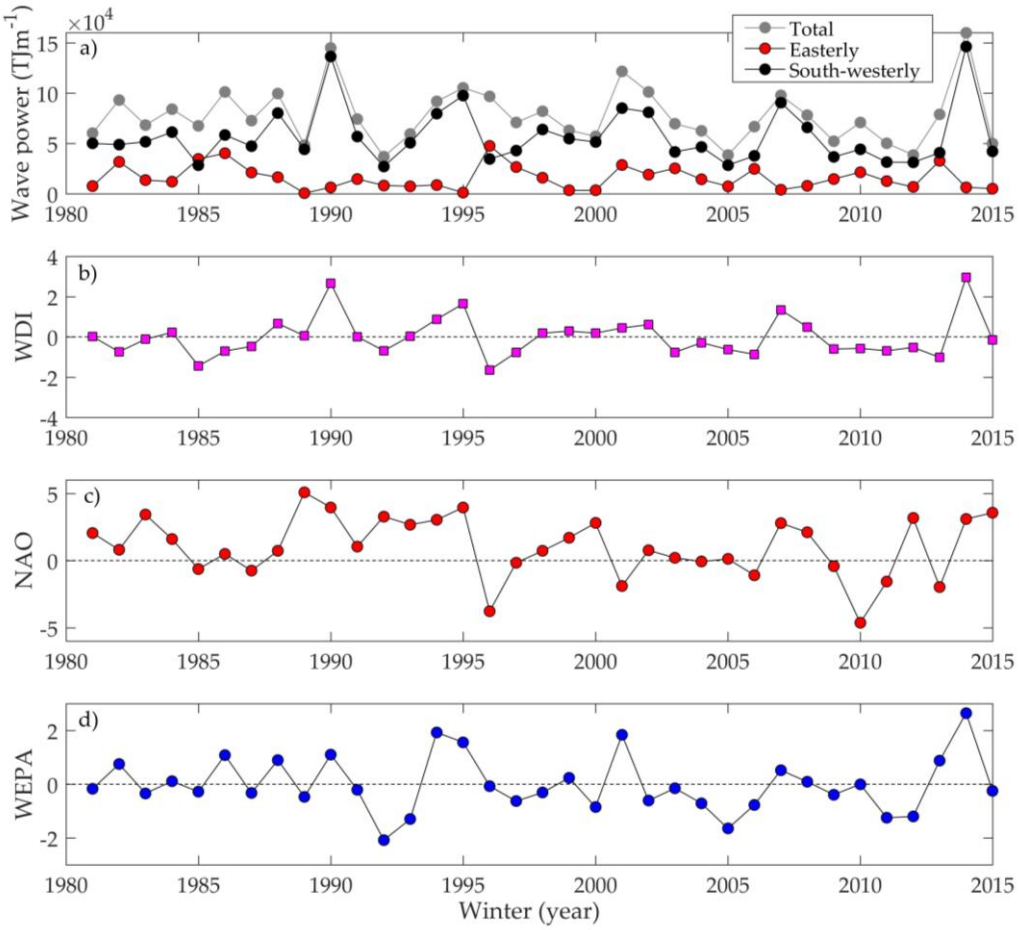

Figure 3.6. Winter average (DJFM) values of wave climate parameters for the Node n6 located off Start Bay showing: (a) 36 years of winter average total wave power (grey), easterly wave power (red) and south-westerly wave power (black) and (b) winter averages of the WDI showing the balance of south-westerly wave power (positive values) or easterly wave power (negative values) compared to the long-term mean. Winter (DJFM) averages of atmospheric indices showing (c) values of NAO and (d) values of WEPA.

The majority of winters were dominated by south-westerly wave power (Figure 3.6a); however, easterly wave power was greater than south-westerly for some winters (e.g., 1985 and 1996). Those high energy easterly winters were reflected in the two greatest negative values of the WDI (Figure 3.6b). Similarly, winters with the highest values of south-westerly wave power, with little contribution from easterly waves, showed the highest positive values of WDI (i.e., 1990, 1995, 2007 and 2014).

Variations in the winter averaged values of NAO and WEPA (Figure 3.6c and Figure 3.6d) were correlated against wave power contributions and the WDI at this node, and

the results are displayed in Table 1. NAO was strongly negatively correlated with easterly wave power, whilst WEPA was strongly positively correlated with south-westerly wave power. The WDI was significantly and positively correlated with both climate indices, suggesting there was some atmospheric control on wave climate.

Table 3.1. Pearson's correlation coefficients for atmospheric and wave climate variables, obtained from WaveWatchIII model data from Node n6 (see Figure 3.4 for location). Correlations between winter averages (DJFM) of total wave power, south-westerly wave power, easterly wave power, WDI, NAO and WEPA are presented, with correlations significant at the 95% confidence limit presented in bold.

Variable	**Total Power**	**SW Power**	**E Power**	**WDI**	**NAO**	**WEPA**
Total Power		**+0.88**	+0.18	**+0.68**	+0.02	**+0.84**
SW Power			−0.29	**+0.94**	**+0.37**	**+0.75**
E Power				**−0.59**	**−0.75**	+0.12
WDI					**+0.58**	**+0.59**
NAO						+0.07
WEPA						

Expanding the analysis across all model nodes and the full spatial extent of the study, wave climate parameters along the length of the English Channel exhibited variable relationships with atmospheric indices (Figure 3.7). At the eastern end of the English Channel, both total (Figure 3.7a) and south-westerly (Figure 3.7b) wave power were positively and statistically (95% confidence interval) correlated with NAO.

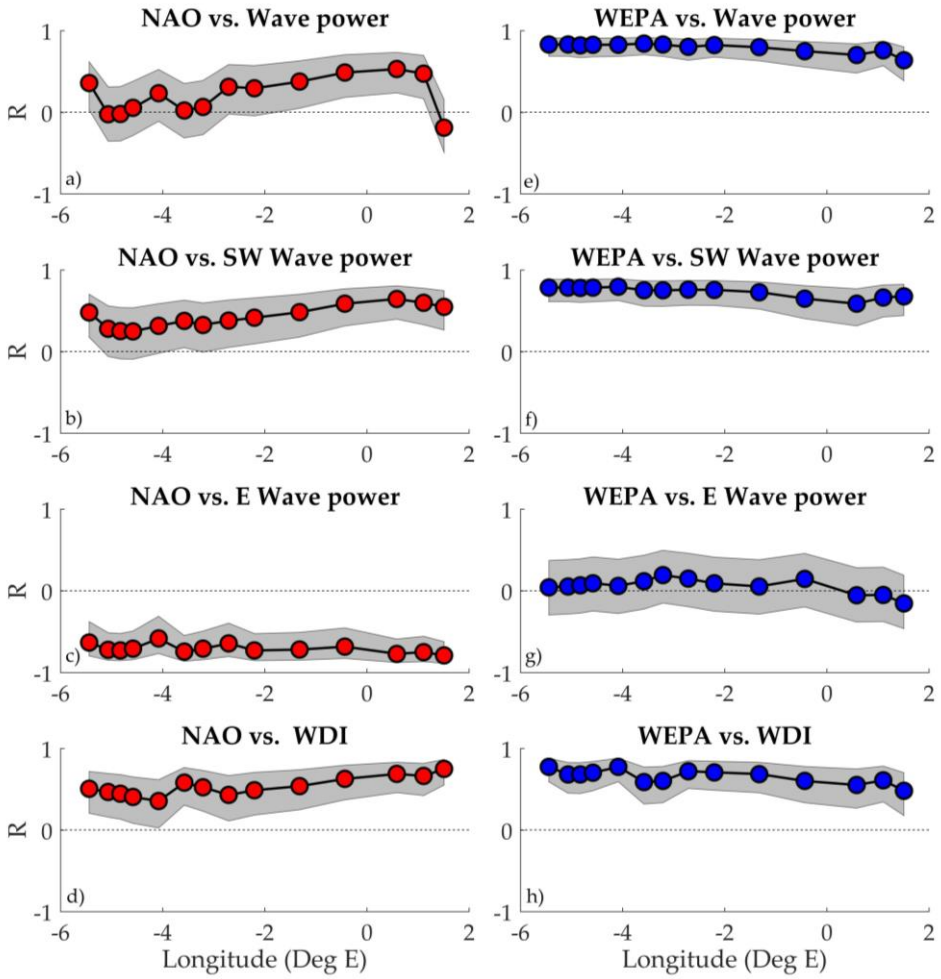

Figure 3.7. Correlations between winter NAO with (a) total winter wave power, (b) south-westerly wave power (P_{Dir1}), (c) easterly wave power (P_{Dir2}) and (e) WDI. Additional correlations are shown between winter WEPA with (e) total winter wave power, (f) south-westerly wave power (P_{Dir1}), (g) easterly wave power (P_{Dir2}) and (h) WDI. In all plots, 95% confidence bounds are shown by the grey shaded boxes.

Correlations with south-westerly wave power at the western end were positive, but weak and lacked significance. In contrast, NAO showed a very strong negative correlation with easterly wave power at all locations along the full length of the coastline (Figure 3.7c). Conversely, WEPA showed a significant and positive correlation with total wave power (Figure 3.7e) and south-westerly wave power (Figure 3.7f) along the full length of the channel, with the strongest correlations and increased significance apparent at the western extent. There was no significant correlation between WEPA and easterly wave power at any node location (Figure 3.7g). The WDI

was positively and significantly correlated with both NAO and WEPA along the full length of the coastline (Figure 3.7d and Figure 3.7h).

3.3.2 Morphological response to wave forcing

For all 22 sites analysed in this study, the BMR was calculated and is presented geographically in Figure 3.8.

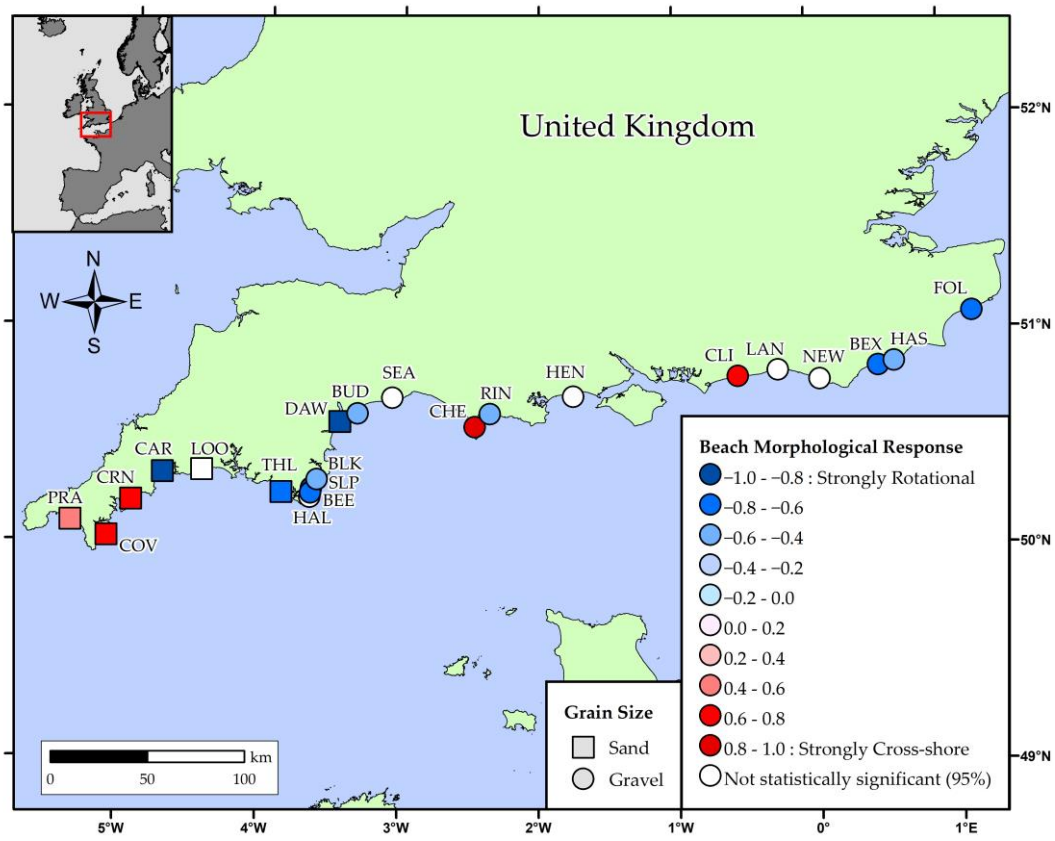

Figure 3.8. Beach morphological response at 22 coastal locations along the length of the south coast of England, U.K., calculated from multi-annual survey records. The strength and direction of the morphological response is indicated by the strength and colour of markers, with strongly rotational (cross-shore) sites identified by dark blue (red) colours. White markers indicate sites in which the behavioural response is insignificant at the 95% confidence limit ($p > 0.05$). Square markers indicate sand sites, whilst circles indicate gravel beaches.

Sites with highly negative correlations such as Carlyon Bay (CAR), $R = -0.82$, Slapton Sands (SLP), $R = -0.86$ and Dawlish (DAW), $R = -0.87$ suggest that the beach response was highly rotational, with the two opposing beach ends responding out of

phase with each other, likely attributable to longshore sediment transport. At other locations, where BMR values were positive, for example Climping Harbour (CLI), R = 0.78, Praa Sands (PRA), R = 0.50, and Chesil Beach (CHE), R = 0.85, both ends of the beach appeared to be responding together, and the beach gained or lost volume as a single unit, suggesting transport was cross-shore dominated and spatially uniform across the beach length.

BMR values for each site are displayed relative to their average shore normal angle in Figure 3.9a, with the majority of sites that demonstrated significant negative (rotational) BMR values, orientated to face southeast, with average shore normal angles less than 180°. For sites with significantly positive (cross-shore) BMR values, beaches tended to face southwest (shore normal angles greater than 180°), towards the incoming dominant south-westerly waves. In addition, at all sites, for each time step of the survey record, the RI was linearly regressed against the WDI for the period between morphological surveys. The correlation between the two is presented in Figure 3.9b. Where correlations were positive, clockwise beach rotation occurred with increased positive values of the WDI, with dominance of south-westerly over easterly waves, and anti-clockwise rotation occurred where there was a reversal in wave directional dominance. Where correlations were negative, the opposite was true, with anti-clockwise rotation of the beach state under increased south-westerly waves. For all significant correlations, beach locations that exhibited clockwise rotation to increased WDI values were facing south east, with a shore normal angle that split the angle of the two bi-directional wave modes (south-westerly and easterly).

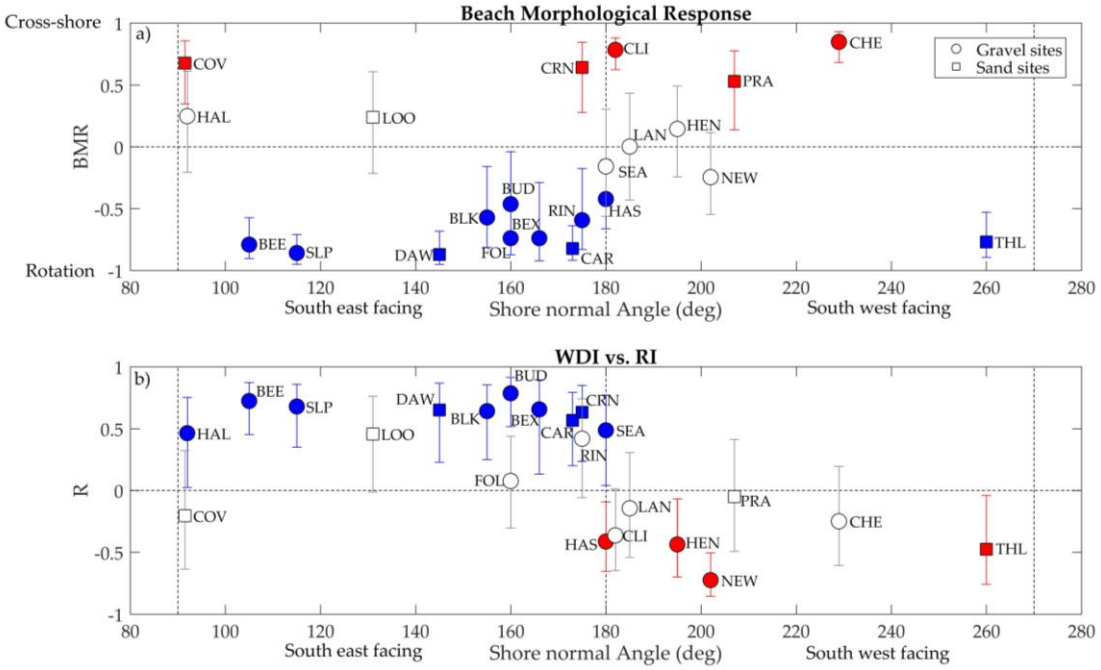

Figure 3.9. (a) Average shore-normal angle for each morphological site, plotted against its Beach Morphological Response (BMR) value. (b) The average shore-normal angle of coastline for each morphological site, plotted against the linear correlation coefficient (R) between the WDI and RI. Vertical dashed lines display the 90° and 180° shore-normal angles, with the areas in between representing south-easterly- and south-westerly-facing beaches. In both plots, gravel sites are denoted by circles, and sand sites by squares. Where site markers are white, correlation coefficients are not statistically significant at the 95% confidence limit ($p > 0.05$).

In addition to the shore normal angle, average beach slope (berm crest to MLWS) was calculated for each site and plotted against values of BMR (Figure 3.10). Sites with steeper slopes ($\tan\beta > 0.08$) displayed statistically significant rotational values (negative BMR values). The majority of sites displaying cross-shore morphological responses (positive BMR values) had shallower slopes, with $\tan\beta < 0.08$ for all but one site, Chesil (CHE). Additionally, most cross-shore responses were found at sand beaches, whereas rotational responses were more apparent at steeper, gravel beaches.

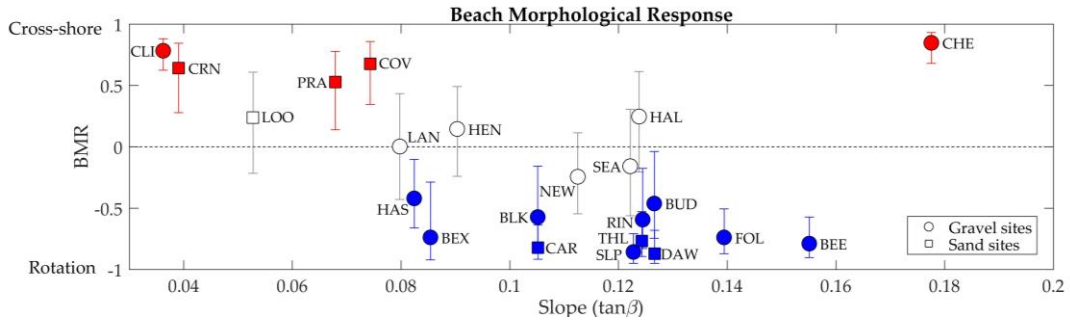

Figure 3.10. Average beachface slope (tanβ), plotted against its BMR value. Gravel sites are denoted by circles and sand sites by squares. Where site markers are white, correlation coefficients are not statistically significant at the 95% confidence limit ($p > 0.05$).

3.3.3 Atmospheric control of morphological response

As shown previously, the WDI imparts strong controls on rotational beach behaviour at many of the south east-facing sites assessed in this study. Given the significant correlations of WDI with both NAO and WEPA, direct connections between atmospheric indices and beach rotation were investigated. Slapton Sands (SLP), a long gravel barrier beach, and Carlyon Bay (CAR), a shorter, sandy embayed beach, both displayed strong rotational beach morphological responses over the duration of the study, and in both cases, RI was significantly correlated to WDI. Both sites had relatively complete morphological datasets, and the direct linear regression of RI against NAO and WEPA is displayed in Figure 3.11.

Both sites displayed a weak positive correlation between the RI and NAO (Figure 3.11a and Figure 3.11c); however, both were statistically insignificant ($p > 0.05$). In contrast, both sites displayed a strong, significant positive correlation (Figure 3.11b and Figure 3.11d) between winter values of WEPA and the RI (Slapton Sands, $R = 0.88$; Carlyon Bay, $R = 0.86$). For both locations, the strongest positive (negative) RI values were associated with positive (negative) values of both NAO and WEPA, resulting in clockwise (anti-clockwise) rotation.

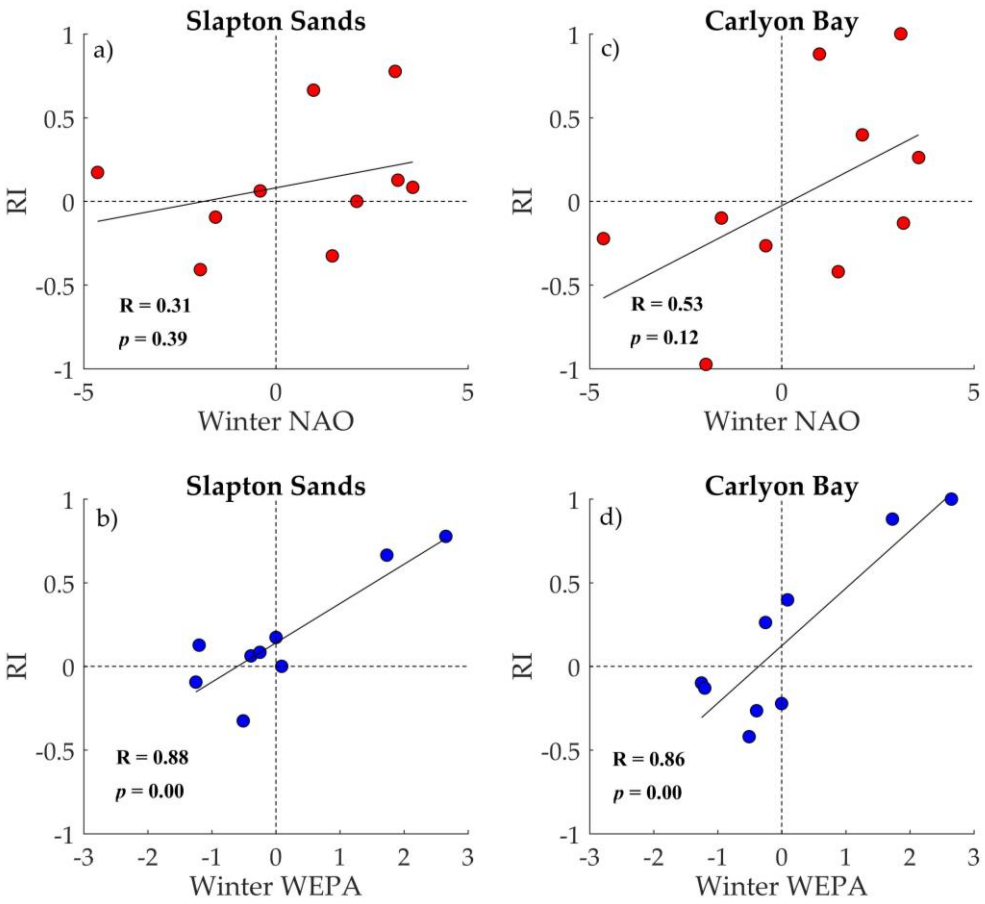

Figure 3.11. Direct correlations of the winter RI at Slapton Sands with winter values of (a) NAO and (b) WEPA. Additional correlations of winter RI at Carlyon Bay with winter values of (c) NAO and (d) WEPA.

3.4 Discussion

This chapter identified a bi-directional wave climate along the length of the English Channel, with dominant waves arriving from south-westerly directions and secondary modes coming from the east. Variability in the contribution of both modes of wave direction, and their relative balance over winter averaged seasons, has been shown to correlate well with the NAO and WEPA climate indices. Whilst winter wave height anomalies in the northern latitudes of the north east Atlantic Ocean were well correlated with both NAO and WEPA by Castelle et al. (2017), Malagon Santos et al. (2017) concluded that WEPA was better suited to predicting increased wave height in the south west region; however, directionality was not taken into account, and the results of the

current chapter show that wave bi-directionality is also linked to NAO and WEPA along the entirety of the English Channel. Easterly wave power contributions were well correlated to negative phases of the winter NAO whilst high contributions of south-westerly waves were correlated with positive values of winter WEPA. Both indices had some spatial variability in their influence on wave conditions along the coastline, with WEPA imparting a stronger control in the western extent of the channel whilst NAO was shown to have stronger, more significant correlations in the eastern reaches.

Chapter 2 presented the site-specific evidence of beach rotation at an embayed series of interlinked gravel barriers, and suggested that the WDI could be used to predict alongshore changes in beach morphology at similar semi-sheltered sites over different timescales. Within this chapter, several beach sites had been identified that displayed rotational behaviour, with beach extremities responding out of phase with each other. It must be noted that only intertidal beach volumes have been assessed within this chapter, and in some cases, rotational signals may be weakened or obscured due to exchanges occurring from the inter-tidal to sub-tidal domain. In almost all significant cases, beach rotation appeared to be linked with shoreline alignment, with coastlines oriented towards the south east, experiencing the most oblique incident waves under dominant south-westerly conditions, driving clockwise beach rotation, whilst counter rotating under easterly waves.

Where sites faced south west, towards the angle of dominant south-westerly wave approach, significant cross-shore morphological responses were observed, with both ends of the beach gaining or losing volume at the same time. This response is likely attributable to increased exposure to south-westerly waves and perhaps increased shelter, and reduced influence, from easterly waves. Burvingt et al. (2016) observed a similar result, identifying a strong relationship between shoreline orientation and beach

rotation, at a multitude of south-easterly-facing beaches following an exceptionally energetic winter season, dominated by south-westerly storm events (Masselink et al., 2015, 2016; Scott et al., 2016). Despite their observations only spanning a single winter season, rotational behaviour was consistent within the western beaches of the English Channel and was furthermore correlated to normalised beach length (not assessed in this thesis), with longer, narrower beaches experiencing greater levels of rotation. Additionally, the studies conducted by Burvingt et al. (2016) and Scott et al. (2016) both identified the same cross-shore response at south west-facing beaches, where dominant storm waves approached from a shore-normal angle, although the wave climate at these locations under the observed winter period was unidirectional. Within this chapter, beach slope and sediment type were also found to impart some control on the observed morphological responses (Figure 3.10). Steeper, predominantly gravel beaches, exhibited rotational behaviour, and shallower, sandier beaches displayed a cross-shore response; however, quantitative assessment of beach grain size was not conducted here.

Where rotational behaviour was identified in this chapter, the RI at each site was well correlated with the WDI, especially for south-east facing beaches, implying that the magnitude and direction (clockwise/anti-clockwise) of beach rotation is controlled by the balance of south-westerly to easterly wave power. This agrees with the findings of Chapter 2, which presents evidence of clockwise and anti-clockwise rotation under south-westerly and easterly winters, respectively. Similar results of beach rotation at the same location were presented by Ruiz de Alegria-Arzaburu and Masselink (2010), for contrasting storm events from opposing directions. Although their results showed agreement with the results of this chapter, in that the balance of contrasting wave directions controls the rotational beach state, they also noted that storm-induced sediment transport rates may be asymmetrical between the two wave directions, given

the shoreline angle and differing wave types. This may also explain why there are some anomalous results within the regional assessment. For example, both Coverack beach (COV) and Hallsands (HAL) displayed a cross-shore BMR response (Figure 3.9a), despite being the most easterly facing beaches in the analysis. At both locations, shelter from south-westerly waves is provided by proximity to prominent headlands, meaning exposure to oblique south westerlies may be limited, and approaching easterly waves are shore-normal. Additionally, both beaches are very short in length, which is less conducive to rotation, as suggested by Burvingt et al. (2016, 2017). Additionally, the morphometric parameters of headland geometry in relation to the incoming wave climate can lead to wave shadowing from different directions, inducing gradients in alongshore wave energy. In some cases, this can result in beach rotation as a function of variable cross-shore exchanges at different alongshore locations (Harley et al., 2011, 2015), rather than directly due to changes in dominant wave direction.

Due to the strong correlations between atmospheric indices and wave climate, in addition to the significant link between WDI and RI, beach rotation may potentially be inferred from atmospheric indices, perhaps allowing wave climate to be omitted when assessing coastline vulnerability to erosive rotational events. For the majority of sites presented in this chapter, RI was not significantly well correlated with either winter NAO or winter WEPA, at the timescales assessed here. This is potentially due to the limited temporal dataset, restricting available data points to no more than 10 years; however, both Slapton Sands and Carlyon Bay did show strong BMR values (Figure 3.9a), correlations between RI and WDI (Figure 3.9b), and a statistically-significant positive correlation between RI and winter WEPA (Figure 3.11b and Figure 3.11d). This consistency within the analysis suggests that positive (negative) rotation may be predicted at each site with positive (negative) winter forecasts of WEPA.

Despite both sites showing statistically insignificant correlations between RI and winter NAO, the index should not be ignored. For the south-east facing beaches, it is likely that strong negative NAO winters result in increased easterly wave events, reducing the extent of winter-induced clockwise rotation, as a result of south-westerly waves. Conversely, when both the NAO and WEPA are in phase, it is likely that the combined influence of the two indices may amplify the effects of rotation, whether clockwise or anti-clockwise. This is apparent from the synchronous high values of the NAO and WEPA during the winter of 2013/2014, recently described as the most energetic since at least 1953 (Masselink et al., 2015, 2016; Scott et al., 2016). During that winter, significant clockwise rotation was observed at many south coast locations, leaving coastal communities and infrastructure at risk from future storm events. Both Slapton Sands and Carlyon Bay experienced their largest rotation in the 10-year survey record during the 2013/2014 winter, well described by high values of both WEPA and NAO (Figure 3.11), despite Castelle et al. (2017) identifying that NAO and WEPA indices were not correlated. The combination of high values for both indices within the same winter led to higher than average wave heights in the North Atlantic (Castelle et al., 2017) and storms tracking more southerly than usual (Masselink et al., 2016). Similar signals of enhanced beach rotation have been observed under several winters with increased El Niño (negative ENSO) along the coast of the Pacific North West (Peterson et al., 1990). Many dissipative sandy beaches were observed to rotate anti-clockwise (northwards) under large storm waves approaching from increased southerly directions (Anderson et al., 2018); however, their findings were somewhat different from those found here, as this chapter has identified opposing wave directions under climate variability, rather than subtle shifts in average wave angle and storm wave height.

In many cases, associated recovery (reversals in direction) of beach rotational events can take several years (Scott et al., 2016), particularly if sediment is transported out of

littoral cells around headlands (Scott et al., 2016; Valiente et al., 2019; Wiggins et al., 2019a) and directional longshore transport is asymmetrical (Ruiz de Alegria-Arzaburu and Masselink, 2010). A key example is the embayment scale rotation observed in Start Bay following the winter of 2013/2014, where 294,000 m^3 of gravel were recorded as bypassing significant headlands, leaving littoral sub-cells depleted of volume (presented in Chapter 2). As of 2018, measurements have shown that despite some reversals in wave directions (Wiggins et al., 2019a), the material has yet to return to its original cell, and the embayment continues to maintain its decadal-scale rotation northwards.

Despite this chapter evidencing that individual climate indices have a regional impact on wave climate, combinations of multiple indices may be required for direct predictions of bi-directional wave climates and rotational beach behaviour across larger spatial scales. At site-specific locations, where increased beach rotation poses a risk to sea defences, tourist infrastructure, roads and ecological and environmental assets, even qualitative predictions of rotational direction, or timescales of recovery, derived from forecast climate indices would be a welcome addition to the tools available to coastal managers.

Recent improvements to seasonal forecasts of winter NAO (Scaife et al., 2015; Dunstone et al., 2016; Wang et al., 2017) mean that year-ahead estimates of beach response may be possible, especially for regions similar to those assessed here, where many sites are identified as having a highly-rotational BMR. This would allow coastal managers and engineers to prepare for potential winter rotational impacts, taking a pro-active approach to either soft engineering works (e.g. beach recycling/recharge) or hard coastal defences.

3.5 Conclusions

Strong bi-directionality of the winter wave climate along the south coast of England was identified at 14 model node locations, with south-westerly waves dominant over easterly waves. The winter averaged atmospheric indices of NAO and WEPA were strongly negatively and positively correlated with easterly and south-westerly waves, respectively.

The morphological response of 22 beach locations was assessed over a decadal timescale (winter seasons). Eleven of these sites displayed a statistically-significant rotational beach morphological response, with rotation being strongest at south east-facing beaches, attributed to increased obliquity to both the south-westerly and easterly wave directions. A cross-shore response was identified at south west-facing beaches, with limited rotation observed as beaches tend towards the dominant direction of wave approach.

Of the rotating beaches, eight of the 11 were gravel beaches, and all had relatively steep beachfaces ($\tan\beta > 0.08$). Cross-shore beach responses were more prominent in sandy beaches with shallow beachface slopes ($\tan\beta < 0.08$).

The rotation index, calculated from morphological beach volume change, and an index of the balance of directional wave power were significantly positively correlated with each other at the majority of south-east facing, rotational sites.

4 Predicting beach rotation using multiple atmospheric indices

The previous chapter identified correlations between the winter WDI and both winter climate indices (NAO and WEPA), across a regional scale, which naturally leads research into the potential of combining the two indices to improve the predictive skill. This final results chapter assesses to what level the winter WDI can be predicted from atmospheric indices and attempts to verify this over a centurial scale of beach rotation for the case of Start Bay (specifically Slapton Sands).

This chapter contains work published in Marine Geology: Wiggins, M.; Scott, T.; Masselink, G.; McCarroll, R.J: Russell, P.; 2020, Predicting beach rotation using multiple atmospheric indices. Marine Geology, 426, 106207.

4.1 Introduction

Predicting shoreline change and evolution is an ever-growing issue for coastal managers, engineers and communities, particularly in light of observed and forecasted sea level rise (Nicholls et al., 2011). Whilst increases in storminess and significant wave height (Dodet et al., 2010) have been shown to cause significant cross-shore erosion of exposed beaches (Burvingt et al., 2016; Masselink et al., 2016; Scott et al., 2016), beach rotation due to longshore sediment transport under changes in the incoming wave direction (Klein et al., 2002), plays an equally important role in coastal vulnerability for many semi-sheltered embayments with bi-directional wave climates (Ruiz de Alegria-Arzaburu and Masselink, 2010; Wiggins et al., 2019a). Single storm events and annual winter rotational responses can leave embayments depleted of sediment at the up-wave extent, reducing overall beach volume and increasing the risk of damage, flooding and cliff retreat. If the wave climate maintains a bias towards a particular direction over

multi-annual to decadal timescales, these potential risks increase, due to the lack of recovered beach volumes, reducing the protection offered against damage under storm wave attack.

Understanding the controls that wave power and direction have on beach response has been investigated globally, with phases of atmospheric indices showing strong links to wave height and direction on local to basin-wide scales (Ranasinghe et al., 2004; Barnard et al., 2015; Harley et al., 2017). Within the North Atlantic, recent studies have identified both the North Atlantic Oscillation (NAO) and West Europe Pressure Anomaly (WEPA) as playing a significant role in controlling both the winter-averaged wave height and dominant wind directions (Bacon and Carter, 1993; Dodet et al., 2010; Castelle et al., 2017, 2018). Positive phases of the NAO have been shown to predict increased winter wave height and westerly winds in the upper latitudes of the North Atlantic, northward of 52° N, whilst positive phases of WEPA outscore other indices in predicting increased wave heights southward of this latitude, until the coast of Portugal (Castelle et al., 2018). Along the entire length of the south coast of the U.K. (<52° N), where waves are bi-directional (south-westerly and easterly), Chapter 3 highlighted that winter NAO and WEPA were best suited to predicting easterly and south-westerly winter-averaged wave power, respectively, with weak or no correlation in their opposite directions. In turn, the beach response for many south-east facing beaches along the same coastline, showed rotation was controlled by the Wave Directional Index (WDI), defined as the standardised winter power balance between the primary and secondary winter wave directions (Wiggins et al., 2019a). Despite the strong correlations between WDI and beach rotation, individually, NAO and WEPA were only weakly positively correlated with the WDI, and only significantly correlated with beach rotation in two of the 22 measured locations.

Given the current state of winter NAO forecasting (Scaife et al., 2015; Dunstone et al., 2016; Weisheimer et al., 2017), and the ability to predict several months ahead for the coming winter season, any improvements to our understanding of the relationship between atmospheric indices and morphology could lead us towards season ahead beach response forecasts for rotational sites, a tool that would be welcomed by coastal managers from local to regional scales. Furthermore, an improved relationship between climate variability and beach response could offer the capability to investigate historic beach state, providing a representative indicator of potential future variability, and place the observed contemporary changes into a longer-term context. For example, centurial-scale reconstructions of the NAO (Cook et al., 2002; Trouet et al., 2012; Faust et al., 2016) and the use of proxy records to model the NAO as far back as 3000BP (e.g. Baker et al., 2015), suggest that low frequency fluctuations of significant magnitude have occurred over multi-centurial timescales, many of which have been linked to well documented climate anomalies (e.g. Mediaeval Climate Anomaly, Little Ice Age), causing variations in precipitation, temperature and storminess, potentially driving large scale morphological activity such as sustained coastal dune transgression (Clarke and Rendell, 2006; Jackson et al., 2019). This chapter aims to investigate whether an improved relationship between climatic indices and winter WDI can be obtained by multivariate analysis, helping to place our current observations of wave climate controls on beach rotation into context with centurial scale fluctuations, allowing for proactive decisions in terms of long-term planning and coastal management.

4.2 Study site

Start Bay lies along the south coast of Devon, United Kingdom (50.27° N, 3.65° W), facing south east into the English Channel. The embayment consists of four interconnected coarse gravel barriers (D_{50} = 2 - 10mm), backed by freshwater lagoons

and separated at high tides by protruding rocky headlands and shore platforms. Aligned from south-west to north-east, its wave climate is bi-directional, consisting of predominantly diminished Atlantic swell waves from the south-west and short fetch easterly wind waves from the English Channel. Offshore wave angles are modulated by the presence of Skerries Bank (McCarroll et al., 2020) and Start Point (Figure 4.1), which refract and attenuate south-westerly waves to become southerly at the shoreline, whilst easterly waves maintain their angle as they propagate into the bay.

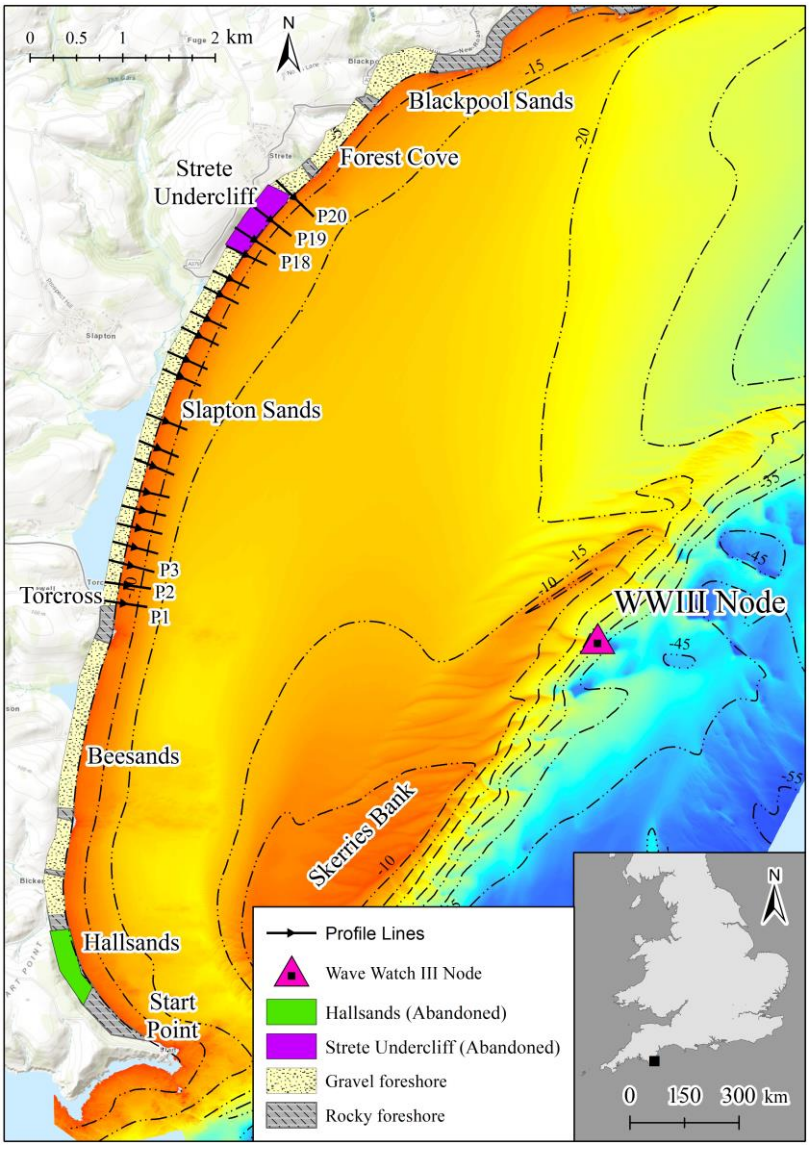

Figure 4.1. Location map of Start Bay with bathymetric contours (UKHO, 2013) and WW3 (U.K. Met Office) model node location. Topographic profile survey line locations are displayed as black arrows. The locations of two abandoned villages are displayed by the coloured polygons located towards the northern and southern ends of the embayment.

The southerly and easterly wave angles drive northward and southward sediment transport respectively, and the embayment is continually in a state of dynamic equilibrium, with the planform shape rotating in response to the current wave approach. The full embayment sediment cell as a whole, was demonstrated to be closed in Chapter 2, bounded by significant northern and southern headlands; however, beach rotation and exchange of sediment between the individual sub-embayments was observed through headland bypassing under extreme wave conditions (McCarroll et al., 2019) and sustained periods of a particular wave direction (Wiggins et al., 2019a).

Both full-embayment and sub-embayment beach rotation has long been a concern within Start Bay, with significant historical and contemporary examples being the subject of numerous scientific studies (Hails, 1975a; Chadwick et al., 2005; Ruiz de Alegria-Arzaburu and Masselink, 2010; Wiggins et al., 2017, 2019a, 2019b; McCarroll et al., 2019). The loss of the old village of Hallsands in 1917 is one of the highest profile cases of coastal erosion impacts in the United Kingdom. Lying at the southern corner of Start Bay (Figure 4.1), its collapse into the sea during a severe easterly storm followed a sustained lowering of the beach level in the years earlier, largely attributed to the dredging of sub-tidal beach material between 1897 and 1902 (Worth, (1904), cited in May and Hansom, (2003)). In addition to the dredging, evidence suggests that beach lowering at this end of the embayment was exacerbated due to a coincidental shift in winter NAO to a sustained positive phase for almost 30 years from the commencement of dredging (1898), leading to increased southerly waves, and clockwise rotation of the beach under prolonged northward sediment transport (Wiggins et al., 2017). Historical accounts of an earlier lost village at the opposite end of Start Bay, suggests the local community may have formed settlements based on the rotation and planform of the beach. Strete Undercliff, a small fishing village formed during the early 17th century (Goodall, 2007) and located at the northern end of Slapton Sands (Figure 4.1), was

documented on early nautical maps (Denbigh, 2017), until its subsequent disappearance by 1780 (Waterhouse, 2009; Stranack, 2017), around the time the village of Hallsands (in the south) became more established. Despite the lack of quantitative data from this period, it could be suggested that due to the closed nature of the sediment budget within Start Bay (Wiggins et al., 2019a), variations in multi-decadal phases of wave direction may have influenced the settlement locations of the past and present communities of Start Bay.

More recently, during the winter of 2013/14, Start Bay's beaches experienced significant clockwise rotation under a single winter season characterized by unprecedented south-westerly storm events (Masselink et al., 2015; Scott et al., 2016; Wiggins et al., 2019a), leaving the southern ends of embayments depleted of sediment. This increased the vulnerability of coastal defences at southern beach extremities, and in the following winter years (2015 and 2016), lack of beach volume resulted in the undermining and collapse of sea walls at Torcross, Slapton Sands, and loss of infrastructure including the car park at Hallsands (BBC, 2014).

4.3 Materials and methods

4.3.1 Wave data

WaveWatchIII modelled wave data was obtained for a coastal node offshore of Start Bay (Figure 4.1) in approximately 20 m water depth. Total winter wave power was computed at each year for the period of December through March (DJFM), and subsequently split into contributions of the primary (south westerly) and secondary (easterly) directions, designated P_{Dir1} and P_{Dir2}, respectively.

The wave directionality index (WDI) was computed for each winter from 1980 to 2018 using equation (1) as set out in Chapter 2;

$$\text{WDI} = \frac{(P_{Dir1} - P_{Dir2}) - \overline{(P_{Dir1} - P_{Dir2})}}{\sigma(P_{Dir1} - P_{Dir2})} \quad \text{Eq. (10)}$$

where $(P_{Dir1} - P_{Dir2})$ is the difference in wave power between the primary and secondary wave directions, $\overline{(P_{Dir1} - P_{Dir2})}$ is the long-term mean and

$\sigma(P_{Dir1} - P_{Dir2})$ is the long-term standard deviation of that difference. Positive (negative) values of the WDI represent winter periods where the wave climate was more southerly (easterly) than average.

4.3.2 Atmospheric indices

Winter averaged (DJFM) atmospheric index values for the station-based NAO (based on the difference of normalized sea level pressure (SLP) between Lisbon, Portugal and Stykkisholmur/Reykjavik, Iceland since 1864) were obtained from The Climate Data Guide (downloaded from the National Centre for Atmospheric Research, https://climatedataguide.ucar.edu/). Additionally, values of the West Europe Pressure Anomaly (WEPA) were obtained via hindcasts of SLP between Valentia (Ireland) and Santa Cruz de Tenerife (Canary Islands), as developed by Castelle et al (2017) from Twentieth Century Reanalysis data (https://www.esrl.noaa.gov/psd/). Despite SLP derived NAO records being available as far back as the mid to late 1800s, and proxy reconstructions (described later in section 5) going even further up to 3000 years before present, records of WEPA only date back to 1906 due to limited SLP records and inconsistent hindcasts beyond this.

The previous chapter showed that individual wave power contributions from the primary and secondary wave directional modes are well correlated with WEPA and NAO respectively, along the entire length of the south coast of England. Chapter 2 also highlighted that winter values of the WDI for Start Bay are positively correlated with both NAO and WEPA, suggesting that a combination of the two indices may improve

the predictive skill (improved R^2 values) at this location. To assess this further, an empirical stepwise multi-linear regression (SMLR) model was constructed using both NAO and WEPA.

4.3.3 Modelled longshore sediment flux

A look-up table modelling approach was applied by McCarroll et al. (2020), for the period 1980 – 2018, to transform offshore wave conditions to breakpoint values in order to estimate alongshore wave power and potential longshore sediment flux within the Start Bay embayment. The estimated flux is 'potential' as the model assumes unlimited sediment availability. Bathymetry for the model was obtained using inshore multibeam (Wiggins et al., 2019a), combined with offshore multibeam from 2013 (UKHO, 2013). To generate the inshore wave conditions for the look-up model, Delft3D-WAVE was run in stationary mode for ~400 scenarios, covering the full range of naturally occurring boundary wave conditions. Boundary conditions for a 1980-2018 wave time series were obtained from a coarse-grid hindcast model (WaveWatchIII, U.K. Met Office). These boundary conditions were transferred to points along the 14-m depth contour using the look-up table approach. A simple refraction-shoaling parameterisation (Van Rijn, 2014) was used to transform waves from 14 m depth to the break point, with nodes at 25-m spacing. The breaking wave conditions were used to estimate alongshore wave power using linear wave theory. Alongshore sediment flux was estimated using the CERC equation (USACE, 2002), for a range of K-value coefficients (0.04 to 0.26). The output from the look-up model is a 38-year time series of longshore wave power and potential sediment flux, which was validated against prior model results and field observations (McCarroll et al., 2019). A detailed description of the model setup and forcing can be found within McCarroll et al. (2020). Total winter transport was summed for the DJFM months, and at each location, correlations were drawn between both the observed WDI and the predicted WDI.

4.3.4 Topographic data and rotation index

Since 2006, monthly RTK-GPS cross-shore profile surveys of Slapton Sands have been conducted by the University of Plymouth, labelled from south to north as "P1" to "P20", with average spacings of 250m (Figure 4.1). Pre-winter autumn and post-winter spring surveys along the length of the beach provide alongshore averaged volume change at the southern (P1 to P3) and northern (P18 to P20) ends, both of which have been shown to linearly correlate with winter values of the WDI (Wiggins et al., 2019a). The Rotation Index (RI), shown was computed for winter change as per Chapter 3, by subtracting the normalized winter volume change ($\mathrm{d}V_i$) at the southern end of the beach from the northern end, such that;

$$RI = \mathrm{d}V_i\ (north) - \mathrm{d}V_i\ (south) \qquad \text{Eq. (11)}$$

Positive values of the rotation index represent periods of clockwise northwards rotation and negative values indicate winters where anti-clockwise southward rotation has occurred.

4.3.5 Photographic rotation index

Despite the availability of high accuracy beach surveys from 2007 onwards, prior to this date, quantitative records of beach volume change are scarce. Any surveys that have been found lack consistency in both temporal and spatial frequency as well as method. As such, metrics for beach rotation have been obtained via proxy records of historic photographs, Ordnance Survey (OS) topographic maps and limited aerial photography. For the purposes of this study, beach width at Torcross (at the southern end of the Slapton Sands embayment, Figure 4.1) was chosen based on the availability of historical photographs taken from the same location (a prominent headland just south of the sea wall), and the significant negative correlation between measured beach

width/volume and the WDI over the period of 2007 to 2018 identified in Chapter 2. Additionally, this location of the beach was identified as being indicative of beach rotation, with a significant negative correlation with the northern end of Slapton Sands, implying beach width at one end of the embayment can be used as an indicator of beach rotation. In total, 32 oblique photographs were used, taken from the same location (dating from 1875 to 2019), without the need for rectification. In addition, seven sets of aerial photography (1944 to 2017), and three geo-rectified OS maps with high and low water contours (1887, 1852 and 1983) were also used. To assess historical changes in beach width with the limited dataset available, an integer scale of -2 ("Very Narrow") to +2 ("Very Wide") was assessed qualitatively (as shown in Figure 4.7), based on manual interpretation of the entire dataset, providing a simple, categorical metric of relative beach width for each dated photograph and map for this location. The range of observed beach widths was taken into account in devising the scale, from the most accreted in 1890, to most eroded in 2016.

4.4 Results

4.4.1 WDI predictions from atmospheric indices

Initial exploration of the relationships between the WaveWatchIII-derived WDI (WDI_{WW3}) with NAO and WEPA for a 38 year timeseries between 1980 and 2018 show statistically significant ($p < 0.05$) positive correlations (Figure 4.2); however, relative skill (R^2 values) in predicting the WDI_{WW3} is low for both indices ($R^2 < 0.31$).

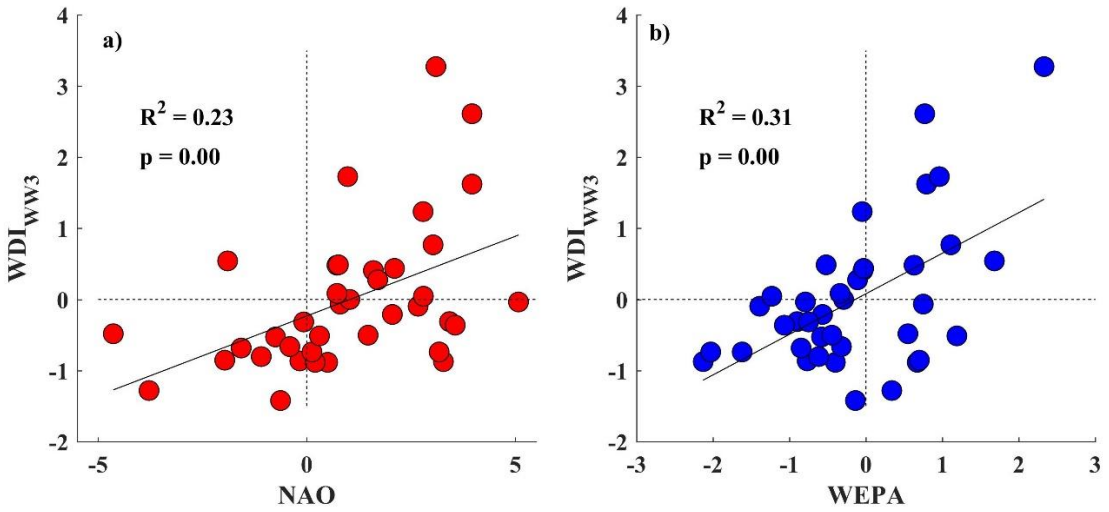

Figure 4.2. Correlations between winter averaged atmospheric indices NAO, WEPA and the WDI_{WW3} for the period of 1980 to 2018.

A SMLR model was created using both NAO and WEPA as predictor variables, with results suggesting that a regression model computed from a combination both NAO and WEPA variables provide improvement in the skill of predicted WDI (WDI_{Pred}). First and second order polynomial models were tested, in addition to two-term exponential regressions, with a linear fit offering the most explanatory power in predicting the WDI_{Pred}, such that:

$$\mathrm{WDI_{Pred}} = \beta_0 + \beta_1 \mathrm{NAO} + \beta_2 \mathrm{WEPA} \qquad \text{Eq. (12)}$$

where β_0 represents the intercept and β_1 to β_2 are coefficients of the predictor variables, with their estimates, confidence bounds and statistics shown in Table 4.1.

Table 4.1. SMLR model statistics for predictor variables used for modelling winter values of the WDI.

Coefficient	Predictor	Estimate	Lower (95%)	Upper (95%)	SE	tStat	P-value
β_0	(Intercept)	-0.19	-0.41	0.03	0.11	-1.78	0.083
β_1	NAO	0.29	0.19	0.38	0.05	6.11	5.54×10^{-7}
β_2	WEPA	0.69	0.48	0.90	0.10	6.74	8.36×10^{-8}

Overall improvements to the predictive skill (R^2) of combining the indices are shown in Table 4.2, with the RMSE reducing from 0.9 when using NAO alone, to 0.60 when using NAO and WEPA. Similar improvements are seen when assessing the R^2 value, with an improvement of from 0.23 to 0.66 ($p = 4.71 \times 10^{-10}$). The coefficients for the two indices (Table 4.1) show that WEPA contributes more (0.69) to the overall predicted values of the WDI_{Pred} than NAO (0.29).

Table 4.2. Improvements to the SMLR models statistics for a range of input variables and sum index used for predicting winter values of the WDIPred.

Predictor Terms	**RMSE**	**R-squared**	**P-value**
NAO	0.90	0.23	2.39 x 10-3
WEPA	0.86	0.31	3.15 x 10-4
NAO + WEPA	0.60	0.66	5.08 x 10-9

Outputs of WDI_{Pred} for the period of the modelled wave data (Figure 4.3) show the addition of both indices reproduce the winter WDI_{WW3} values with an R^2 value of 0.66.

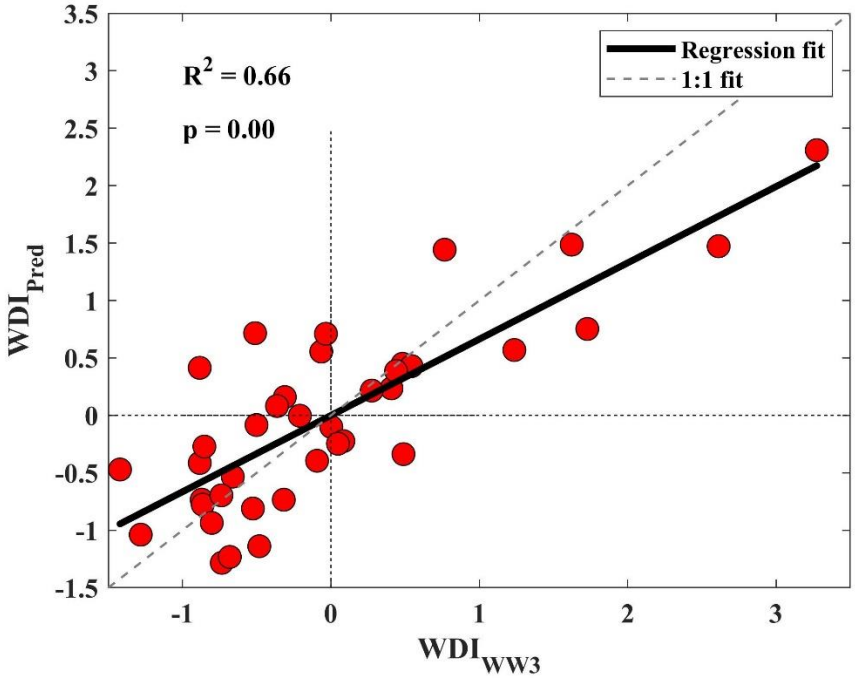

Figure 4.3. WDI_{WW3} for the winter periods of 1980 to 2018 plotted against WDI_{Pred} predicted using a SMLR model of winter atmospheric indices. The regression fit is shown as the bold line, whilst the 1:1 fit is displayed as the dashed grey line.

Using the regression model, values of NAO and WEPA are used to hindcast the WDI_{Pred} back to the beginning of the record of atmospheric indices (1906). The predicted output can be seen in the top panel of Figure 4.4, with the accumulated value of the WDI_{Pred} plotted in the middle panel.

Clear inter-annual variation can be seen within the long-term WDI_{Pred} values (Figure 4.4a); however, there are periods of sustained negative or positive winter values, persisting for up to five years in a row (e.g. 2008 to 2013). Despite the high R^2 value between the WDI_{WW3} and the WDI_{Pred} hindcast from atmospheric indices (for the overlapping period of 1980 to 2018, Figure 4.3), there are some years where the sign of the WDI_{Pred} is opposite to the WDI_{WW3}, e.g. 2000 to 2003. This can be attributed to years where winter averaged values of NAO and WEPA are low (close to zero) or opposite in sign, leading to the larger of the two indices impacting the WDI_{Pred}. In addition, although the regression analysis was conducted using a linear relationship, the fit between winter averaged climate indices and WDI_{WW3} is not perfectly linear,

especially for extremely high values of NAO and WEPA within the limited 37-year timeseries (Figure 4.2). This explains why the regression model under predicts the value of the WDI_{Pred} for some years; however, in the majority of cases where the WDI_{WW3} is either highly positive or negative, hindcast values of the WDI_{Pred} share the same sign and are also larger in magnitude relative to the overall time series average.

The annual hindcast WDI_{Pred} values have a limited trend over the last 113 years; however, the cumulative WDI_{Pred} values (Figure 4.4b) show a negative trend of -0.17 yr^{-1}. The detrended values of the cumulative WDI_{Pred} (Figure 4.4. bottom panel) indicate that there is potential periodicity in phases of positive and negative WDI_{Pred}.

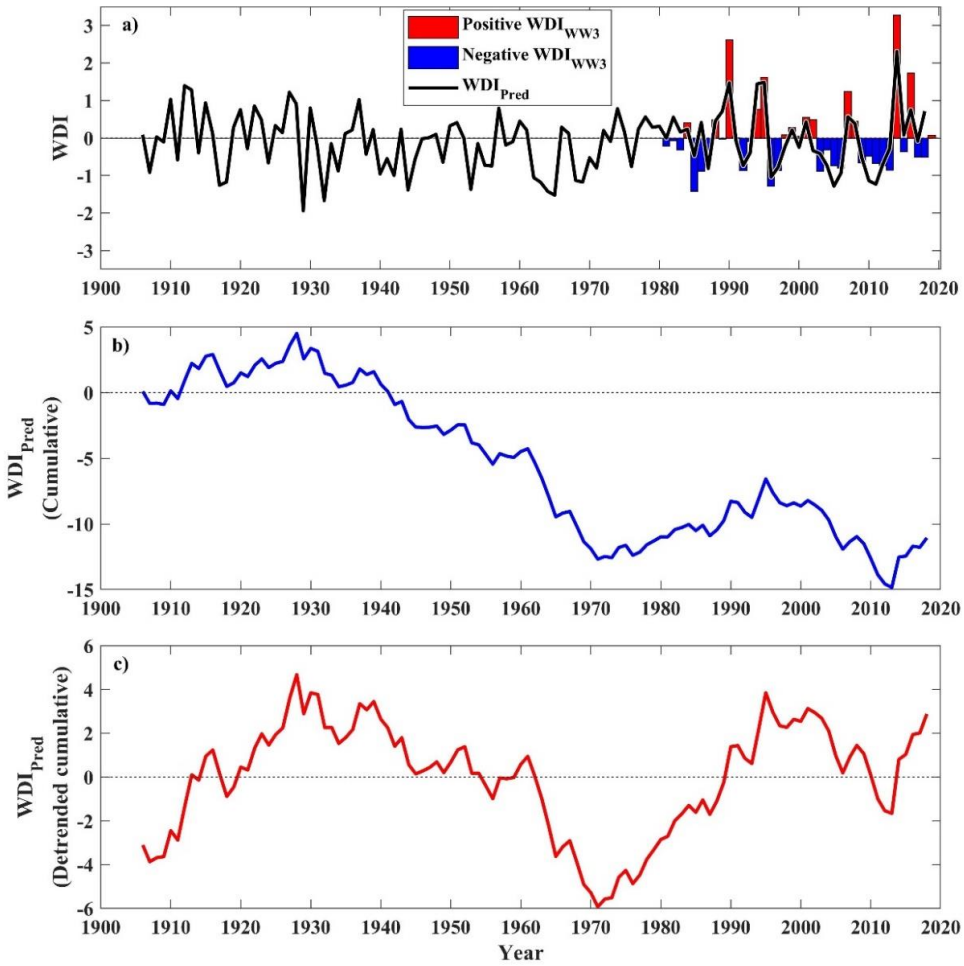

Figure 4.4. a) SMLR modelled WDI_{Pred} values from atmospheric indices NAO and WEPA, predicted back to 1906, as well as the values of WDI_{WW3} as obtained from the WaveWatchIII model. b) The cumulative WDI_{Pred} values from 1906 to 2018, as predicted by the SMLR model of NAO and WEPA. c) The detrended cumulative values of WDI_{Pred} from 1906 to 2018.

4.4.2 Modelled longshore sediment flux

To examine the relationship between the two different offshore WDI parameters (WDI_{WW3} and WDI_{Pred}) and transport rates within the embayment, potential alongshore sediment flux was computed for a series of six fixed shoreline positions (Figure 4.5a), using an inshore wave transformation model comprising real bathymetry (see further, McCarroll et al. (2020)). Total potential winter transport totals (Figure 4.5b, e, h, k, n, q) were compared with WDI_{WW3} values for the period of 1980 to 2018. In all locations, significant positive correlations are observed between the WDI_{WW3} and directional sediment transport (Figure 4.5c, f, i, l, o, r), with the strongest correlation being at Strete ($R^2 = 0.84$), the northern end of Slapton Sands (Figure 4.5f). Other nodes located in the northern sections of the embayment show a balance of northward (southward) transport under highly positive (negative) WDI_{WW3} winters, whereas almost all winter WDI_{WW3} conditions drive northward transport at Hallsands in the far south of the embayment.

The positive correlations throughout the bay suggest that the WDI_{WW3} calculated at the offshore model node is an adequate proxy of the balance of inshore wave directions, responsible for driving sediment transport and beach rotation within the embayment.

In addition to the comparisons between modelled sediment transport and WDI_{WW3}, the same comparison was conducted against values of the WDI_{Pred}, as produced by the SMLR (Figure 4.5d, g, j, m, p and s). At all sites, weaker but similarly positive correlations were observed, with all results being significant at the 95% confidence interval, highlighting that the WDI_{Pred} computed from climate indexes is a suitable proxy for estimating flux at the shoreline.

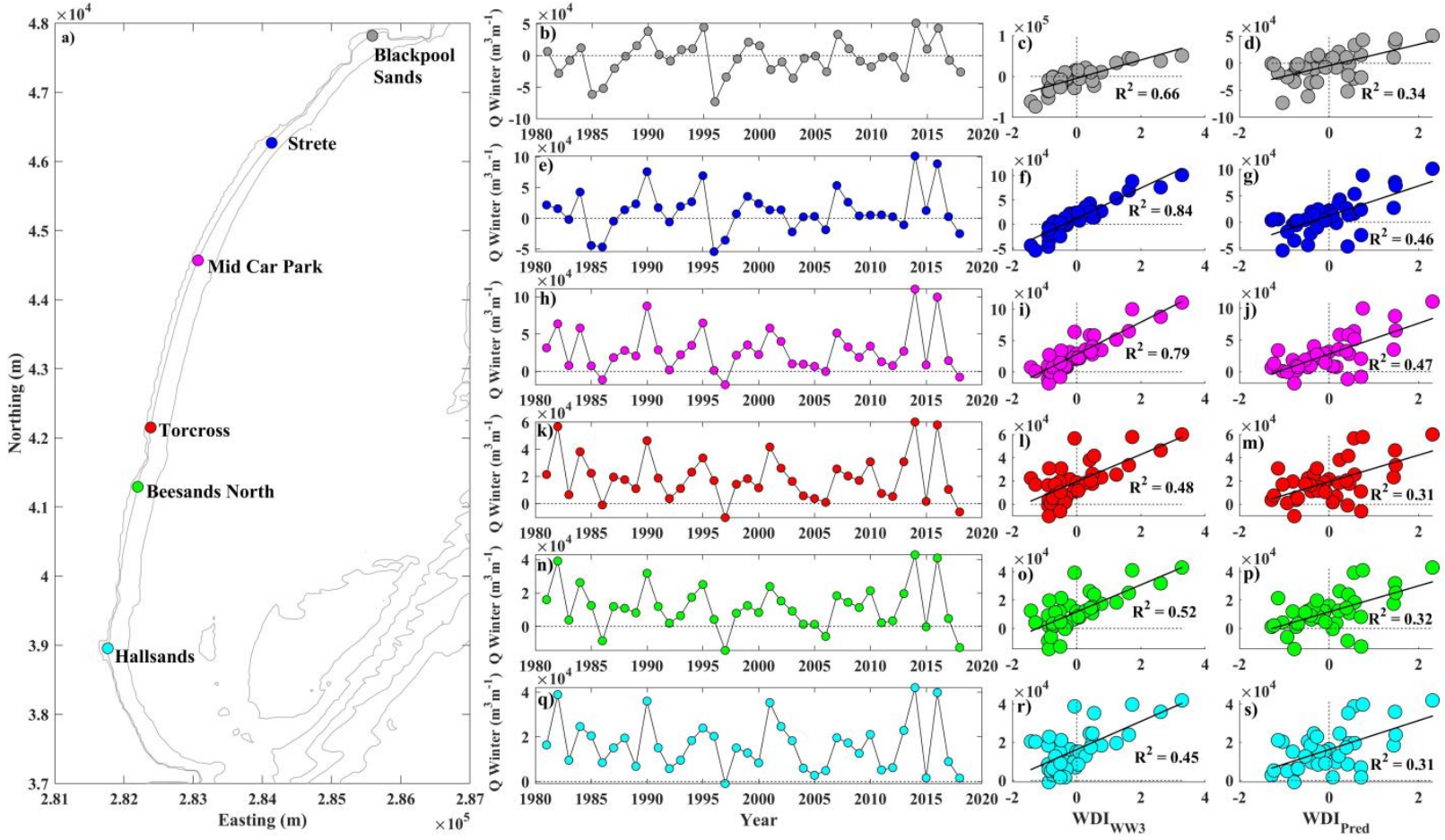

Figure 4.5. a) location map of inshore nodes at which total potential winter sediment flux has been calculated, b) total potential winter alongshore sediment flux at Blackpool Sands, e) Strete, h) Middle car park, k) Torcross, n) Beesands North and q) Hallsands. Panels c), f), i), l), o) and r) show the correlation between the WDI_{WW3}, and longshore sediment transport at the six locations, whilst panels d), g), j), m), p) and s) show the same correlations but with values of WDI_{Pred}.

4.4.3 Validation against beach surveys and historical records

To demonstrate the potential application of WDI_{Pred} in predicting beach rotation, correlations with contemporary and historical beach rotation are presented. Similar to previous studies of both Slapton Sands and other locations in the south west, values of the WDI_{WW3} are well correlated with the rotation index (defined in eq. 2) for the period of 2008 to 2019, derived from topographic survey data. The sign of the rotation index tracks well with the sign of WDI_{WW3} (Figure 4.6a), whilst the linear correlation of the two is significant and strong ($R = 0.77$, $p = 0.00$, Figure 4.6b). Similarly, the correlation between the WDI_{Pred} and rotation index is positive ($R = 0.47$), despite not being statistically significant at 95%; however, it is observed that the correlation is much stronger and statistically significant ($R = 0.74$, $p = 0.01$), if the winter change from 2017/18 is removed as an outlier. During this year, a single, large-scale easterly storm event at the end of February and beginning of March 2018 caused substantial anti-clockwise rotation of the beach. Although that winter featured a negative WDI_{WW3} value, both the NAO and WEPA were positive at 0.30 and 1.18, respectively, resulting in a positive WDI_{Pred} value. That winter also stands out as having the highest anti-clockwise rotation index during the observational period, so its impact on reducing the strength of the correlation coefficient is substantial.

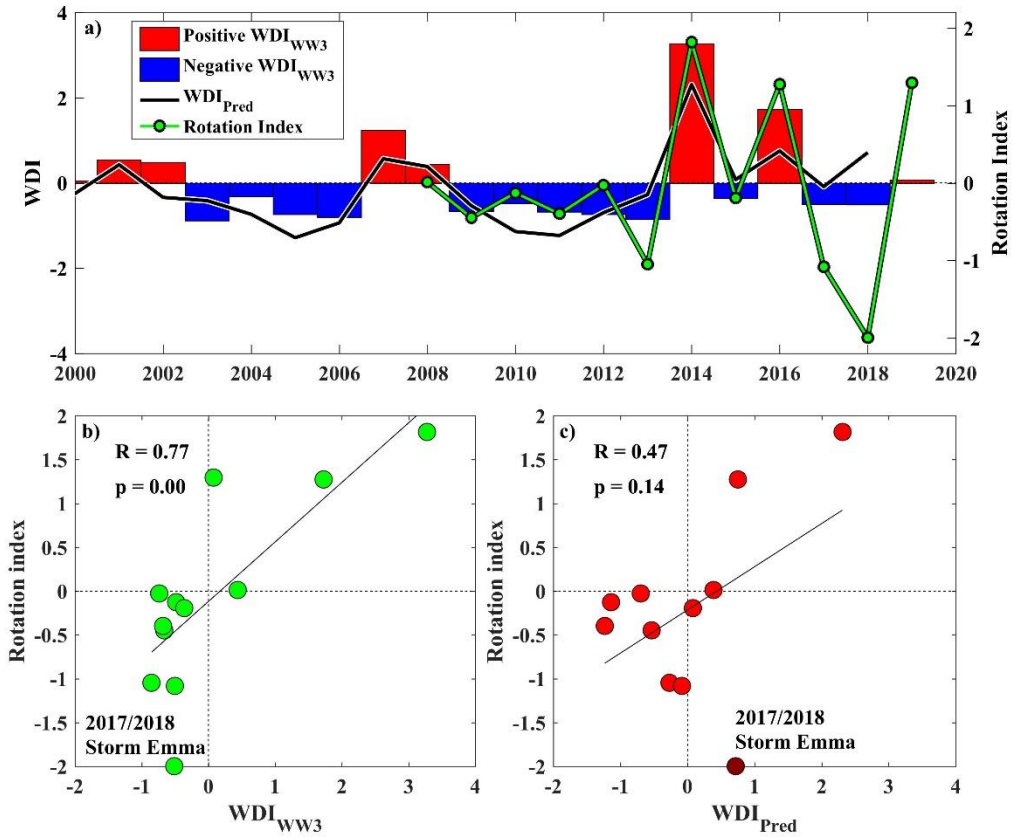

Figure 4.6. a) Time series of short term (~20 years) WDI_{WW3} values, shown by the red and blue bars, overlaid with WDI_{Pred} from the NAO and WEPA SMLR model, shown as the black line. The rotation index (green line) over the period of 2008 to 2019, derived from measured winter change (November to March) in beach volume at opposing ends of Slapton Sands, with positive (negative) values indicating northward clockwise (southward *anti-clockwise*) beach rotation. b) Correlation between WDI_{WW3} and winter rotation index for the period of 2008 to 2019. c) Correlation between winter WDI_{Pred} and the winter rotation index for the period of 2008 to 2018.

The lack of consistent high-quality shoreline data before 2006 means proxy records are the only possibility for validation of the longer-term WDI_{Pred} values. Time series of the qualitative beach width assessment for Torcross and the detrended cumulative WDI_{Pred} values for the period spanning 1906 to 2019 are shown in Figure 4.7a. The beach appears widest during the last decade of the 1800s, then beginning to narrow up to the 1920's, remaining a similar width in photographs and maps until around 1945. A period of beach widening then occurs until the early 1970's, before narrowing again until 2016, the lowest beach volume in both the short-term surveys, and photo archive.

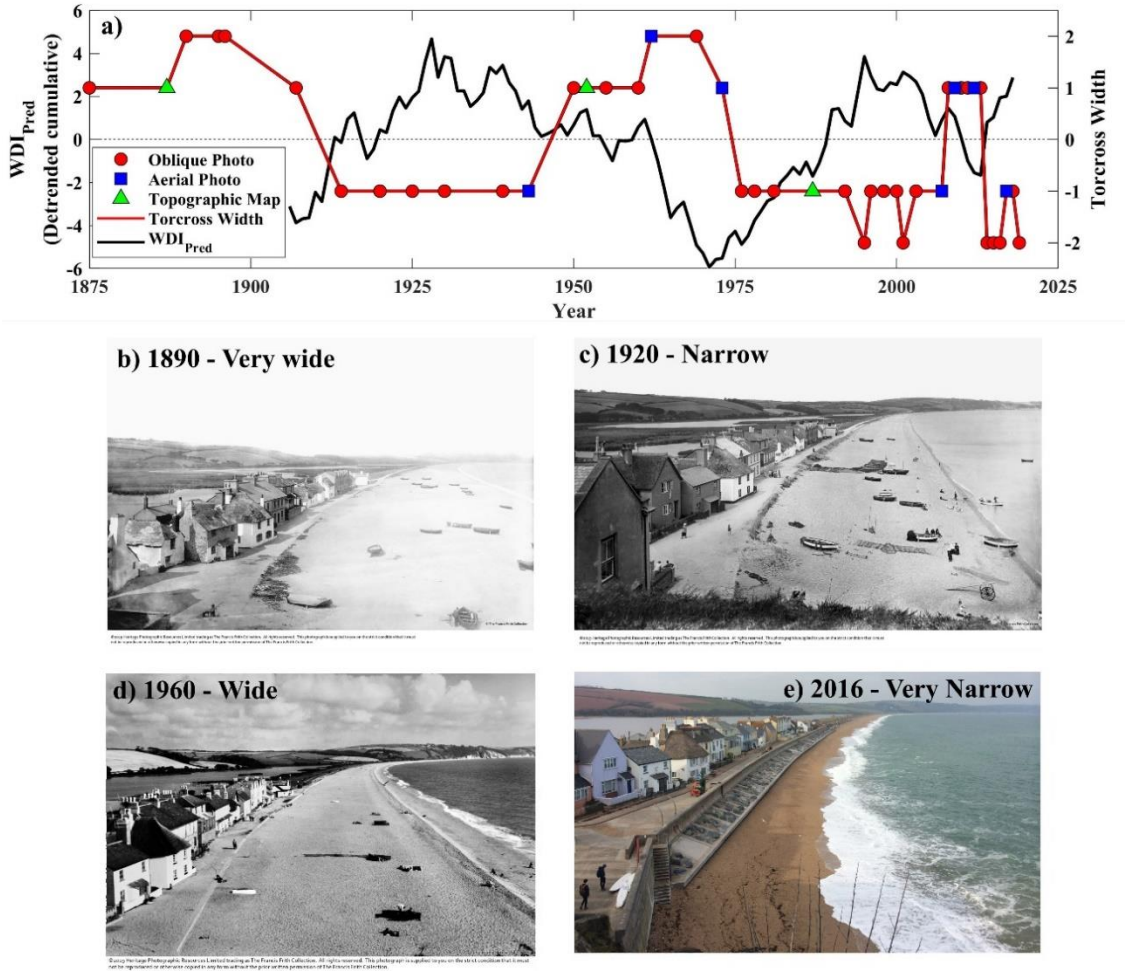

Figure 4.7. a) Detrended cumulative values of the WDI_{Pred} (left axis) from 1906 to 2018, overlaid on the right axis is a qualitative assessment of beach width at Torcross (southern end of Slapton Sands), with positive values indicating a wide beach, suggesting southward sediment transport and anti-clockwise beach rotation, whilst negative values indicate a narrower beach, signifying a period of potential northward sediment transport and clockwise beach rotation. b) Photos of Torcross taken in 1890, c) 1920, d) 1960 (Copyright The Francis Frith Collection) e) 2016 (Copyright G. Masselink), showing different beach widths throughout the last 200 years.

Both beach width and detrended cumulative WDI_{Pred} values display low frequency fluctuations over the last 113 years, with beach width appearing to narrow during periods of cumulative positive WDI_{Pred} and widen during sustained negative phases (Figure 4.7a). Long-term detrended cumulative values for the WDI_{Pred} as well as the NAO and WEPA were computed and the results are displayed in Figure 4.8.

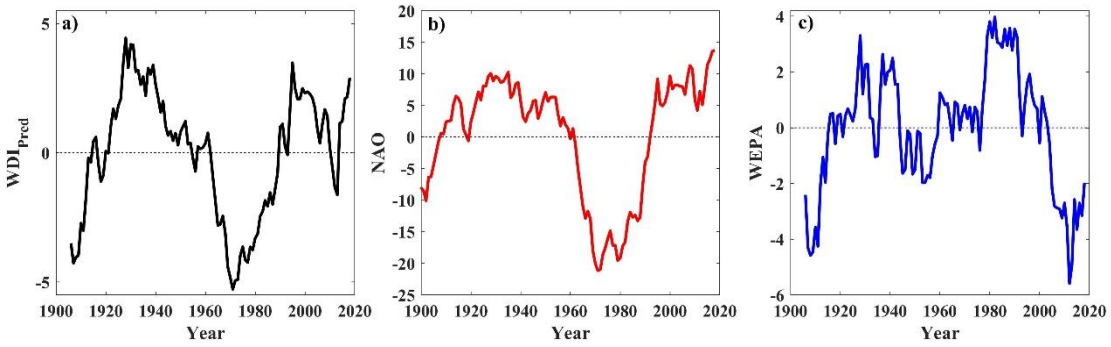

Figure 4.8. Detrended cumulative values of winter averaged a) WDI_{Pred}, b) NAO and c) WEPA.

For the WDI_{Pred} values (Figure 4.8a), there appears to be a multi-decadal variation (approximately 60-70 years between peaks) in cumulative positive and negative phases, whilst the NAO (Figure 4.8b) displays a similar multi-decadal oscillation on the same order of magnitude (~60-80 years) (Figure 4.8d). WEPA values presented a double peak, with a potential multi-decadal (>50 years) fluctuations in respective positive and negative phases.

4.5 Discussion

This chapter has shown that combination of two major winter-averaged climate indices, NAO and WEPA, in a SMLR model significantly improves skill when trying to predict winter-averaged offshore directional wave climate (WDI), when compared to using the individual indices. Given that the WDI is key predictor of the magnitude and direction of beach rotation at this, and many similar sites along the length of the southern U.K. coastline (Chapter 3), the ability to forecast its value from two significant indices represents a step forward in assessing the accuracy in historical records of beach rotation, and the future potential to predict wave climate and morphological behaviour at seasonal to centurial timescales. Whilst previous studies have been able to link changes in atmospheric variability to deviations in wave height or direction (Ranasinghe et al., 2004; Dodet et al., 2010; Barnard et al., 2015; Castelle et al., 2017, 2018; Harley

et al., 2017; Burvingt et al., 2018), the combination of multiple indices for direct calculation of a bi-directional wave climate parameter for opposing directions is unique.

Both the WDI_{WW3} and WDI_{Pred} were shown to correlate with winter integrated potential longshore transport rates throughout the embayment (McCarroll et al., 2020). Statistically significant ($p < 0.05$) correlation coefficients for WDI_{WW3} and WDI_{Pred} ranging from 0.67 to 0.92, and 0.56 to 0.68, respectively, show that the WDI calculated for a single point offshore is a robust proxy for the inshore wave climate and sediment transport. Similar to this study, significant correlations were found by Splinter et al., (2012) between yearly modelled net longshore transport rates and positive phases of the Inter-decadal Pacific Oscillation (IPO) and the Southern Oscillation Index (SOI); however, regression models combining both indices required a five-year smoothing average of both predictor and response variables, in addition to separate model equations for positive and negative phases of the IPO, incorporating different coefficients and predictor values at different time lags. The simplicity of the SMLR model used in this study, suggests that where WDI calculations are well correlated with beach rotation (Chapter 2 and 3), similar analysis can be conducted at other rotation dominated sites.

The results of Section 4.3 show the rotation index of Slapton Sands (as calculated from <10 year topographic survey record) is well correlated with values of the WDI_{WW3}, but not significantly correlated with the atmospheric index based WDI_{Pred} values predicted by the model over a 10-year period of observations. Further investigation into the limited dataset showed that the winter of 2017/18 featured a large single easterly storm event (Storm Emma, further description in McCarroll et al. (2019)) which caused a significant anti-clockwise rotation of the beach at the end of the winter season (March 2nd 2018). The morphological response was observed in the anti-clockwise rotational beach record and the observed negative WDI_{WW3} value (-0.51); however, it was not

reflected in the positive winter averages of NAO and WEPA (0.30 and 1.17 respectively). As a result, such values of atmospheric indices resulted in the model predicting a positive WDI_{Pred} value (+ 0.70), suggesting a more southerly than average dominance of wave power. That winter also stands out as having the highest anti-clockwise rotation index during the observational period, so its impact on reducing the strength of the correlation coefficient is substantial. Clearly single extreme events such as this can cause significant beach rotation and substantial damage to infrastructure, and whilst the WDI_{Pred} is shown to correlate well with beach rotation when the 2017/18 winter is removed from the analysis ($R = 0.74$ $p = 0.01$), ignoring potential outliers of the general trend presents problems in application within a coastal management setting. If a longer period of accurate morphological survey data was available, better understanding of the skill and limitations of the relationship between WDI_{Pred} and beach rotation could be obtained.

Beyond the immediate correlations between both winter WDI values and recent multi-annual beach rotation, it is interesting to examine the detrended cumulative record of WDI_{Pred} as conceptually it provides insights into the rotational state of the embayment. Using the SMLR model a hindcast record of WDI_{Pred} shows low frequency (~60-70 years) multi-decadal fluctuations over the last century (Figure 4.8), driven by combined changes in the cumulative values of winter NAO and WEPA. Although the methodology for constructing a proxy record of observed beach rotation is quantitatively limited (i.e. manual interpretation of southern beach width from photography and topographic maps), it does present a qualitative coherence with the periodicity in the long-term cumulative WDI_{Pred} values (Figure 4.7a). Temporal gaps and lack of consistency in the seasonal timing of photographs may lead to aliasing of higher frequency variations in beach width, but the longer-term signal presented in the historical record shows a clear coherence with the detrended cumulative WDI_{Pred} values,

providing some validation for using detrended cumulative WDI_{Pred} in this context. Several decades of the last century which show a positive phases in detrended cumulative WDI_{Pred} values (e.g. 1900 to 1930; sustained southerly winter waves) coincide with periods of beach narrowing (clockwise rotation), whilst phases of sustained negative detrended cumulative WDI_{Pred} values (e.g. 1940 to 1970; higher percentage of easterly winter waves) coincide with beach widening (anti-clockwise rotation). Current improvements to shoreline detection from satellite images dating back to the 1980s could provide the extended datasets required (e.g. Vos et al., 2019b), and would further assist in validating regression models of atmospheric indices and their control on wave climates and beach response.

Successive winters of the same WDI_{Pred} sign (positive or negative) may drive cumulative beach rotation in a particular direction or maintain the planform shape if already rotated. Event-scale wave action can cause rapid changes to the beach profile and planform shape, and reversals of wave direction have been shown to quickly counter-rotate the embayments of Start Bay (Ruiz de Alegria-Arzaburu and Masselink, 2010; McCarroll et al., 2019; Wiggins et al., 2019a); however, this study has identified that multi-decadal trends in the detrended cumulative WDI_{Pred}, are mirrored in beach rotation proxies over the last 113 years. Such multi-decadal beach rotation patterns have been identified in other locations over a comparable time period, such as the south coast of Pembrokeshire, Wales, U.K., with similar correlations found between wave angle variations driving beach rotation under contrasting phases of the NAO (Thomas et al., 2013). The longer-term trends in cumulative WDI values appear to dictate the general planform state of Start Bay, indicating that within the next 100 years, a continued upward trend in cumulative WDI values, or a potential phase shift into a sustained negative period may lead to sustained clockwise rotation or reversal and anti-clockwise rotation.

To place the observed contemporary changes in context with long-term reconstructions of the NAO, detrended cumulative values of the WDI_{Pred}, NAO and WEPA from the current study are plotted on a log time scale in Figure 4.9a, b, and c. For comparison, detrended cumulative values of two extended NAO reconstructions are also presented. The first (Figure 4.9d), dating back to 1400, is derived from tree-ring and ice-core proxies from Cook et al. (2002). The second (Figure 4.9e) is presented as a ~3000 year record of detrended cumulative normalised stalagmite growth rates (Baker et al., 2015), inverted for ease of comparison, with high growth rates representative of drier conditions, reflective of negative NAO phases.

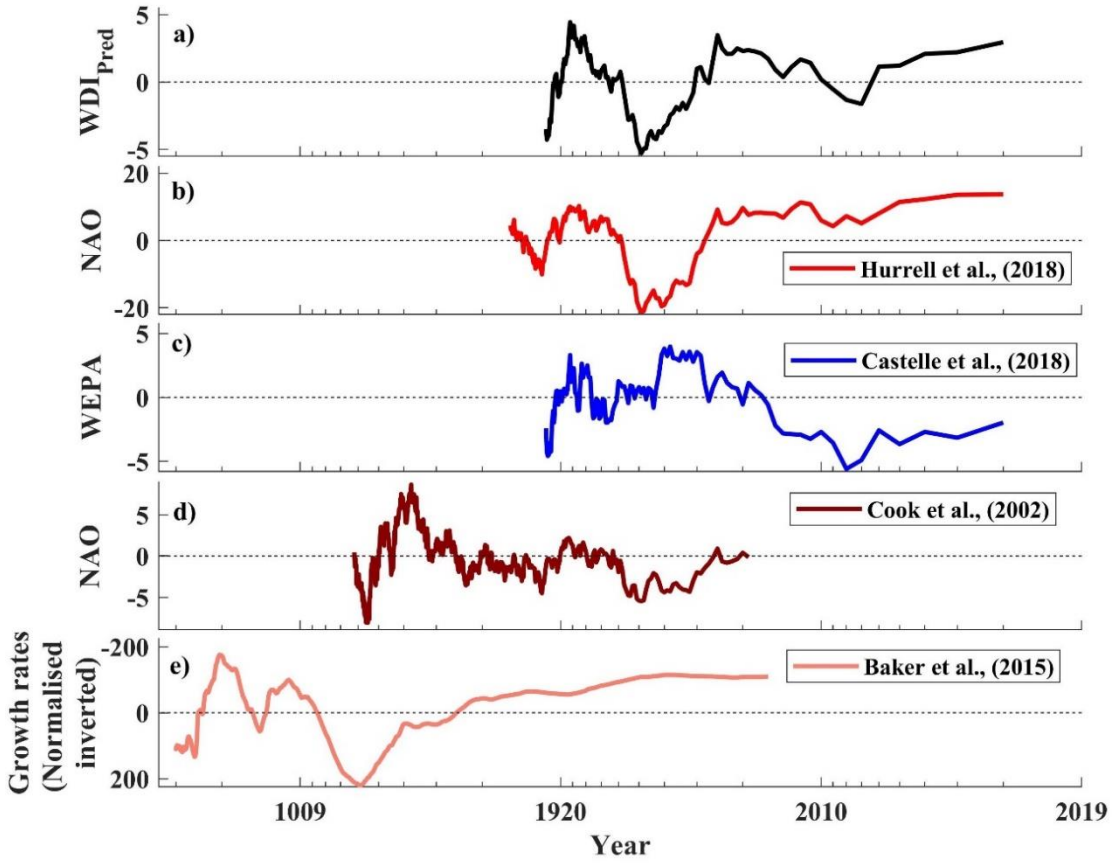

Figure 4.9. Detrended cumulative values of a) WDI_{Pred}, b) NAO from Hurrell et al. (2018) c) WEPA derived by Castelle et al. (2018), d) long-term NAO reconstructions from Cook et al. (2002), e) normalised stalagmite growth rates (inverted) from Baker et al. (2015). Time in year date (A.D.) is presented on a log scale.

Both additional records demonstrate sustained multi-decadal to multi-centurial phases of significant magnitude which have been confirmed by several other authors (e.g. Faust et al., 2016; Trouet et al., 2012). These observed fluctuations are of significantly greater scale and duration than those exhibited within the 113 years assessed in this study. Long-term variations in NAO have seen noticeable climate shifts identified in Europe over the last 2000 years, including a relative warming during the MCA (~800 to 1300 A.D.) due to persistent positive NAO (Trouet et al., 2009a), as well as a cooler period during the LIA (~1400 – 1850 A.D.) linked to a persistent negative NAO phase (Luterbacher et al., 2001). European coastal response to these changes has been documented, with large-scale dune growth and inland sand migration evidenced during the LIA under negative NAO conditions, due to increased sand availability and stronger onshore winds (Clarke and Rendell, 2006), as well as cooler temperatures limiting vegetation growth and destabilising dunes (Jackson et al., 2019). Historical accounts of many settlements and agricultural land being abandoned due to wind driven sand migration throughout Europe (Clarke and Rendell, 2009), indicates that atmospheric effects on coastal communities have been always been apparent, driving a constant need for shoreline adaptation. Within the context of the present study site, the shoreline of Start Bay has likely undergone many previous sustained rotational states, evidenced by the loss of two historical settlements at opposing ends of the embayment (Figure 4.1), Strete Undercliff and Hallsands (Wiggins et al., 2017), within only the last 300 years. Exact dates of Strete Undercliff's formation are unclear, but it was well established by 1652 A.D. at the northern end of the embayment, likely following a sustained positive phase of cumulative NAO winters (Figure 4.10), driving clockwise rotation and northward sediment transport, resulting in a wide beach. Its eventual decline and demise 130 years later (1782 A.D.) followed an opposing phase of cumulative negative NAO winters, possibly driving anti-clockwise rotation and southward sediment transport.

Around the same time, early records of the formation of Hallsands, in the southern corner of the embayment, suggest anti-clockwise rotation produced a wider beach and encouraged settlement at this location, before dredging of beach shingle (Worth, 1904) and a reversal towards more positive NAO winters at the turn of the 20th century (Wiggins et al., 2017), depleted the protective beach and the village was abandoned in 1917.

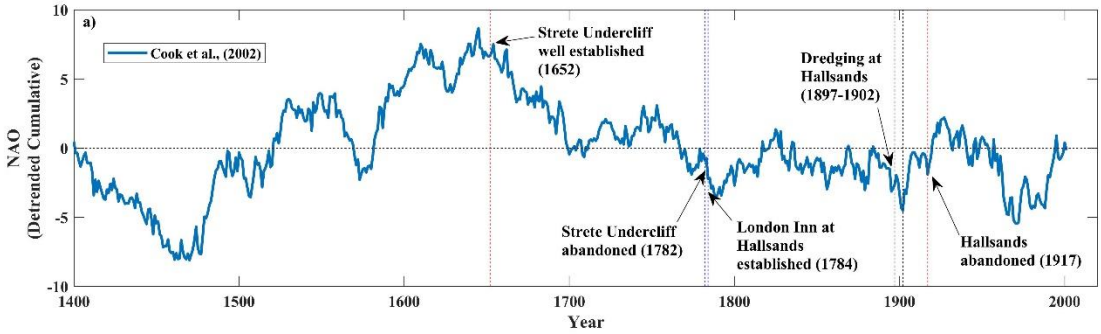

Figure 4.10. Detrended cumulative NAO reconstruction from Cook et al. (2002), with annotations describing the establishment and subsequent demise of two historic settlements within Start Bay, Strete Undercliff in the north, and Hallsands in the south.

The observed low frequency variations in long-term NAO suggest that sustained morphological rotations may have been occurring over substantially longer timescales in Start Bay, and much of Europe, particularly in rotation-prone sites where wave climates are bi-directional.

The skill (increased R^2) demonstrated in using combined NAO and WEPA for predicting the WDI and hence beach rotation, leads to the question of whether skilful forecasts of both indices can be obtained for either short-term (seasonal) or longer-term (multi-annual to decadal) timescales. Given that Castelle et al. (2017) have shown that NAO and WEPA are not correlated, independent forecasts of each index would need to be made well ahead of the coming winter season if the predictability of the WDI can be achieved at timescales useful to coastal managers. For example, Colman et al. (2011) made use of the NAO's positive correlation with wave height in the North Sea, to

predict expected operational downtime of oil and gas rigs using season ahead forecasts of the NAO, made available several months in advance; however, our work presents the ability, and therefore enhanced application, of predicting the direction and magnitude of the wave power balance in a region where it significantly impacts coastal rotation and subsequent vulnerability. Improvements to seasonal NAO forecasts are currently being showcased by many authors (Scaife et al., 2015; Dunstone et al., 2016; Wang et al., 2017; Baker et al., 2018); however, hindcast predictions of the NAO over the last 100 years has shown that forecast skill may be variable, with particular weakness during sustained phases of low magnitude negative NAO winters, and better skill during the stronger, positive phases during the beginning and end of the 20th century (Weisheimer et al., 2017). The results of this chapter, and the previous two, highlight that the NAO's strong negative correlation with easterly wave events is critical in the formulation of WDI values for the present location. In such a case study, skilful prediction of negative NAO winters is crucial for identifying the anti-clockwise rotations observed during increased easterly waves. WEPA has been shown to have much greater skill in predicting the occurrence of the more dominant south-westerly waves but, as yet, is largely unpredictable at the season-ahead timescale, in part due to current climate models reliance on accurate predictions of winter mean SLP, which are weaker for the areas around the U.K. and Ireland (Scott et al., in prep), leading to a lack of forecast skill in areas where NAO has little influence, and WEPA is unresolved.

4.6 Conclusions

This chapter has shown that a combination of two major atmospheric indices significantly improves the predictive skill for a SMLR model of the bi-directional winter wave power balance (WDI), which in turn has been shown to directly control morphological beach rotation on seasonal to multi-annual timescales. The model was

then used to hindcast WDI_{Pred} using long-term records of NAO and WEPA, with the detrended cumulative values showing periodicity linked to similar fluctuations in detrended cumulative values of both indices. Further results showed that trends in the WDI_{Pred} are mirrored in the historic records of beach rotation for this site, suggesting that beyond seasonal and event-scale rotational events, the long-term planform of this, and many similar embayments may be controlled by multi-decadal to centurial scale trends in phases of atmospheric indices.

Application of this multi-index regression method suggests that the increased ability to predict climate indices some months in advance of the coming winter period, may allow for season-ahead forecasts of forthcoming wave climates, and hence potential rotational beach impacts. Practically, this would provide coastal managers with an informed forecast of likely risks in high-impact areas, enabling proactive decisions to be made regarding hard or soft engineering works within rotational sites.

The following conclusions of this chapter are as follows;

1. Increased skilful prediction ($R^2 = 0.66$) of the WDI_{Pred} was be obtained from a regression model comprised of two atmospheric indices, when compared to the skill of individual indices alone.

2. Modelled alongshore wave power and potential sediment flux at fixed shoreline positions were significantly correlated with observed and predicted WDI at a range of locations within the study site; suggesting that the WDI is a valid proxy for inshore sediment transport.

3. Medium term (10-year) measured beach rotation correlates with the observed and model predicted WDI record (with the exception of an individual extreme event), showing multiple atmospheric indices may hindcast beach rotational state at many other locations, given extensive and reliable records.

4. The detrended cumulative WDI_{Pred} shows multi-decadal fluctuations over the years of 1906 to 2018, which is qualitatively mirrored by historic changes in beach planform, suggesting that low frequency variations in climate indices control longer-term beach rotational state.

5. Longer-term records of low frequency NAO phases suggest that larger scale rotational events may have occurred at multi-centurial timescales, potentially driving shoreline adaptation of communities in response to variations in climate indices.

5 Synthesis and conclusions

Embayment rotation has been observed at several locations worldwide, and in many cases, its effect has potential to increase the vulnerability of shoreline-based infrastructure to coastal hazards across a variety of timescales. Its morphodynamic mechanism may be varied (Klein et al., 2002; Ruiz de Alegria-Arzaburu and Masselink, 2010; Harley et al., 2011); however, for longshore beach rotation due to contrasting and oblique wave directions, atmospheric forcing can directly influence incident wave climates over seasonal to centurial timescales (Thomas et al., 2011a, 2013; Castelle et al., 2018), resulting in beach rotation driven by climatic variability (Wiggins et al., 2019a, 2019b).

The overarching aim of this research was to increase our understanding of embayed beach rotation over different timescales (annual to multidecadal), linking observations of beach response to bi-directional wave climates and atmospheric forcing. This thesis used a variety of different techniques to address these aims, including; (i) multi-annual (4 years) field observations, using a novel multi-method survey technique and robust sediment budget analysis (Chapter 2), (ii) identification and quantification of decadal scale rotational response due to wave-driven forcing and atmospheric controls at local and regional scales (Chapters 2 and 3), (iii) multivariate linear modelling of the wave climate and hence beach state in Start Bay, assessing historic (140 years) beach rotation in response to atmospheric variability (Chapter 4). This thesis has fulfilled the objectives set out in Section 1.2 through the relevant chapters, and several key findings have been identified which provide a step-change in our understanding of beach rotation driven by bi-directional wave climates and atmospheric forcing.

5.1 Key findings

This section provides a summary of the main findings in relation to the specific research objectives of each chapter, some of the key discussion topics, and finally draws together the thesis conclusions and briefly discusses potential avenues for future research.

5.1.1 Chapter 2 - Coastal embayment rotation: Response to extreme events and climate control, using full embayment surveys

Individual rotations of embayed beaches have been observed at many site specific locations (Harley et al., 2011; Thomas et al., 2011a; Burvingt et al., 2016; Scott et al., 2016), but in most cases, measurements have been restricted to the intertidal shoreface, using single survey methods (e.g. LiDAR or RTK-GPS), limiting insights into the significance of both sub-tidal transport processes, and potential sediment exchange between embayments (or sub-embayments). Chapter 2 of this thesis directly measured the sediment budget of an entire 12-km coastal cell, from sub-aerial to sub-tidal extents, using a novel application of extensive multi-method surveys, including sub-aerial topography from airborne LiDAR, UAV photogrammetry, RTK-GPS and laser scan surveys, in addition to sub-tidal bathymetry from multi-beam vessel-based surveys. Robust assessments of measurement uncertainties and their spatial variability when DEM differencing, propagating through the analysis, allowed the provision of uncertainty bounds for total volumetric change in both the sub-aerial to sub-tidal extent. This facilitated the assessment of volume changes throughout and between sub-embayments, providing a detailed account of the rotational response of an entire embayment under two unique sets of wave conditions. It was then discovered, using 10 years of beach profile surveys and modelled wave data, that intertidal beach volume change at opposing ends of sub-embayments was directly correlated with a newly developed wave climate parameter, the Wave power Directionality Index (WDI), which

describes the balance of wave power contributions from the two dominant directions, relative to the long-term mean.

The following objectives and findings for Chapter 2 were identified:

i. **Quantify the short-term rotational response of an entire coastal embayment to bi-directional wave conditions.**

In answering this first objective, key findings of Chapter 2 highlighted that under two contrasting wave directions, two distinct rotational responses were identified across an entire sediment cell.

Extensive field surveys and the application of a multimethod survey technique allowed analysis of the total sediment budget for a single site (Start Bay, U.K) comprising several sub-embayments, which revealed that under extreme and sustained dominance of a particular wave direction, **full embayment rotation** (through the process of headland sediment bypassing) was possible, whilst only **sub-embayment rotation** was observed under weaker but opposing wave directions, limiting recovery of sediment volumes lost during extreme wave conditions.

The first epoch of study (2013 to 2016) included the unprecedented stormy winter of 2013/14 (Masselink et al., 2015, 2016; Scott et al., 2016; Malagon Santos et al., 2017), characterised by intense Atlantic storms, with 15 southward tracking storms propagating up the English Channel, driving southerly wave angles at Start Bay (H_s = 1.65 m), resulting in the most energetic winter season in 50 years (Masselink et al., 2016). Within Start Bay, southerly waves comprised 84% of the winter period and under this increased dominance of south-westerly waves and storm sequencing, an intense mode of clockwise rotational response was identified through the sediment budget analysis conducted in Section 2.4.1. In this case, individual sub-embayments rotated up to and beyond the point at which large volumes of sediment bypassed previously constraining

headlands and sediments were deposited into the down-wave sub-embayments. The resulting net losses and gains at opposing ends of the embayment were balanced (closed embayment) but led to a full-embayment rotational response. Figure 5.1a **Error! Reference source not found.**highlights this full embayment rotational mechanism through a conceptual diagram, using a modified embayment geometry of Start Bay. Where embayments rotate and shorelines accrete on updrift side of bounding headlands, sediment bypass may occur, drastically altering sediment budgets within sub-embayments (either losing or gaining substantial volume).

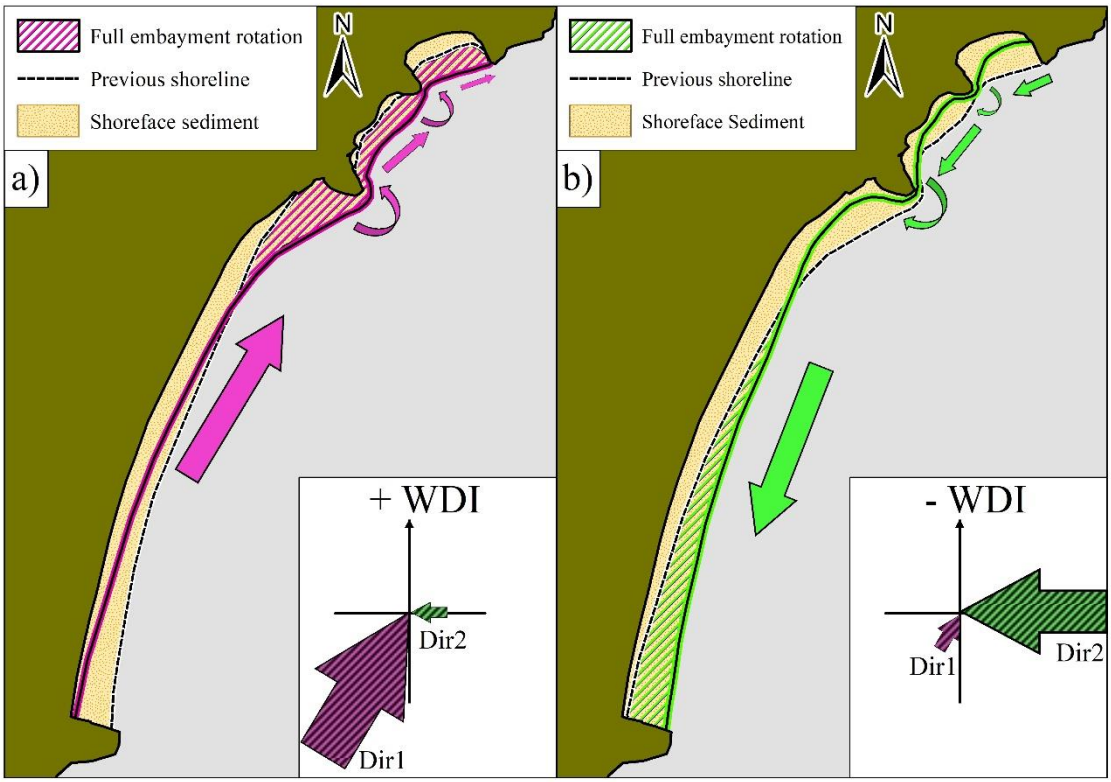

Figure 5.1 Conceptual diagram of full embayment rotation under extreme directional wave dominance for a) southwesterly waves and b) easterly waves. In these examples, purple (green) sections represent clockwise (anti-clockwise) rotation of the shoreline position under an extreme positive (negative) WDI regime, shown by the arrows about the compass in the inset subsection. Sediment transport directions are shown by the solid filled arrows, including the potential for headland bypassing between embayments.

Whilst this observed headland bypassing (and subsequent full embayment rotation) response was initially hypothesised for this site by Scott et al. (2016) and Burvingt et al.

(2018), their assessments only addressed intertidal sediment budgets of a limited number of sub-embayments within Start Bay, and could not account for the potential observed changes in the sub-tidal extent, or within all adjacent sub-embayments of the complete coastal cell. Within this study, 651,000m^3 of transport was measured, with 290,000 m^3 detected to have bypassed headlands, and sub-tidal sediment transport across the full embayment was shown to account for 33% of the total observed change under extreme wave conditions. In some areas of the embayment, up to 50% of volume changes occurred within the sub-tidal, suggesting that previous and future sediment budget analyses may be missing half of the longshore components of sediment volume change. Without the inclusion of the sub-tidal extent, net volume changes to the intertidal beach remain unidentified (potential sources/sinks alongshore or offshore). This is significant, and represents a key finding of this thesis, showcasing that the application of the total sediment budget approach, with critical uncertainty assessments (Lane et al., 2003; Wheaton et al., 2010; Milan et al., 2011), can provide increased insight into the mechanisms and pathways for sediment transport within a coastal cell.

In addition to the full embayment rotational response, a second, sub-embayment rotational mechanism was identified under a winter dominated by easterly waves (2016 to 2017), with material transported from one end of a sub-embayment to another, but with minimal (~56,000 m^3) to zero detectable exchange between. A similar conceptual diagram highlights this sub-embayment rotational response to contrasting seasonal wave conditions (Figure 5.2).

The increase in easterly waves over the 2016/2017 period resulted in southward transport of sediment (40% of the total observed between 2013 and 2016), but was not sustained, or energetic enough to meet the threshold required to facilitate significant volume transport around headlands. As highlighted for Start Bay under positive or negative values of the WDI such embayed beaches may respond by rotating in either a

clockwise or anti-clockwise direction (depending on orientation). In these cases, although no sediment may be lost from the total budget of the sub-embayment (Klein et al., 2002), sustained sub-embayment rotation over a variety of timescales can still leave shorelines depleted and beach width narrowed at key locations alongshore, reducing the protection offered by a healthy beach, potentially increasing the vulnerability of infrastructure and coastal assets to future storms impacts through overwash and flooding. In Start Bay, the net losses calculated between embayments due to the storm induced full embayment rotation (Figure 5.1a) may not be recovered due to a single season of characteristic easterly waves (H_s = 1.24 m, average of 1.15 m). Scott et al. (2016) suggested that recovery of lost sediment volumes at such locations would require equal and aggregate wave energy from the opposing direction to facilitate headland bypassing in the reverse direction, leading to an opposing full-embayment counter-rotation as highlighted in Figure 5.1b.

Recent measurements of Start Bay (McCarroll et al., 2019) during an extremely high energy (> 1-in-50 year) easterly wave event (Storm Emma, March 2018) highlighted that although extreme anti-clockwise rotation was observed within sub-embayments, limited headland bypassing occurred, particularly at the northern-most headlands. This was explained by the cross-shore extent and toe depth of the northern headlands, with larger and deeper headlands acting to constrain bypass rates. Additionally, as shorelines rotate and accrete at the down-drift extent of wave direction, the angle of the shoreline orientation changes, becoming less oblique to storm waves. This effectively reduces alongshore wave power and transport of sediment, suggesting that predictions of headland bypassing may be difficult, requiring knowledge of headland morphometry, shoreline orientation and sediment supply. Further work by McCarroll et al. (2020) has expanded this idea and highlighted that wave-induced headland bypass rates can be estimated using a combination of wave conditions, shoreface slope, sediment size and

headland cross-shore extent. The key parameter which controls bypass rates was found to be the ratio of headland cross-shore extent to surf zone width, with headland shape being of less importance. This new evidence supports a key finding for this objective, which suggests that headland bypassing within Start Bay and other rotation-prone locations may be asymmetrical under different wave directions, with significant implications for recovery of sediment between sub-embayments.

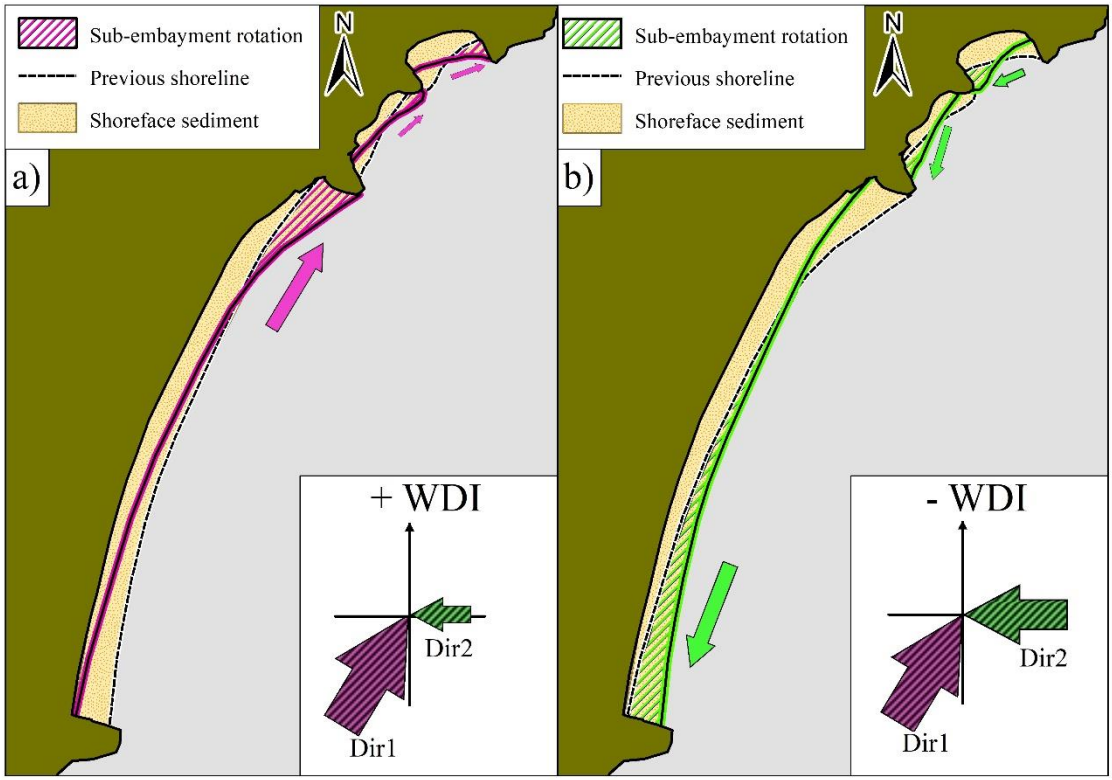

Figure 5.2. Conceptual diagram of sub-embayment rotation for a) southerly waves and b) easterly waves. In these examples, purple (green) sections represent clockwise (anti-clockwise) rotation of the shoreline position under a positive (negative) WDI regime, shown by the arrows about the compass in the inset subsection. Sediment transport directions are shown by the solid filled arrows, with headlands acting to constrain transport.

ii. Assess the extent to which the bi-directional wave balance controls beach rotation over multi-annual timescales.

In addition to the event scale rotational response, Chapter 2 addressed the research objective of identifying the bi-directional wave climate control on multi-annual (<10 year) rotation of the sub-embayments within Start Bay. As alluded to by Ruiz de Alegria-Arzaburu and Masselink (2010), and identified in the first objective of Chapter 2, alternate rotations (clockwise, anti-clockwise) of Start Bay occur under the two dominant, and opposing directions of wave approach within the bay. Building on this, using offshore modelled wave data, Chapter 2 developed the Wave power Directionality Index (WDI) parameter (Section 2.3.9), which described and quantified the balance of standardized wave power contributions from the two dominant directions (south-westerly and easterly), relative to the long-term mean. Winter, intertidal beach volume changes (calculated from a 10-year record of beach profile surveys) across the entire embayment were shown to be positively or negatively correlated with winter-averaged WDI values (Figure 2.16), suggesting that beach rotation over multi-annual to decadal scales was controlled not only by the high energy, episodic storm events from distinct directions (Ruiz de Alegria-Arzaburu and Masselink, 2010; Bergillos et al., 2017; McCarroll et al., 2019), but also by subtle shifts in the directional wave climate balance, and hence winter WDI parameter, over multi-annual timescales. This has implications for coastal management at rotational sites, particularly with bi-directional wave climates, as it shows the balance of wave power from opposing directions (WDI) is as important as, or potentially more so, than simply the total average wave height or power received at a particular shoreline. In addition, the rotational state of an embayment may be a function of changes to the WDI occurring at variable timescales (not just storm events). As a result, the monitoring of shorelines over multi-annual to decadal scale highlights planform changes which are subtle but nonetheless important for coastal

vulnerability and planning. The WDI approach to predicting the magnitude and direction of beach rotation could be applied on global scale at sites which experience embayment rotation under bi-directional wave climates, for example; the Atlantic coast of Portugal (Loureiro et al., 2012), the west and east coasts of Australia (Masselink and Pattiaratchi, 2001; Harley et al., 2015), the east coast of New Zealand (Bryan et al., 2013; Van de Lageweg et al., 2013) and Brazil (Klein et al., 2002; Vintém et al., 2006).

iii. Examine the relationship between climatic indices and bi-directional wave forcing.

The key findings of the first two objectives have identified strong forcing relationships between the bi-directional wave climate and short to medium term beach rotation, suggesting that if the wave climate can be predicted with some degree of skill, beach rotational state may also be inferred. Well established correlations between atmospheric variability and wave climates have been identified for the North Atlantic (Hurrell and Deser, 2009; Dodet et al., 2010; Masselink et al., 2016; Castelle et al., 2017; Burvingt et al., 2018), and, as such, initial correlations were drawn between the directional winter wave power contributions for Start Bay, and winter averaged values of the NAO and WEPA. In addressing this objective, a split response was identified in the correlations of winter averaged WEPA and NAO with southerly and easterly winter wave power, respectively (Figure 2.18). Over the 37-year period of modelled wave data for Start Bay, southerly winter wave power was shown to be weakly positively correlated ($R = 0.27$) with winter NAO, whilst being strongly correlated with winter values of WEPA ($R = 0.81$). Conversely, easterly wave power was strongly negatively correlated with NAO ($R = -0.73$) whilst showing no significant correlation with WEPA ($R = 0.04$). Additionally, the WDI was shown to correlate with both with both NAO ($R = 0.47$) and WEPA ($R = 0.69$) (Figure 2.19), suggesting that bi-directional wave climates and hence

beach rotation may potentially be predicted or hindcast using key climate indices over a range of timescales.

Both NAO and WEPA have been shown to control the nature of the wave climate within Start Bay, which may allow for prediction of beach rotational state, based on climate indices alone. The implications of this finding show that climate indices could potentially predict rotation on a wide range of semi-exposed coastlines, useful to coastal managers at local to regional scales.

5.1.2 Chapter 3 - Regionally coherent, medium-term beach rotation and climate control

For the key findings of Chapter 2 to be relevant at other locations beyond the initial study site (Start Bay), application of the methods are expanded and assessed at a regional scale in Chapter 3, utilising modelled wave data and records of beach profile surveys along the length of the south coast of England, U.K. The same winter storm period (2013/14) which caused the full embayment rotation of Start Bay (Chapter 2), was also noted as producing a regionally coherent seasonal scale rotational response for many beaches along the south west region of the U.K. (Masselink et al., 2015; Burvingt et al., 2016; Scott et al., 2016); however, multi-annual (<10 year) identification of beach rotational behaviour had not previously been conducted for this stretch of coastline. This assessment addressed the potential for rotational beach sites to be identified in locations with similar bi-directional wave climates, and by their local environmental factors.

The following objectives and findings for Chapter 3 were identified:

i. **Investigate the regional coherence of bi-directional wave climates and relationships with atmospheric indices.**

In addressing this objective, the medium-term approach and findings for the Start Bay case study (Chapter 2) were explored further by expanding the spatial domain and assessing the nature of the wave climate for the length of the English Channel.

Modelled wave data for 14 node locations along the full length of the English Channel identified that wave climates were similarly bi-directional over the period of 1980 to 2016, with a primary south-westerly mode and a secondary easterly mode (Figure 3.4). Additionally, wave power from the two directions was likewise correlated with differing phases of both NAO and WEPA (Figure 3.7), with south-westerly waves being strongly positively correlated with WEPA ($0.9 > R > 0.68$, at 95% confidence limits), and easterly waves being strongly negatively correlated with NAO ($-0.58 > R > -0.79$, at 95% confidence limits). The WDI was calculated at each model node and was positively correlated with NAO and WEPA for the length of the English Channel.

The regional scale similarities in both wave climate bi-directionality and correlations with atmospheric forcing suggested that there is potential coherence in the morphological response between similar coastal sites over a range of timescales, and that single indices of large scale patterns of atmospheric variability have wide-reaching effects in this region.

ii. Identify and quantify regional beach response, in order to examine the extent to which wave bi-directionality controls beach rotation.

The second section of Chapter 3 addressed this research objective by analysing beach profile data for 22 coastal sites, looking to discover similar responses in shoreline behaviour. To identify beach rotation, the Beach Morphological Response (BMR) parameter was developed, which identifies and quantifies either a cross-shore (positive BMR, Figure 5.3c and Figure 5.3d) or rotational (negative BMR, Figure 5.3a and Figure 5.3b) beach response, based on the linear correlation between volume change at

opposing (north/south or east/west) ends of the beach. Additionally, the Rotation Index (RI) was devised, which provides a metric of the magnitude and direction of rotational events, relative to the survey record. Highly positive (negative) RI values are indicative of strong clockwise (anti-clockwise) rotational events, whereas smaller values (tending towards zero) indicate weaker rotational events (Figure 5.3a and Figure 5.3b).

Eleven of the 22 sites exhibited a statistically significant rotational response ($R < -0.4$ - at 95% confidence intervals, Figure 3.8), whilst only five sites were shown to be strongly cross-shore in nature (the remainder of sites did not show a significant correlation for either response). The RI was positively correlated with the localised WDI at almost all rotating sites (Figure 3.9), showing that bi-directional wave climates impart similar controls on beach state at regional scales.

Similar to previous studies (Masselink et al., 2015; Burvingt et al., 2016, 2017, 2018; Scott et al., 2016), a key finding for this objective was the identification of regionally coherent beach behaviour, but in this case over multi-annual timescales. South-east facing beach orientation, and hence increased exposure to both primary and secondary directions of bi-directional wave climates, was the key factor controlling beach rotation. This critical relationship has been also been observed in south eastern Australia by Short et al. (2014), who identified synchronous cross-shore oscillation and rotation of three beaches, hundreds of km apart, but with similar orientations and lengths.

In addition to beach orientation, the results of Chapter 3 found that beach slope and sediment type were also coherent with the mode of beach response, where steeper gravel beaches tended to rotate, whilst flatter sandier beaches exhibited cross-shore behaviour.

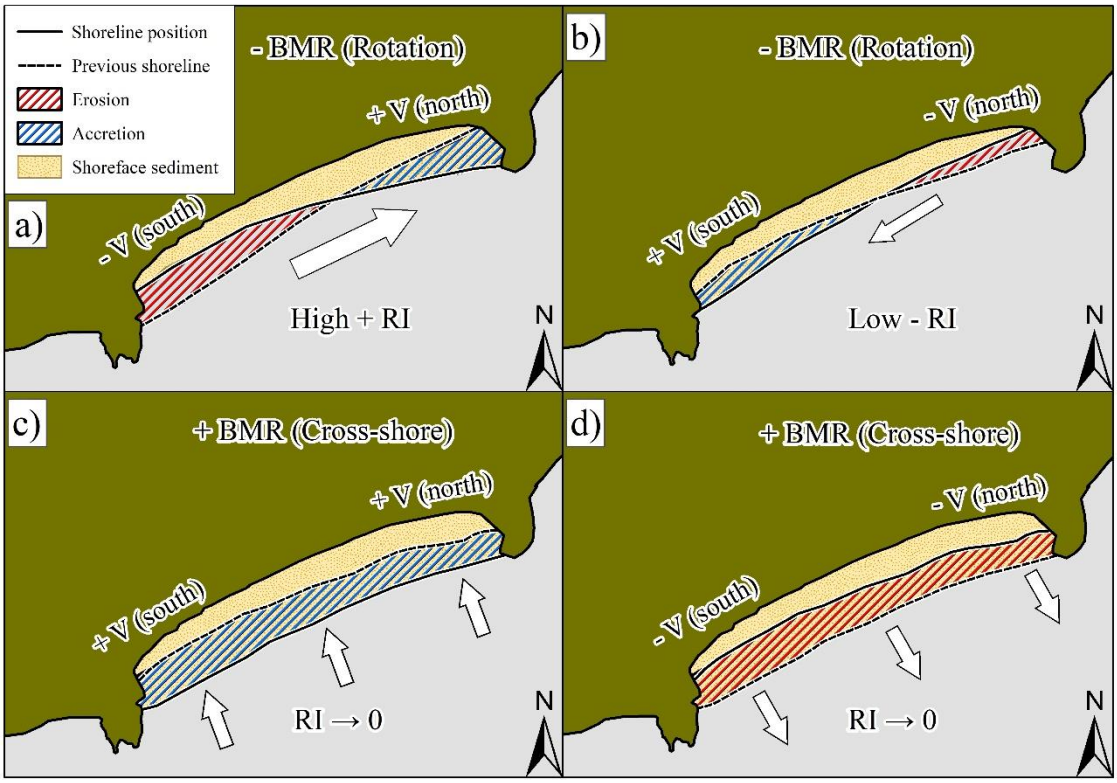

Figure 5.3 Conceptual diagram demonstrating the two forms of Beach Morphological Response (BMR) and the Rotation Index (RI) showing a) negative BMR (rotational site) with a high positive RI, indicative of strong clockwise rotation, b) negative BMR (rotational site) with a lower negative RI, indicative of a weaker anti-clockwise rotation, c) and d) positive BMR (cross-shore site) with RI tending to zero, showcasing alongshore uniform accretional and erosional responses. In all cases white arrows indicate the direction of sediment transport.

The implications of these findings suggest that beaches at risk of significant rotational events may be identified from their key parameters (e.g. orientation to wave climate, sediment type, slope etc.), and where monitoring or satellite shoreline data exists, a similar assessment of beach response can be conducted for comparable sites with bi-directional wave climates. Additionally, this analysis will only be improved with sustained monitoring programmes and increased resolution, geo-location accuracy and frequency of satellite derived shorelines (Vos et al., 2019a), increasing the temporal dataset and potentially increasing the statistical significance and confidence of the analysis.

5.1.3 Chapter 4 - Predicting beach rotation using multiple atmospheric indices

Both Chapter 2 and Chapter 3 identified the strong correlations between the winter-averaged bi-directional wave climate and climate indices NAO and WEPA at site-specific and regional scales. The time series of beach rotation presented in both Chapter 2 and 3 is temporally limited (~10 years), which potentially reduces the significance of direct correlations between beach state and atmospheric indices (low sample number), initial exploration in Chapter 3 showed that WEPA was positively correlated with beach rotation at two sites (Figure 3.11). This finding, coupled with the fact that NAO and WEPA are uncorrelated (Castelle et al., 2017), suggested that combining both indices could lead to improved explanatory skill in predictions of the bi-directional wave climate (WDI) and potential beach response.

The following objectives and findings for Chapter 4 were identified:

i. **Evaluate the skill of atmospheric indices for predicting beach rotation through multivariate modelling.**

Given the observed correlations of bi-directional wave climates with NAO and WEPA, Chapter 4 took this approach further, dealing with the research objective of improving the predictive skill (increase of R^2) of the WDI in Start Bay, by the possible combination of the two indices.

The development of a stepwise multi-linear regression model (Section 4.4.1) resulted in the addition of the two indices, with separate coefficients, improving the skill in predicting the WDI (Figure 4.3), with an associated R^2 of 0.66, when compared to 0.23 and 0.31 for NAO and WEPA individually, over a 38-year period (1980-2018). The model was then used to hindcast WDI from the beginning of the SLP station-based WEPA record (1906). Multi-decadal fluctuations on the order of ~60-70 years were

identified in the detrended cumulative WDI timeseries (Figure 4.4). This potential multi-decadal periodicity in predicted WDI is likely induced through cumulative positive and negative phases (70-80-year periodicity) of the NAO (Figure 4.8b), in addition to ~50-60 year cycles in detrended cumulative values of WEPA. This atmospheric index control on wave climate variability is consistent with other studies, for example Castelle et al. (2018) showed that over the latter half of the 20th Century NAO is increasing with a trend of + 0.013 per year, whilst WEPA has exhibited increased periodicity at a timescale of 7 years in the last 30 years with a striking correlation with wave height increases in the area of the North Atlantic southward of 52° N. This significant combined influence of NAO and WEPA on wave climate in this region, suggest the multi-variate modelling approach is well grounded in predicting both bi-directional wave variability and potential beach rotation.

The driving forces of the observed fluctuations in atmospheric indices are still uncertain, but longer term variations in NAO have been linked to sea surface temperature changes (McCarthy et al., 2015), with some observational and modelling studies suggesting that variations in the Atlantic Multidecadal Oscillation (AMO), a low frequency mode of natural variability between sea surface temperature anomalies in the North Atlantic basin (Kerr, 2000), can impart some control on changes in the NAO (Seip et al., 2019). The AMO has an estimated period of 60-80 years, and positive phases of AMO have been shown to lead negative phases of the NAO, at multi-annual scales (Gastineau and Frankignoul, 2012; Hodson et al., 2014). In turn, the AMO is thought to be driven by the Atlantic Meridional Overturning Circulation (AMOC) (Delworth and Mann, 2000; Knight et al., 2005), although suggestions of anthropogenic radiative forcing have been also been proposed (Mann and Emanuel, 2006); however, recent observations of subsurface ocean temperature (Zhang et al., 2007; Zhang, 2008;

Wang and Zhang, 2013) show previous records of AMOC are coherent with observed AMO, suggesting that AMO and therefore NAO are controlled by AMOC variations.

Whilst previous studies have identified links between increased directional wave height and climate indices (Ranasinghe et al., 2004; Dodet et al., 2010; Barnard et al., 2015; Castelle et al., 2017, 2018; Harley et al., 2017; Burvingt et al., 2018), the findings presented for this objective highlight that the wave directional balance can be predicted with increased skill by the combination of two climate indices. This has key implications for the potential to hindcast past wave climates at other locations, beyond the length of modelled wave datasets, where records of station-based climate indices extend much further back in time (Hurrell, 2018). Additionally, current improvements to "season ahead" forecasts of such indices as the NAO, with up to 1-year lead times (Scaife et al., 2015; Dunstone et al., 2016; Wang et al., 2017) could allow prediction of the bi-directional wave climate at timescales useful to coastal engineering and management. Individual SMLR models could be developed to predict bi-directional wave climates at rotation-prone sites, incorporating multiple additional indices, for example NAO, WEPA, Scandinavian index (SCAND), Arctic Oscillation index (AO), East Atlantic/West Russian (EA/WR) etc. as per Scott et al. (submitted), depending on the most relevant for each local site or region. This multivariate approach has also been used to predict other climate-forced phenomena in other disciplines, such as climate/rainfall for agriculture (Zambrano et al., 2018) and wave heights for oil and gas operations (Colman et al., 2011).

ii. Validate the value of long-term hindcasts of wave directionality index (WDI) against proxy records of beach rotation.

This objective was achieved by investigating the suitability of a climate index modelled directional wave climate for predicting observed beach rotation. The predicted values of

the WDI were shown to validate against a measured beach rotation index (Figure 4.6) from 2008 to 2018 (correlation of R = 0.74) and modelled inshore potential longshore energy fluxes from 1980 to 2018 (Figure 4.5), highlighting the effective skill in predicting beach rotation and longshore transport from atmospheric indices alone.

The hindcast values of the WDI, and its subsequent multi-decadal periodicity (~60-70-year) were then validated against qualitative assessments of historic beach rotation within Start Bay (Figure 4.7), derived from proxy datasets, with the results suggesting that longer-term climatic oscillations lead to rotational changes at time scales beyond seasonal to multi-annual, highlighted by potential multi-decadal periodicity in phases of the NAO and WEPA over the observed record. The findings for this objective highlight that climate indices may be used to not only hindcast historical directional wave climates, but also possibly predict previous shoreline orientations. In addition, predictions of future beach rotational behaviour may be possible based on forecasts on climate indices.

iii. Place the contemporary beach rotational behaviour into a longer-term context of climatic variability.

The observed atmospheric control of NAO and WEPA on the WDI parameter has highlighted that changes to the two indices may impact wave climate and beach rotation over a range of timescales, from multi-annual to multi-decadal. Large scale contemporary rotations of Start Bay (2013/14 winter season) have been observed within the last decade (Chapter 2), as well as centurial-scale changes to beach planform inferred from the historical abandonment and relocation of two settlements at opposing ends of the embayment (Worth, 1904; Martins et al., 2010; Stranack, 2017), potentially in relation to fluctuations in cumulative NAO values (Figure 4.10) over multi-centurial scales (Wiggins et al., 2017).

To address the objective of placing these changes into longer term context, Chapter 4 investigated extended millennial scale reconstructions of the NAO (Baker et al., 2015), which highlighted that there have been much larger scale phases of NAO periodicity at significantly higher magnitudes and durations (Figure 4.9) than those observed within the last few centuries, suggesting that previous and future beach rotations may occur as a function of long period atmospheric variability .

Large-scale morphological responses to such millennial-scale climate variability have been examined by other authors, particularly for dune transgression during large scale global changes in climate (Clarke and Rendell, 2006; Jackson et al., 2019), linked with extended phases of the NAO (Trouet et al., 2009a, 2009b), suggesting that the previously observed atmospheric controls on beach rotation are likely to continue, with potentially greater impacts on coastal communities observed at accelerated levels due to increased rates of sea-level rise (Nicholls et al., 2011) and potential for increased storminess.

5.2 Limitations and suggestions for future research

At the site-specific scale, the novel application of a robust multi-method survey technique (Chapter 2) allowed the quantification of total volumes of sediment, inferred to have bypassed headlands through the full embayment rotation mechanism; however, actual bypass rates around headlands under different wave conditions are difficult to obtain, particularly in gravel environments, potentially limiting the strength of the conclusions possible from such a study. Chapter 2 also suggested that headland bypassing may be asymmetrical under differing wave approach angles, depending on headland geometry, depth, extent and shoreline angle, which would prove critical for recovering sediment lost between rotational events. These parameters were not directly obtained within this study; however, future work should look to calculate headland

bypassing rates, either using field observations (e.g. McCarroll et al., 2019) or numerical modelling (e.g. George et al., 2019). This work also lacked the inclusion or development of a full shoreline model for rotating beaches, which could potentially incorporate both longshore and cross-shore processes (e.g. Bergillos et al., 2017; Turki et al., 2013), as well as the ability to deal with embayment headlands and bypass rates. This could then be run for simulations of different wave conditions, perhaps driven by synthetic values of key climatic indices as per the results of Chapter 4, validating the results and conclusions drawn here. Furthermore, current forecasts of atmospheric indices are limited to season ahead projections (~ 1-year timescales), and the work of climatologists to improve both the skill and lead time of such predictions may lead to operational forecasts of beach rotation.

Further limitations of the work presented here are founded in data availability. At regional spatial scales, the work presented in Chapter 3 and 4 of this thesis is based largely on field observations of beach volumes and shoreline position, in some cases spanning no more than 10 years, partly due to the lack of consistent, regular monitoring of beaches worldwide. This limited the strength of correlations that were able to be drawn between both observed and modelled wave data with the morphological changes discovered. The observations, parameters (e.g. BMR, RI) and correlations (e.g. WDI vs RI, WDI vs NAO) derived within this Chapter 3 and 4 could be improved and strengthened if applied to other coastal locations, on increased spatial and temporal scales. Recent improvements in detection from satellite imagery (Liu et al., 2017; Vos et al., 2019b) may provide historic and future observations of shorelines for assessment of beach rotation on a continental scale.

Whilst the majority of the analysis in this thesis is conducted where data is largely available (i.e. a single site or region), this limits the the global significance of the results observed, as conditions and processes may not always be comparable at other scales. To

combat this, a cross-comparison between the North American and European coastal response to phases of different climate indices could be conducted for the North Atlantic basin, with satellite data potentially providing observations for the last 40 years in places. Similar work is currently being conducted following (Vos et al., 2019a) for the southern Pacific basin, with preliminary results showing an out of phase relationship between the Australian and South American coastlines, to different modes of ENSO. Increasing the temporal and spatial scale of the work conducted in Chapter 3, such high-level assessment of beach response to atmospheric forcing would be of great value to engineers, planners and governments, enabling them to make informed decisions for beach management over a range of timescales.

5.3 Thesis conclusions

Through a combination of site specific to regional scale analysis, this thesis directly contributes new insights into embayment rotation at different spatial and temporal scales, in addition to demonstrating the potential for operational "season-ahead" forecasting.

Application of a new total sediment budget approach, including all sub-embayments and supra- to sub-tidal extents (with robust spatial uncertainty assessments) is shown to be critical for understanding full embayment rotation and recovery processes (Chapter 2), whilst winter-averaged bi-directional waves, that are significantly correlated with atmospheric indices (Chapter 3) are shown to predict beach rotation at multi-annual to multi-decadal timescales (Chapter 4).

Key conclusions:

- Under extreme directional wave energy (>1:50 year southerly winter season), full embayment rotation (6.5 x 10^5 m^3 transport) was observed through headland

bypassing (50% of total) and sub-tidal change (33% of total), providing new insights into sediment transport pathways for gravel beaches.

- Asymmetrical headland bypassing may limit retrieval of previously lost sediment under opposing wave directions, extending timescales of beach recovery.

- Regional analysis (22 beaches) has shown that rotational response to bi-directional wave climates can be predicted by a new index of the normalized wave power directional balance (WDI).

- Atmospheric variability imparts significant control on bi-directional wave climates and beach rotation, with the WDI parameter well correlated to both NAO (R = 0.47) and WEPA (R = 0.69).

- Hindcast prediction of the WDI using multivariate modelling is greatly improved by combining NAO and WEPA (R^2 of 0.66 between model data and index predicted values of the WDI), allowing hindcasts of historical beach rotation, in addition to potential forecasting of season ahead rotation.

- Low frequency (~60 years) phases of historical clockwise/anticlockwise beach rotation follow positive/negative phases of the detrended cumulative hindcast WDI record, controlled by similar phases of NAO (~60-80 year) and WEPA (~50-60 year), dictating directional wave climate and beach rotation over centurial timescales.

- Millennial scale variability in NAO indicate that previously inferred phases of extreme coastal realignment may recur in the future, presenting a significant long-term issue for locations affected by beach rotation.

Appendix A

Table A1. Morphological survey site code, with local name, UK County, coordinates, beach length and sediment type.

Code	Name	County	Coordinates	Length (km)	Sediment
PRA	Praa Sands	Cornwall	50.1045° N, 5.3857° W	1.6	Sand
COV	Coverack	Cornwall	50.0244° N, 5.0976° W	0.5	Sand
CRN	Carne	Cornwall	50.2071° N, 4.9380° W	1.2	Sand
CAR	Carlyon Bay	Cornwall	50.3370° N, 4.7467° W	1.3	Sand
LOO	Looe Beach	Cornwall	50.3522° N, 4.4522° W	0.3	Sand
THL	Thurlestone	Devon	50.2655° N, 3.8541° W	0.6	Sand
HAL	Hallsands	Devon	50.2361° N, 3.6597° W	0.2	Gravel
BEE	Beesands	Devon	50.2532° N, 3.6575° W	1.4	Gravel
SLP	Slapton Sands	Devon	50.2833° N, 3.6333° W	5.2	Gravel
BLK	Blackpool Sands	Devon	50.3194° N, 3.6102° W	0.7	Gravel
DAW	Dawlish Town	Devon	50.5809° N, 3.4640° W	1.0	Sand
BUD	Budleigh Salterton	Devon	50.6310° N, 3.3202° W	3.1	Gravel
SEA	Seaton	Devon	50.7053° N, 3.0719° W	2.1	Gravel
CHE	Chesil Beach	Dorset	50.6267° N, 2.5605° W	4.1	Gravel
RIN	Ringstead	Dorset	50.6309° N, 2.3512° W	0.5	Gravel
HEN	Hengistbury	Dorset	50.7191° N, 1.7661° W	1.4	Gravel
CLI	Climping	W Sussex	50.7978° N, 0.5734° W	1.8	Gravel
LAN	Lancing	W Sussex	50.8282° N, 0.3281° W	1.8	Gravel
NEW	Newhaven	E Sussex	50.7931° N, 0.0456° E	1.0	Gravel
BEX	Bexhill	E Sussex	50.8499° N, 0.4662° E	1.0	Gravel
HAS	Hastings	E Sussex	50.8543° N, 0.5735° E	1.0	Gravel
FOL	Folkestone	Kent	51.0737° N, 1.1703° E	0.9	Gravel

Table A2. Morphological survey site code, with local name, total number of surveys, start year of survey programme and frequency.

Code	Name	Surveys	Start year	Frequency
PRA	Praa Sands	25	2007	6 monthly
COV	Coverack	22	2007	6 monthly
CRN	Carne	21	2007	6 monthly
CAR	Carlyon Bay	27	2007	6 monthly
LOO	Looe Beach	22	2007	6 monthly
THL	Thurlestone	25	2007	6 monthly
HAL	Hallsands	22	2007	4/6 monthly
BEE	Beesands	26	2007	4/6 monthly
SLP	Slapton Sands	25	2007	4/6 monthly
BLK	Blackpool Sands	20	2007	6 monthly
DAW	Dawlish Town	23	2007	6 monthly
BUD	Budleigh	22	2007	6 monthly
SEA	Seaton	21	2007	6 monthly
CHE	Chesil Beach	30	2007	4/6 monthly
RIN	Ringstead	19	2007	6 monthly
HEN	Hengistbury	29	2005	6 monthly
CLI	Climping	31	2007	4/6 monthly
LAN	Lancing	28	2007	4 monthly
NEW	Newhaven	33	2007	4 monthly
BEX	Bexhill	38	2003	4 monthly
HAS	Hastings	38	2003	4 monthly
FOL	Folkestone	34	2003	4 monthly

References

Anderson, D., Ruggiero, P., Antolínez, J.A.A., Méndez, F.J., Allan, J., 2018. A Climate Index Optimized for Longshore Sediment Transport Reveals Interannual and Multidecadal Littoral Cell Rotations. J. Geophys. Res. Earth Surf. 123, 1958–1981. https://doi.org/10.1029/2018JF004689

Anthony, E.J., Gardel, A., Gratiot, N., Proisy, C., Allison, M.A., Dolique, F., Fromard, F., 2010. The Amazon-influenced muddy coast of South America: A review of mud-bank-shoreline interactions. Earth-Science Rev. 103, 99–121. https://doi.org/10.1016/j.earscirev.2010.09.008

Austin, M.J., Masselink, G., Mccall, R.T., Poate, T.G., 2013. Groundwater dynamics in coastal gravel barriers backed by freshwater lagoons and the potential for saline intrusion : Two cases from the UK. J. Mar. Syst. 123–124, 19–32. https://doi.org/10.1016/j.jmarsys.2013.04.004

Autret, R., Dodet, G., Suanez, S., Roudaut, G., Fichaut, B., 2017. Long–term variability of supratidal coastal boulder activation in Brittany (France). Geomorphology 304, 184–200. https://doi.org/10.1016/j.geomorph.2017.12.028

Bacon, S., Carter, D.J.T., 1993. A connection between mean wave height and atmospheric pressure gradient in the North Atlantic. Int. J. Climatol. 13, 423–436. https://doi.org/10.1002/joc.3370130406

Baker, A., C. Hellstrom, J., Kelly, B.F.J., Mariethoz, G., Trouet, V., 2015. A composite annual-resolution stalagmite record of North Atlantic climate over the last three millennia. Sci. Rep. 5, 10307.

Baker, L.H., Shaffrey, L.C., Sutton, R.T., Weisheimer, A., Scaife, A.A., 2018. An Intercomparison of Skill and Overconfidence/Underconfidence of the Wintertime

North Atlantic Oscillation in Multimodel Seasonal Forecasts. Geophys. Res. Lett. 45, 7808–7817. https://doi.org/10.1029/2018GL078838

Barnard, P.L., Short, A.D., Harley, M.D., Splinter, K.D., Vitousek, S., Turner, I.L., Allan, J., Banno, M., Bryan, K.R., Doria, A., Hansen, J.E., Kato, S., Kuriyama, Y., Randall-Goodwin, E., Ruggiero, P., Walker, I.J., Heathfield, D.K., 2015. Coastal vulnerability across the Pacific dominated by El Niño/Southern Oscillation. Nat. Geosci. 8, 801.

Barnard, P.L., Hoover, D., Hubbard, D.M., Snyder, A., Ludka, B.C., Allan, J., Kaminsky, G.M., Ruggiero, P., Gallien, T.W., Gabel, L., McCandless, D., Weiner, H.M., Cohn, N., Anderson, D.L., Serafin, K.A., 2017. Extreme oceanographic forcing and coastal response due to the 2015-2016 El Niño. Nat. Commun. 8, 1–8. https://doi.org/10.1038/ncomms14365

Bater, C.W., Coops, N.C., 2009. Evaluating error associated with lidar-derived DEM interpolation. Comput. Geosci. 35, 289–300. https://doi.org/10.1016/j.cageo.2008.09.001

BBC, 2014. Hallsands residents fear for storm-hit village [WWW Document]. https://www.bbc.co.uk/news/uk-england-devon-26382832.

Bergillos, R.J., López-ruiz, A., Ortega-sánchez, M., Masselink, G., Losada, M.A., 2016a. Implications of delta retreat on wave propagation and longshore sediment transport - Guadalfeo case study (southern Spain). Mar. Geol. 382, 1–16. https://doi.org/10.1016/j.margeo.2016.09.011

Bergillos, R.J., Ortega-Sánchez, M., Masselink, G., Losada, M.A., 2016b. Morpho-sedimentary dynamics of a micro-tidal mixed sand and gravel beach, Playa Granada, southern Spain. Mar. Geol. 379, 28–38. https://doi.org/10.1016/j.margeo.2016.05.003

Bergillos, R.J., Masselink, G., Ortega-Sánchez, M., 2017. Coupling cross-shore and longshore sediment transport to model storm response along a mixed sand-gravel coast under varying wave directions. Coast. Eng. 129, 93–104. https://doi.org/10.1016/j.coastaleng.2017.09.009

Bradbury, A., Stratton, M., Mason, T., 2011. Impacts of wave climate with bi-modal wave period on the profile response of gravel beaches, in: The Proceedings of the Coastal Sediments 2011. World Scientific Publishing Company, pp. 2004–2018. https://doi.org/doi:10.1142/9789814355537_0151

Brasington, J., Rumsby, B.T., McVey, R.A., 2000. Monitoring and modelling morphological change in a braided gravel-bed river using high resolution GPS-based survey. Earth Surf. Process. Landforms 25, 973–990. https://doi.org/10.1002/1096-9837(200008)25:9<973::AID-ESP111>3.0.CO;2-Y

Bromirski, P.D., Cayan, D.R., 2015. Wave power variability and trends across the North Atlantic influenced by decadal climate patterns. J. Geophys. Res. Ocean. 120:, 3419–3443. https://doi.org/10.1002/2014JC010472

Brunier, G., Fleury, J., Anthony, E.J., Gardel, A., Dussouillez, P., 2016. Close-range airborne Structure-from-Motion Photogrammetry for high-resolution beach morphometric surveys: Examples from an embayed rotating beach. Geomorphology 261, 76–88. https://doi.org/10.1016/j.geomorph.2016.02.025

Bryan, K.R., Foster, R., MacDonald, I., 2013. Beach Rotation at Two Adjacent Headland-Enclosed Beaches. J. Coast. Res. 165, 2095–2100. https://doi.org/10.2112/si65-354.1

Burvingt, O., Masselink, G., Russell, P., Scott, T., 2016. Beach response to consecutive extreme storms using LiDAR along the SW coast of England. J. Coast. Res. 75, 1052–1056. https://doi.org/10.2112/si75-211.1

Burvingt, O., Masselink, G., Russell, P., Scott, T., 2017. Classification of beach response to extreme storms. Geomorphology 295, 722–737. https://doi.org/10.1016/j.geomorph.2017.07.022

Burvingt, O., Masselink, G., Scott, T., Davidson, M., Russell, P., 2018. Climate forcing of regionally-coherent extreme storm impact and recovery on embayed beaches. Mar. Geol. 401, 112–128. https://doi.org/10.1016/j.margeo.2018.04.004

Calder, B.R., Mayer, L.A., 2003. Automatic processing of high-rate, high-density multibeam echosounder data. Geochemistry, Geophys. Geosystems 4, 1048. https://doi.org/10.1029/2002GC000486

Calder, B.R., Wells, D., 2007. CUBE User's Manual - Version 1.14.

Castelle, B., Dodet, G., Scott, T., 2017. A new climate index controlling winter wave activity along the Atlantic coast of Europe : the West Europe Pressure Anomaly. Geophys. Res. Lett. 44, 1384–1392. https://doi.org/10.1002/2016GL072379

Castelle, B., Dodet, G., Masselink, G., Scott, T., 2018. Increased Winter-Mean Wave Height, Variability, and Periodicity in the Northeast Atlantic Over 1949–2017. Geophys. Res. Lett. 45, 3586–3596. https://doi.org/10.1002/2017GL076884

Chadwick, A.J., Karunarathna, H., Gehrels, W.R., Massey, A.C., O'Brien, D., Dales, D., 2005. A new analysis of the Slapton barrier beach system, UK. Proc. Inst. Civ. Eng. - Marit. Eng. 158, 147–161. https://doi.org/10.1680/maen.2005.158.4.147

Clarke, M.L., Rendell, H.M., 2006. Effects of storminess, sand supply and the North Atlantic Oscillation on sand invasion and coastal dune accretion in western Portugal. The Holocene 16, 341–355. https://doi.org/10.1191/0959683606hl932rp

Clarke, M.L., Rendell, H.M., 2009. The impact of North Atlantic storminess on western European coasts: A review. Quat. Int. 195, 31–41.

https://doi.org/10.1016/j.quaint.2008.02.007

Colman, A.W., Palin, E.J., Sanderson, M.G., Harrison, R.T., 2011. The Potential for Seasonal Forecasting of Winter Wave Heights in the Northern North Sea. Weather Forecast. 26 (6), 1067–1074. https://doi.org/10.1175/WAF-D-11-00017.1

Cook, E.R., D'Arrigo, R.D., Mann, M.E., 2002. A Well-Verified , Multiproxy Reconstruction of the Winter North Atlantic Oscillation. J. Clim. 15, 1754–1764.

Corbella, S., Stretch, D., 2012. Shoreline recovery from storms on the east coast of South Africa. Nat. Hazards Earth Syst. Sci. 12, 11–22. https://doi.org/https://doi.org/10.5194/nhess-12-11-2012

Davidson, M.A., Splinter, K.D., Turner, I.L., 2013. A simple equilibrium model for predicting shoreline change. Coast. Eng. 73, 191–202. https://doi.org/10.1016/J.COASTALENG.2012.11.002

Delworth, T.L., Mann, M.E., 2000. Observed and simulated multidecadal variability in the Northern Hemisphere. Clim. Dyn. 16, 661–676. https://doi.org/10.1007/s003820000075

Denbigh, A., 2017. The Slapton Line - Living with a Changing Coast. F. Stud. 1–4.

Dodet, G., Bertin, X., Taborda, R., 2010. Wave climate variability in the North-East Atlantic Ocean over the last six decades. Ocean Model. 31, 120–131. https://doi.org/10.1016/J.OCEMOD.2009.10.010

Dolphin, T.J., Vincent, C.E., Wihsgott, J., Belhache, M., Bryan, K.R., 2011. Seasonal rotation of a mixed sand-gravel beach. J. Coast. Res. SI64, 65–69.

Dunstone, N., Smith, D., Scaife, A.A., Hermanson, L., Eade, R., Robinson, N., Andrews, M., Knight, J., 2016. Skilful predictions of the winter North Atlantic Oscillation one year ahead. Nat. Geosci. 9, 809.

https://doi.org/https://doi.org/10.1038/ngeo2824

Eichentopf, S., Karunarathna, H., Alsina, J.M., 2019. Morphodynamics of sandy beaches under the influence of storm sequences: Current research status and future needs. Water Sci. Eng. 12, 221–234. https://doi.org/10.1016/J.WSE.2019.09.007

Faust, J., Fabian, K., Milzer, G., Giraudeau, J., Knies, J., 2016. Norwegian fjord sediments reveal NAO related winter temperature and precipitation changes of the past 2800 years. Earth Planet. Sci. Lett. 435, 84–93. https://doi.org/10.1016/j.epsl.2015.12.003

Feser, F., Barcikowska, M., Krueger, O., Schenk, F., Weisse, R., Xia, L., 2015. Storminess over the North Atlantic and northwestern Europe—A review. Q. J. R. Meteorol. Soc. 141, 350–382. https://doi.org/10.1002/qj.2364

Gastineau, G., Frankignoul, C., 2012. Cold-season atmospheric response to the natural variability of the Atlantic meridional overturning circulation. Clim. Dyn. 39, 37–57. https://doi.org/10.1007/s00382-011-1109-y

George, D.A., 2016. Circulation and Sediment Transport at Headlands with Implications for Littoral Cell Boundaries. University of Southern California.

George, D.A., Largier, J.L., Pasternack, G.B., Barnard, P.L., Storlazzi, C.D., Erikson, L.H., 2019. Modeling sediment bypassing around idealized rocky headlands. J. Mar. Sci. Eng. 7. https://doi.org/10.3390/jmse7020040

Goodall, F., 2007. Lost Devon. Birliin Publishing.

Goodwin, I.D., Freeman, R., Blackmore, K., 2013. An insight into headland sand bypassing and wave climate variability from shoreface bathymetric change at Byron Bay, New South Wales, Australia. Mar. Geol. 341, 29–45. https://doi.org/10.1016/j.margeo.2013.05.005

Grottoli, E., Bertoni, D., Ciavola, P., 2017. Short- and medium-term response to storms on three Mediterranean coarse-grained beaches. Geomorphology. https://doi.org/10.1016/j.geomorph.2017.08.007

Hails, J.R., 1975a. Offshore Morphology and Sediment Distribution, Start Bay, Devon. Philos. Trans. R. Soc. London. Ser. A, Math. Phys. Sci. 279, 221–228.

Hails, J.R., 1975b. Some Aspects of the Quaternary History of Start Bay, Devon. F. Stud. 4, 207–222.

Harley, M.D., Turner, I.L., Short, A.D., Ranasinghe, R., 2011. A reevaluation of coastal embayment rotation: The dominance of cross-shore versus alongshore sediment transport processes, Collaroy-Narrabeen Beach, southeast Australia. J. Geophys. Res. Earth Surf. 116, 1–16. https://doi.org/10.1029/2011JF001989

Harley, M.D., Turner, I.L., Short, A.D., 2015. New insights into embayed beach rotation : The importance of wave exposure and cross-shore processes. J. Geophys. Res. Earth Surf. 120, 1470–1484. https://doi.org/10.1002/2014JF003390.Received

Harley, M.D., Turner, I.L., Kinsela, M.A., Middleton, J.H., Mumford, P.J., Splinter, K.D., Phillips, M.S., Simmons, J.A., Hanslow, D.J., Short, A.D., 2017. Extreme coastal erosion enhanced by anomalous extratropical storm wave direction. Sci. Rep. 7, 6033. https://doi.org/10.1038/s41598-017-05792-1

Hemer, M.A., Church, J.A., Hunter, J.R., 2010. Variability and trends in the directional wave climate of the Southern Hemisphere. Int. J. Climatol. 30, 475–491. https://doi.org/10.1002/joc.1900

Hodson, D.L.R., Robson, J.I., Sutton, R.T., 2014. An Anatomy of the Cooling of the North Atlantic Ocean in the 1960s and 1970s. J. Clim. 27, 8229–8243. https://doi.org/10.1175/JCLI-D-14-00301.1

Hurrell, J.W., 1995. Decadal trends in the North Atlantic oscillation: Regional temperatures and precipitation. Science (80-.). 269, 676–679. https://doi.org/10.1126/science.269.5224.676

Hurrell, J.W., Deser, C., 2009. North Atlantic climate variability: The role of the North Atlantic Oscillation. J. Mar. Syst. 78, 28–41. https://doi.org/10.1016/J.JMARSYS.2008.11.026

Hurrell, J.W., 2018. The Climate Data Guide: Hurrell North Atlantic Oscillation (NAO) Index (station-based). [WWW Document]. Clim. Data Guid. Hurrell North Atl. Oscil. Index (station-based).

Jackson, D.W.T., Costas, S., Guisado-Pintado, E., 2019. Large-scale transgressive coastal dune behaviour in Europe during the Little Ice Age. Glob. Planet. Change 175, 82–91. https://doi.org/10.1016/j.gloplacha.2019.02.003

Karunarathna, H., Pender, D., Ranasinghe, R., Short, A.D., Reeve, D.E., 2014. The effects of storm clustering on beach profile variability. Mar. Geol. 348, 103–112. https://doi.org/10.1016/j.margeo.2013.12.007

Kelland, N.., 1975. Submarine geology of Start Bay determined by continuous seismic profiling and core sampling. J. Geol. Soc. London. 131, 7–17.

Kelly, J.T., McSweeney, S., Shulmeister, J., Gontz, A.M., 2019. Bimodal climate control of shoreline change influenced by Interdecadal Pacific Oscillation variability along the Cooloola Sand Mass, Queensland, Australia. Mar. Geol. 415, 105971. https://doi.org/10.1016/J.MARGEO.2019.105971

Kerr, R.A., 2000. A North Atlantic Climate Pacemaker for the Centuries. Science (80-.). 288. https://doi.org/10.1126/science.288.5473.1984

Klein, A.H.D.F., Filho, L.B., Schumacher, D.H., 2002. Short-Term Beach Rotation

Processes in Distinct Headland Bay Beach Systems. J. Coast. Res. 18, 442–458. https://doi.org/10.2307/4299093

Klein, A.H.F., Ferreira, Ó., Dias, J.M.A., Tessler, M.G., Silveira, L.F., Benedet, L., de Menezes, J.T., de Abreu, J.G.N., 2010. Morphodynamics of structurally controlled headland-bay beaches in southeastern Brazil: A review. Coast. Eng. https://doi.org/10.1016/j.coastaleng.2009.09.006

Knight, J.R., Allan, R.J., Folland, C.K., Vellinga, M., Mann, M.E., 2005. A signature of persistent natural thermohaline circulation cycles in observed climate. Geophys. Res. Lett. 32. https://doi.org/10.1029/2005GL024233

Lane, S.N., Westaway, R.M., Hicks, Murray, D., 2003. Estimation of erosion and deposition volumes in a large, gravel-bed, braided river using synoptic remote sensing. Earth Surf. Process. Landforms 28, 249–271. https://doi.org/10.1002/esp.483

Lichti, D., Gordon, S.J., 2004. Error propagation in directly georeferenced terrestrial laser scanner point clouds for cultural heritage recording. Proc. FIG Work. Week 1–16.

Liu, Q., Trinder, J.C., Turner, I.L., 2017. Automatic super-resolution shoreline change monitoring using Landsat archival data: a case study at Narrabeen–Collaroy Beach, Australia. J. Appl. Remote Sens. 11, 1–17.

López, I., Aragonés, L., Villacampa, Y., Navarro-González, F.J., 2018. Gravel beaches nourishment: Modelling the equilibrium beach profile. Sci. Total Environ. 619–620, 772–783. https://doi.org/10.1016/J.SCITOTENV.2017.11.156

Loureiro, C., Ferreira, Ó., Cooper, J.A.G., 2012. Geologically constrained morphological variability and boundary effects on embayed beaches. Mar. Geol.

329–331, 1–15. https://doi.org/10.1016/J.MARGEO.2012.09.010

Luterbacher, J., Xoplaki, E., Dietrich, D., Jones, P.D., Davies, T.D., Portis, D., Gonzalez-Rouco, J.F., Von Storch, H., Gyalistras, D., Casty, C., Wanner, H., 2001. Extending North Atlantic Oscillation reconstructions back to 1500. Atmos. Sci. Lett. 2, 114–124. https://doi.org/10.1006/asle.2001.0044

Malagon Santos, V., Haigh, I.D., Wahl, T., 2017. Spatial and Temporal Clustering Analysis of Extreme Wave Events around the UK Coastline. J. Mar. Sci. Eng. 5, 28. https://doi.org/10.3390/jmse5030028

Mann, M.E., Emanuel, K.A., 2006. Atlantic hurricane trends linked to climate change. Eos, Trans. Am. Geophys. Union 87, 233–241. https://doi.org/10.1029/2006EO240001

Martins, C.C., de Mahiques, M.M., Dias, J.M.A., 2010. Daily morphological changes determined by high-energy events on an embayed beach: A qualitative model. Earth Surf. Process. Landforms 35, 487–495. https://doi.org/10.1002/esp.1965

Mason, T., Bradbury, A., Poate, T., Newman, R., 2009. Nearshore wave climate of the English Channel - evidence for bi-modal seas, in: Proceedings of International Conference on Coastal Engineering 2008, Hamburg, World Scientific. pp. 605–616.

Masselink, G., Pattiaratchi, C.B., 2001. Seasonal changes in beach morphology along the sheltered coastline of Perth, Western Australia. Mar. Geol. 172, 243–263. https://doi.org/10.1016/S0025-3227(00)00128-6

Masselink, G., Austin, M., Scott, T., Poate, T., Russell, P., 2014. Role of wave forcing, storms and NAO in outer bar dynamics on a high-energy, macro-tidal beach. Geomorphology 226, 76–93. https://doi.org/10.1016/j.geomorph.2014.07.025

Masselink, G., Scott, T., Poate, T., Russell, P., Davidson, M., Conley, D., 2015. The extreme 2013/2014 winter storms: hydrodynamic forcing and coastal response along the southwest coast of England. Earth Surf. Process. Landforms 41, 378–391. https://doi.org/10.1002/esp.3836

Masselink, G., Castelle, B., Scott, T., Dodet, G., Suanez, S., Jackson, D., Floc'H, F., 2016. Extreme wave activity during 2013/2014 winter and morphological impacts along the Atlantic coast of Europe. Geophys. Res. Lett. 43, 2135–2143. https://doi.org/10.1002/2015GL067492

May, V.J., Hansom, J.D., 2003. Hallsands, Coastal Geomorphology of Great Britain, Geological Conservation Review Series.

McCarroll, R.J., Masselink, G., Wiggins, M., Scott, T., Billson, O., Conley, D.C., Valiente, N.G., Sciences, M., Circus, D., Hill, B., 2019. High-efficiency gravel longshore sediment transport and headland bypassing over an extreme wave event 1–19. https://doi.org/10.1002/esp.4692

McCarroll, R.J., Masselink, G., Valiente, N.G., Wiggins, M., Scott, T., Conley, D.C., King, E. V., 2020. Impact of a headland-associated sandbank on shoreline dynamics. Geomorphology 355, 107065. https://doi.org/10.1016/J.GEOMORPH.2020.107065

McCarthy, G.D., Haigh, I.D., Hirschi, J.J.M., Grist, J.P., Smeed, D.A., 2015. Ocean impact on decadal Atlantic climate variability revealed by sea-level observations. Nature 521, 508–510. https://doi.org/10.1038/nature14491

Michelangeli, P.-A., Vautard, R., Legras, B., 1995. Weather Regimes: Recurrence and Quasi Stationarity. J. Atmos. Sci. https://doi.org/10.1175/1520-0469(1995)052<1237:WRRAQS>2.0.CO;2

Milan, D.J., Heritage, G.L., Large, A.R.G., Fuller, I.C., 2011. Filtering spatial error from DEMs: Implications for morphological change estimation. Geomorphology 125, 160–171. https://doi.org/10.1016/j.geomorph.2010.09.012

Morey, C.R., 1976. The natural history of slapton ley nature reserve XII. The morphology and history of the lake basins. F. Stud. 4, 353–368.

Mortlock, T.R., Goodwin, I.D., 2015. Directional wave climate and power variability along the Southeast Australian shelf. Cont. Shelf Res. 98, 36–53. https://doi.org/10.1016/J.CSR.2015.02.007

Mortlock, T.R., Goodwin, I.D., 2016. Impacts of Enhanced Central Pacific ENSO on Wave Climate and Headland-Bay Beach Morphology. Cont. Shelf Res. 120, 14–25. https://doi.org/10.1016/j.csr.2016.03.007

Nicholls, R.J., Marinova, N., Lowe, J.A., Brown, S., Vellinga, P., De Gusmão, D., Hinkel, J., Tol, R.S.J., 2011. Sea-level rise and its possible impacts given a "beyond 4°C world" in the twenty-first century. Philos. Trans. R. Soc. A Math. Phys. Eng. Sci. 369, 161–181. https://doi.org/10.1098/rsta.2010.0291

Ojeda, E., Guillén, J., 2008. Shoreline dynamics and beach rotation of artificial embayed beaches. Mar. Geol. https://doi.org/10.1016/j.margeo.2008.03.010

Peterson, C.D., Jackson, P.L., O'Neil, D.J., Rosenfeld, C.L., Kimerling, A.J., 1990. Littoral Cell Response to Interannual Climatic Forcing 1983-1987 on the Central Oregon Coast, USA. J. Coast. Res. 6, 87–110.

Pikelj, K., Ružić, I., Ilić, S., James, M.R., Kordić, B., 2018. Implementing an efficient beach erosion monitoring system for coastal management in Croatia. Ocean Coast. Manag. https://doi.org/10.1016/j.ocecoaman.2017.11.019

Plomaritis, T.A., Benavente, J., Laiz, I., Del Río, L., 2015. Variability in storm climate

along the Gulf of Cadiz: the role of large scale atmospheric forcing and implications to coastal hazards. Clim. Dyn. 45, 2499–2514. https://doi.org/10.1007/s00382-015-2486-4

Poate, T., Masselink, G., Mccall, R.T., Russell, P., Davison, M., 2015. UK Storms 2014: Gravel beach response, in: Coastal Sediments 2015. ASCE, San Diego, USA. https://doi.org/doi:10.1142/9789814689977_0257

Poate, T.G., McCall, R.T., Masselink, G., 2016. A new parameterisation for runup on gravel beaches. Coast. Eng. 117, 176–190. https://doi.org/10.1016/j.coastaleng.2016.08.003

Pontee, N., 2013. Defining coastal squeeze: A discussion. Ocean Coast. Manag. 84, 204–207. https://doi.org/10.1016/J.OCECOAMAN.2013.07.010

Ranasinghe, R., McLoughlin, R., Short, A.D., Symonds, G., 2004. The Southern Oscillation Index, wave climate, and beach rotation. Mar. Geol. 204, 273–287. https://doi.org/10.1016/S0025-3227(04)00002-7

Robinson, A.H.W., 1961. The Hydrography of Start Bay and Its Relationship to Beach Changes at Hallsands. Geogr. J. 127, 63–77. https://doi.org/10.2307/1793197

Romeu, M.A.R., Fontoura, J.A.S., Melo, E., 2013. Typical Scenarios of Wave Regimes off Rio Grande do Sul, Southern Brazil. J. Coast. Res. 31, 61. https://doi.org/10.2112/jcoastres-d-12-00085.1

Ruiz de Alegria-Arzaburu, A., Masselink, G., 2010. Storm response and beach rotation on a gravel beach, Slapton Sands, U.K. Mar. Geol. 278, 77–99. https://doi.org/10.1016/j.margeo.2010.09.004

Sanchez-Gomez, E., Somot, S., Déqué, M., 2009. Ability of an ensemble of regional climate models to reproduce weather regimes over Europe-Atlantic during the

period 1961-2000. Clim. Dyn. 33, 723–736. https://doi.org/10.1007/s00382-008-0502-7

Scaife, A.A., Yu Karpechko, A., Baldwin, M., Brookshaw, A., Butler, A., Eade, R., Gordon, M., Maclachlan, C., Martin, N., Dunstone, N., Smith, D., 2015. Seasonal winter forecasts and the stratosphere. Atmos. Sci. Lett. 17, 51–56. https://doi.org/10.1002/asl.598

Schimel, A.C.G., Ierodiaconou, D., Hulands, L., Kennedy, D.M., 2015. Accounting for uncertainty in volumes of seabed change measured with repeat multibeam sonar surveys. Cont. Shelf Res. 111, 52–68. https://doi.org/10.1016/j.csr.2015.10.019

Scott, T., Masselink, G., Russell, P., 2011. Morphodynamic characteristics and classification of beaches in England and Wales. Mar. Geol. 286, 1–20. https://doi.org/10.1016/j.margeo.2011.04.004

Scott, T., Masselink, G., Hare, T.O., Saulter, A., Poate, T., Russell, P., Davidson, M., Conley, D., 2016. The extreme 2013 / 2014 winter storms : Beach recovery along the southwest coast of England. Mar. Geol. 382, 224–241. https://doi.org/10.1016/j.margeo.2016.10.011

Scott, T., Masselink, G., McCarroll, R.J., Castelle, B., Dodet, G., Saulter, A., Scaife, A.A., Dunstone, N., submitted. Atmospheric controls and long range predictability of directional waves in the United Kingdom & Ireland. Earth's Futur.

Seip, K.L., Grøn, Ø., Wang, H., 2019. The North Atlantic Oscillations : Cycle Times for the NAO , the AMO and the AMOC. Climate 7, 1–10. https://doi.org/10.3390/cli7030043

Shaw, J., Duffy, G., Taylor, R.B., Chassé, J., Frobel, D., 2008. Role of a Submarine Bank in the Long-Term Evolution of the Northeast Coast of Prince Edward Island,

Canada. J. Coast. Res. 24, 1249–1259. https://doi.org/10.2112/07-08607.1

Short, A.D., Masselink, G., 1999. Embayed and structurally controlled beaches, in: Short, A.D. (Ed.), Handbook of Beach and Shoreface Morphodynamics. John Wiley & Sons, Ltd, Chichester, Chichester, pp. 230–250.

Short, A.D., Trembanis, A.C., Turner, I.L., 2008. Beach Oscillation, Rotation and the Southern Oscillation, Narrabeen Beach, Australia 2439–2452. https://doi.org/10.1061/40549(276)191

Short, A.D., Bracs, M.A., Turner, I.L., 2014. Beach oscillation and rotation: local and regional response at three beaches in southeast Australia. Proc. 13th Int. Coast. Symp. SI70, 712–717. https://doi.org/10.2112/SI-120.1

Sibson, R., 1981. A brief description of natural neighbor interpolation, in: V. Barnet (Ed.), Interpreting Multivariate Data. pp. 21–36.

Siggery, E., Wiggins, M., 2014. Review of the south west coast beach response to wave conditions during the winter of 2013–2014. South West Reg. Coast. Monit. Program. SW SR01.

Splinter, K.D., Davidson, M.A., Golshani, A., Tomlinson, R., 2012. Climate controls on longshore sediment transport. Cont. Shelf Res. 48, 146–156. https://doi.org/10.1016/j.csr.2012.07.018

Stockdale, T.N., Molteni, F., Ferranti, L., 2015. Atmospheric initial conditions and the predictability of the Arctic Oscillation. Geophys. Res. Lett. 42, 1173–1179. https://doi.org/10.1002/2014GL062681

Stranack, D., 2017. The Lost Village of Undercliff, Blackawton and Strete History Group.

Suanez, S., Cariolet, J.-M., Cancouët, R., Ardhuin, F., Delacourt, C., 2012. Dune

recovery after storm erosion on a high-energy beach: Vougot Beach, Brittany (France). Geomorphology 139–140, 16–33. https://doi.org/10.1016/J.GEOMORPH.2011.10.014

Suursaar, Jaagus, J., Tõnisson, H., 2015. How to quantify long-term changes in coastal sea storminess? Estuar. Coast. Shelf Sci. 156, 31–41. https://doi.org/10.1016/j.ecss.2014.08.001

Taylor, J.R., 1997. An Introduction to Error Analysis: The Study of Uncertainties in Physical Measurements, Second Edi. ed. University Science Books, Sausalito, California (1997).

Thomas, T., Phillips, M.R., Williams, A.T., 2010. Mesoscale evolution of a headland bay: Beach rotation processes. Geomorphology 123, 129–141. https://doi.org/10.1016/j.geomorph.2010.06.018

Thomas, T., Phillips, M.R., Williams, A.T., Jenkins, R.E., 2011b. Medium timescale beach rotation; gale climate and offshore island influences. Geomorphology 135, 97–107. https://doi.org/10.1016/j.geomorph.2011.08.002

Thomas, T., Phillips, M.R., Williams, a. T., Jenkins, R.E., 2011a. Short-term beach rotation, wave climate and the North Atlantic Oscillation (NAO). Prog. Phys. Geogr. 35, 333–352. https://doi.org/10.1177/0309133310397415

Thomas, T., Phillips, M.R., Williams, A.T., Jenkins, R.E., 2012. Rotation on two adjacent open coast macrotidal beaches. Appl. Geogr. 35, 363–375. https://doi.org/10.1016/j.apgeog.2012.08.010

Thomas, T., Phillips, M.R., Williams, a T., 2013. A Centurial Record of Beach Rotation. J. Coast. Res. 594–599. https://doi.org/10.2112/SI65-101.1

Thompson, D.A., Karunarathna, H., Reeve, D.E., 2018. An Analysis of Swell and

Bimodality Around the South and South-west Coastline of England. Nat. Hazards Earth Syst. Sci. 1–28.

Trouet, V., Esper, J., Graham, N.E., Baker, A., Scourse, J.D., Frank, D.C., 2009a. Persistent positive north atlantic oscillation mode dominated the medieval climate anomaly. Science (80-.). 324, 78–80. https://doi.org/10.1126/science.1166349

Trouet, V., Trouet, V., Esper, J., Graham, N.E., Baker, A., Scourse, J.D., Frank, D.C., 2009b. Medieval Climate Anomaly 78. https://doi.org/10.1126/science.1166349

Trouet, V., Scourse, J.D., Raible, C.C., 2012. North Atlantic storminess and Atlantic Meridional Overturning Circulation during the last Millennium: Reconciling contradictory proxy records of NAO variability. Glob. Planet. Change 84–85, 48–55. https://doi.org/10.1016/j.gloplacha.2011.10.003

Turki, I., Medina, R., Coco, G., Gonzalez, M., 2013. An equilibrium model to predict shoreline rotation of pocket beaches. Mar. Geol. 346, 220–232. https://doi.org/10.1016/j.margeo.2013.08.002

UKHO, U.K.H.O., 2013. INSPIRE Portal & Bathymetry DAC [WWW Document]. Available at. http//aws2.caris.com/ukho/mapViewer/map.action.

Valiente, N.G., Masselink, G., Scott, T., Conley, D., McCarroll, R.J., 2018. Role of waves and tides on depth of closure and potential for headland bypassing Role of waves and tides on depth of closure and potential for headland bypassing. Mar. Geol. 407, 60–75. https://doi.org/10.1016/j.margeo.2018.10.009

Valiente, N.G., McCarroll, R.J., Masselink, G., Scott, T., Wiggins, M., 2019. Multi-annual embayment sediment dynamics involving headland bypassing and sediment exchange across the depth of closure. Geomorphology 343, 48–64. https://doi.org/10.1016/J.GEOMORPH.2019.06.020

Van de Lageweg, W.I., Bryan, K.R., Coco, G., Ruessink, B.G., 2013. Observations of shoreline-sandbar coupling on an embayed beach. Mar. Geol. https://doi.org/10.1016/j.margeo.2013.07.018

van Nieuwkoop, J.C.C., Smith, H.C.M., Smith, G.H., Johanning, L., 2013. Wave resource assessment along the Cornish coast (UK) from a 23-year hindcast dataset validated against buoy measurements. Renew. Energy 58, 1–14. https://doi.org/10.1016/j.renene.2013.02.033

van Rijn, L.C., 2014. A simple general expression for longshore transport of sand, gravel and shingle. Coast. Eng. 90, 23–39. https://doi.org/https://doi.org/10.1016/j.coastaleng.2014.04.008

Vieira da Silva, G., Toldo, E.E., Klein, A.H. d. F., Short, A.D., Woodroffe, C.D., 2016. Headland sand bypassing - Quantification of net sediment transport in embayed beaches, Santa Catarina Island North Shore, Southern Brazil. Mar. Geol. 379, 13–27. https://doi.org/10.1016/j.margeo.2016.05.008

Vintém, G., Freitas, M., Menezes, J., Klein, A., 2006. Beach rotation processes: 35 month survey of embayed beaches of Santa Catarina Brazil. J. Coast. Res. 1752–1755.

Vos, K., Harley, M.D., Splinter, K.D., Simmons, J.A., Turner, I.L., 2019a. Sub-annual to multi-decadal shoreline variability from publicly available satellite imagery. Coast. Eng. 150, 160–174. https://doi.org/10.1016/j.coastaleng.2019.04.004

Vos, K., Splinter, K.D., Harley, M.D., Simmons, J.A., Turner, I.L., 2019b. CoastSat: A Google Earth Engine-enabled Python toolkit to extract shorelines from publicly available satellite imagery. Environ. Model. Softw. 122, 104528. https://doi.org/10.1016/j.envsoft.2019.104528

Wang, C., Zhang, L., 2013. Multidecadal Ocean Temperature and Salinity Variability in the Tropical North Atlantic: Linking with the AMO, AMOC, and Subtropical Cell. J. Clim. 26, 6137–6162. https://doi.org/10.1175/JCLI-D-12-00721.1

Wang, L., Ting, M., Kushner, P.J., 2017. A robust empirical seasonal prediction of winter NAO and surface climate. Sci. Rep. 7, 279. https://doi.org/10.1038/s41598-017-00353-y

Waterhouse, R., 2009. Blackawton & Strete heritage appraisal: an archaeological history. South Hams District Council, Totnes.

Weisheimer, Antje, Schaller, N., Reilly, C.O., Macleod, A., Palmer, T., Centre, E., Weather, M., Ecmwf, F., Weisheimer, A, 2017. Atmospheric seasonal forecasts of the twentieth century : multi-decadal variability in predictive skill of the winter North Atlantic Oscillation (NAO) and their potential value for extreme event attribution. Q. J. R. Meteorol. Soc. 143, 917–926. https://doi.org/10.1002/qj.2976

Westoby, M.J., Brasington, J., Glasser, N.F., Hambrey, M.J., Reynolds, J.M., 2012. "Structure-from-Motion" photogrammetry: A low-cost, effective tool for geoscience applications. Geomorphology 179, 300–314. https://doi.org/10.1016/j.geomorph.2012.08.021

Wheaton, J.M., 2008. Uncertainty in morphological sediment budgeting of rivers. Ph. D. thesis.

Wheaton, J.M., Brasington, J., Darby, S.E., Sear, D.A., 2010. Accounting for uncertainty in DEMs from repeat topographic surveys: Improved sediment budgets. Earth Surf. Process. Landforms 35, 136–156. https://doi.org/10.1002/esp.1886

Wiggins, M., Scott, T., Masselink, G., Russell, P., Castelle, B., Dodet, G., 2017. The

role of multi-decadal climate variability in controlling coastal dynamics: re-interpretation of the “Lost Village of Hallsands,” in: Proceedings Coastal Dynamics 2017. pp. 96–107.

Wiggins, M., Scott, T., Masselink, G., Russell, P., McCarroll, R.J., 2019a. Coastal embayment rotation : Response to extreme events and climate control , using full embayment surveys. Geomorphology 327, 385–403. https://doi.org/10.1016/j.geomorph.2018.11.014

Wiggins, M., Scott, T., Masselink, G., Russell, P., Valiente, N.G., 2019b. Regionally-Coherent Embayment Rotation : Behavioural Response to Bi-Directional Waves and Atmospheric Forcing. J. Mar. Sci. Eng. 7, 116.

Williams, R.D., 2012. DEMs of Difference. Geomorphol. Tech. (Online Ed. 2, 1–17.

Wilson, S., 2006. Slapton Coastal Zone Management Main Study Volume 1: Phase 1.

Woolf, D., Wolf, J., 2013. Impacts of climate change on storms and waves. Mar. Clim. Chang. IMPACTS Partnersh. Sci. Rev. 20–26.

Worth, R.H., 1904. Hallsands and Start Bay. Devonsh. Assoc. 36, 302–346.

Wright, L.D., Short, A.D., 1984. Morphodynamic variability of surf zones and beaches: A synthesis. Mar. Geol. 56, 93–118. https://doi.org/10.1016/0025-3227(84)90008-2

Zambrano, F., Vrieling, A., Nelson, A., Meroni, M., Tadesse, T., 2018. Prediction of drought-induced reduction of agricultural productivity in Chile from MODIS, rainfall estimates, and climate oscillation indices. Remote Sens. Environ. 219, 15–30. https://doi.org/https://doi.org/10.1016/j.rse.2018.10.006

Zhang, R., Delworth, T.L., Held, I.M., 2007. Can the Atlantic Ocean drive the observed multidecadal variability in Northern Hemisphere mean temperature? Geophys. Res.

Lett. 34. https://doi.org/10.1029/2006GL028683

Zhang, R., 2008. Coherent surface-subsurface fingerprint of the Atlantic meridional overturning circulation. Geophys. Res. Lett. 35. https://doi.org/10.1029/2008GL035463